KINETICS OF THE REACTION OF INTRINSIC AND N-TYPE SILICON WITH

ATOMIC AND MOLECULAR BROMINE AND CHLORINE

BY

ZANE HARRY WALKER

B.Sc. (Hons.), Dalhousie University, 1983

M.Sc., University of British Columbia, 1986

A THESIS SUBMITTED IN PARTIAL FULFILLMENT OF THE

REQUIREMENTS FOR THE DEGREE OF DOCTOR OF PHILOSOPHY

in

THE FACULTY OF GRADUATE STUDIES

Department of Chemistry

We accept this thesis as conforming

to the required standard

THE UNIVERSITY OF BRITISH COLUMBIA

November 1990

In presenting this thesis in partial fulfilment of the requirements for an advanced degree at the University of British Columbia, I agree that the Library shall make it freely available for reference and study. I further agree that permission for extensive copying of this thesis for scholarly purposes may be granted by the head of my department or by his or her representatives. It is understood that copying or publication of this thesis for financial gain shall not be allowed without my written permission.

Department of Chemistry

The University of British Columbia
Vancouver, Canada

Date November 27, 1990

DE-6 (2/88)

Abstract

The etching of silicon by atomic and molecular chlorine and bromine was studied as a function of etchant pressure and reaction temperature. Various types of silicon were employed in the etching experiments including intrinsic and n-type polycrystalline silicon as well as the (100) face of intrinsic single crystal silicon. The pressures of Cl_2 and Br_2 varied from 0.1 to 30 Torr and the partial pressure of Cl and Br atoms was between 0.08 and 0.2 Torr. Temperatures of between 365 and 600 °C were required for Cl_2 and Br_2 etching, while lower temperatures of 25 to 470 °C were sufficient for the more reactive Cl and Br atoms.

The reaction between silicon and Br atoms was shown to be first order with respect to the partial pressure of atoms and a first order dependence was assumed for Cl atom etching. The rate constants were determined for the Cl and Br atom etching of intrinsic and n-type polycrystalline silicon, with a dopant concentration of 5×10^{18} atoms cm^{-3}. The reactivity of Cl atoms with n-type silicon was approximately 90 times greater than with intrinsic silicon. This enhancement in reaction rate is primarily due to an increase in the preexponential factor in k_1, with the activation enthalpy for the process remaining unchanged at approximately 28 kJ mol^{-1}. For Br atom etching, the reaction rate for the n-type silicon was over 300 times greater than for intrinsic silicon and was characterized by activation enthalpies of 55 and 63 kJ mol^{-1} respectively. The enhancement in reactivity can also be attributed principally to an increase in the preexponential factor. The preexponential factors for the rate constants are larger than those expected, based on the collision frequencies of Cl and Br atoms. This is interpreted as evidence for a preadsorption step in these reactions.

The reactions of silicon with Cl_2 and Br_2 were found to display a complex pressure dependence. The etch rates varied linearly with (etchant pressure)$^{1/2}$ and the intercepts from a linear regression of the data were slightly negative. To account for the half order pressure dependencies observed in these etching reactions, a reversible dissociative adsorption mechanism is proposed whereby Br_2 (or Cl_2) is dissociatively adsorbed, in a reversible reaction, onto the silicon surface yielding two atoms bound to the surface. This step is then followed by a first order

reaction leading to the formation of a species which is either gaseous product or some precursor which forms that product in a subsequent non rate-determining step.

From the slopes of etch rate versus (pressure)$^{1/2}$ plots, composite half order rate constants were calculated and from the intercepts it was possible to evaluate the rate constant for dissociative adsorption of the halogen molecules. At high etchant pressures, where the reaction was half order with respect to Br_2 (or Cl_2), a half order "composite" rate constant characterized the etching reaction. Values for the half order rate constant were determined for a number of wafers at various temperatures. From the temperature dependencies of these rate constants, activation enthalpies of 131 ± 8 and 116 ± 7 kJ mol^{-1} were calculated for Br_2 and Cl_2 etching of intrinsic polycrystalline silicon respectively. A value of 121 ± 7 kJ mol^{-1} was determined for the Br_2 etching of silicon (100). Higher reaction rates were observed for the etching of n-type polycrystalline silicon, with greater enhancements observed for Br_2 relative to Cl_2 etching. The enhancements in etch rates were found to be principally due to a lower activation enthalpy for the half order rate constant. An activation enthalpy for the composite rate constant of 82 ± 3 kJ mol^{-1} was determined for Cl_2 etching of n-type silicon with a dopant atom concentration of 5×10^{18} atoms cm^{-3}. Br_2 etching of the same wafer yielded an activation enthalpy of 86 ± 3 kJ mol^{-1}. At low pressures, the reaction becomes first order and the temperature dependence of the corresponding first order rate constant yielded activation enthalpies of 109 and 83 kJ mol^{-1} for intrinsic and n-type polycrystalline silicon.

Table of Contents

Chapter 2. Experimental

Chapter 3. Results

List of Tables

List of Figures

Acknowledgements

I would like to extend thanks to Professor Elmer Ogryzlo for his guidance and encouragement throughout the course of this study and for the many valuable discussions on chemical kinetics over the past three years. I would like to acknowledge the electronic, glass blowing and mechanical shops for their assistance in constructing the experimental apparatus necessary for the collection of the data presented in this thesis. Finally, my deepest appreciation is reserved for my parents and wife for their continued support and encouragement throughout my acedemic studies.

Chapter 1. Introduction

1.1 Overview

The reaction of atomic and molecular chlorine and bromine with silicon can be viewed from two perspectives. Fundamentally, the study of these heterogeneous reactions provides insight into the poorly understood realm of gas-solid reaction kinetics, especially in those systems characterized by gaseous reaction products. The majority of work that has been done on gas-solid systems has focussed on heterogeneous catalysis, whereby the surface provides only adsorption sites for one or more gas phase species to undergo chemical reaction. Considerable work has also been carried out on gas-solid reactions in which the products are solids, as in the case of surface oxidation of metals and semiconductors. From a more applied perspective, the reactions of halogens or halogen containing gases with crystalline silicon are widely employed in etching processes during the fabrication of semiconductor devices. Thus information on the reactivities of the halogens with silicon is of interest in the microelectronics industry. To this end much of this thesis will be written from the viewpoint of microelectronic fabrication, including the terminology and methodology associated with it. However, it is hoped that the approach taken in carrying out this study, as well as the conclusions drawn from this work, will find general application in the understanding of gas-solid reactions.

The development of the microelectronic industry during the latter half of this century has revolutionized our day to day lives as seen from the widespread application of semiconductor devices in the home and work place. This is reflected in the magnitude of sales estimated to reach $60 billion this year world wide and forecasted to double to $120 billion by 1994[1]. One reason for the universality of microelectronics has been their low cost. Low cost has been partially achieved through the development of fabrication processes suitable for mass production. A second contributing factor has been the continued drive towards smaller and smaller feature sizes, which today may be less than 1 micron. This miniaturization has lead to an increase in the scale of integration, resulting in the production of chips containing 4 to 16 million discrete devices.

Semiconductors, as the name implies, are materials which have semi-insulating and semi-conducting properties. However it is the ability to selectively increase the electrical conductivity of

an intrinsic semiconductor through the introduction of dopants that has made semiconductors so important in microelectronic device fabrication. Some of the early semiconductor materials included selenium, silicon carbide, and gelena (naturally occurring lead sulfide) and were used to construct rectifiers, photodetectors and point contact diodes in the years prior to World War II. It was the war, and the development of radar, that focussed interest on silicon and germanium as these materials were found to be the most suitable for construction of mixer and detector diodes required in the radar circuitry.

The first transistor was introduced in 1947 by John Bardeen and Walter Brattain of Bell Telephone Laboratories and employed polycrystalline germanium. Within a year similar devices based on polycrystalline silicon were constructed. The second major advance in as many years came in 1949 when single crystal silicon was used to build transistors. It was the introduction of single crystal silicon with well defined properties that allowed the high volume production of small devices and the development of large scale integrated circuits. During the fifties both silicon and germanium were widely used for devices, but by the early sixties silicon was beginning to dominate. Germanium's low band gap of 0.7 eV resulted in major limitations on device operating temperatures making it less attractive. There was also the advantage with silicon of being able to thermally grow a high quality oxide on the surface, which was impossible with germanium. The number of silicon transistor sales began increasing rapidly and by 1966 surpassed those of germanium transistors for the first time[2]. Silicon had become the dominant semiconductor in the microelectronics industry and remains so today.

1.2 Silicon

Silicon has been the most widely employed semiconductor for over 25 years and there are a number of reasons why it has proven to be so advantageous. It is the second most abundant element on earth with a natural abundance of just over 25%, albeit in the form of the oxide SiO_2, providing an inexpensive and inexhaustible supply of raw material. Its bandgap of 1.1 eV allows successful operation of devices up to temperatures of 175 °C[3]. Once purified, silicon becomes a hard, crystalline solid with a diamond-like structure. It is relatively easy to machine into wafers and

eventually into chips with minimal damage from breakage. Silicon is also an elemental semiconductor ensuring chemical stability after being subjected to various processing techniques. This is a distinct advantage over binary semiconductors such as GaAs and InP where high temperature processing often leads to an outgassing of arsenic and phosphorus respectively. One outstanding property of silicon is the ability to form a surface oxide (SiO_2) by thermal oxidation. The oxide is hard, crystalline and resistant to attack by most chemicals, thus passivating the surface as well as providing an ideal mask for many of the processing steps. The high quality of the thermally grown oxide for silicon is unique among semiconductors.

However, silicon does have two major limitations. (1) Silicon is an indirect bandgap semiconductor and therefore not well suited for optoelectronic devices. Indirect bandgap semiconductors are characterized by a minimum in the conduction band which does not lie directly over the maximum in the valence band in a band structure diagram. Thus in order for an electron to be promoted from the valence band to the conduction band, the electron must undergo a change in momentum. This reduces the optical transition probability, resulting in an inefficient energy transfer between photons and electrons. (2) Electron mobilities in silicon are 6 times slower than in GaAs at low applied fields resulting in a lower operating frequency for devices fabricated from silicon. Although silicon is not an ideal semiconductor, the advantages discussed above, along with the extensively developed processing techniques currently being employed and low cost, will ensure its continued widespread use in the foreseeable future. However, it is likely that a number of other semiconductors such as GaAs, AlGaAs, diamond, etc., will emerge and find their niches in specialty applications where silicon is considered unsatisfactory.

The raw material used in the production of silicon is quartz sand. Elemental silicon is obtained by reducing silicon dioxide with carbon, in the form of coke, at high temperatures. Once elemental silicon is formed, the level of purity is increased to that required by the microelectronics industry (10^{15} impurity atoms cm^{-3}) through an oxidation/reduction process. Silicon is oxidized by anhydrous HCl at high temperatures forming $SiHCl_3$ and $SiCl_4$ which can then be distilled to the desired purity level. The purified chlorosilanes are then reduced by H_2 to yield semiconductor grade silicon.

3

1.2.1 Single Crystal Silicon

Crystalline silicon has a diamond-like structure. That is to say it is a face centered cubic structure with half of the tetrahedral holes filled as shown in the unit cell diagram in Figure 1.1. All silicon atoms are tetrahedrally bonded with all bond lengths being equal. The five small black circles in the figure represent the interstitial sites which may become occupied by either a silicon or impurity atom resulting in defects. The silicon (100) and (111) faces are the two most important crystal faces in the fabrication of semiconductor devices (Figure 1.2). The silicon [111] direction consists of alternating planes of atoms, as shown in Figure 1.2. One plane of atoms have their tetrahedral bonds orientated such that each atom has one bond directed to an atom in the plane above with the remaining three bonds going to atoms in the plane below. The atoms in the second plane are orientated just the opposite with each atom having three bonds directed to atoms in the plane above it and one to an atom in the plane below it. In contrast, the less densely packed silicon [100] direction consists of equally spaced planes of atoms, with each atom having two bonds directed to atoms in the plane above and two bonds to atoms in the plane below.

Single crystal silicon is most commonly produced using the Czochralski technique whereby seed crystals with the desired crystal orientation are dipped into a crucible of molten silicon and the ingots are then pulled from the melt. During crystal formation, growth is easiest along the closely packed [111] direction. The etching of this face is also the slowest, leaving behind a smooth etched surface. The (111) material is the most widely used in device manufacturing, although silicon (100) is often used in manufacturing devices such as low-threshold MOS circuits and low-noise operational amplifiers. Silicon (100) is found experimentally to have fewer surface states (i.e. fewer "dangling bonds") than silicon (111) and hence results in lower flicker noise. Doping of the silicon can be achieved by adding the desired type and amount of dopant to the melt. Due to the small quantities required (concentrations in the range of ppm often suffice), the dopants are usually added in the form of heavily doped silicon powder. Elements from groups IIIA and VA are added to produce p- and n-type silicon respectively. Boron and phosphorus are the two most commonly employed, although aluminium and antimony are also used.

4
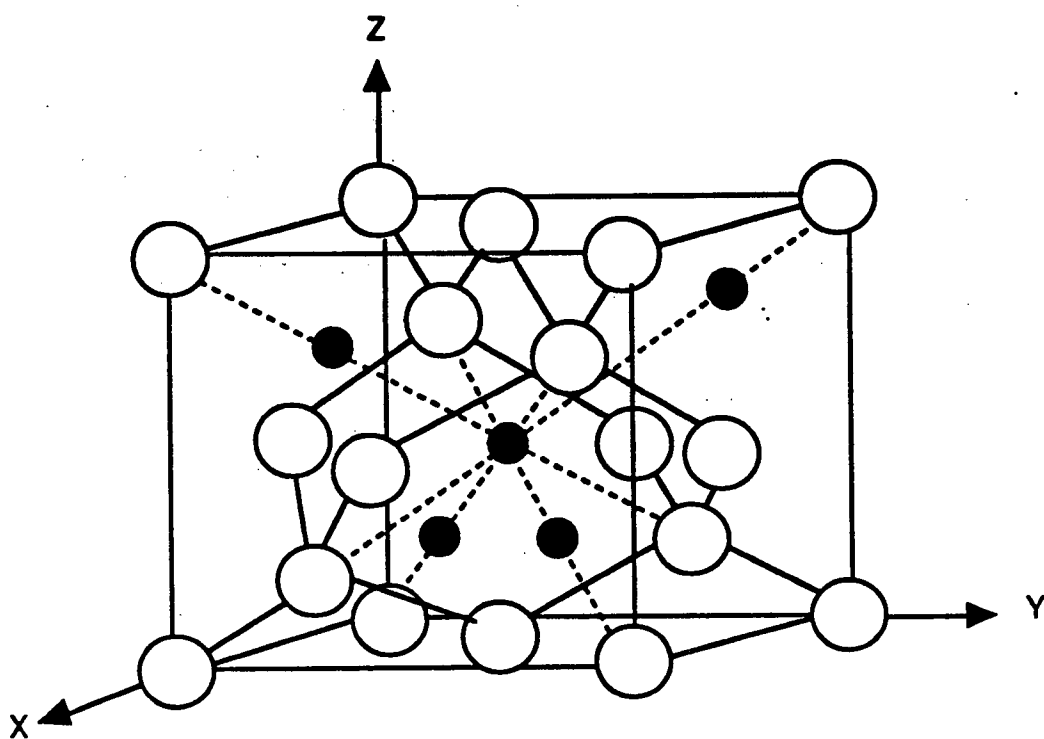
Figure 1.1 Unit cell of crystalline silicon. Solid circles represent interstitial sites.

5

Silicon (111)

Silicon (100)
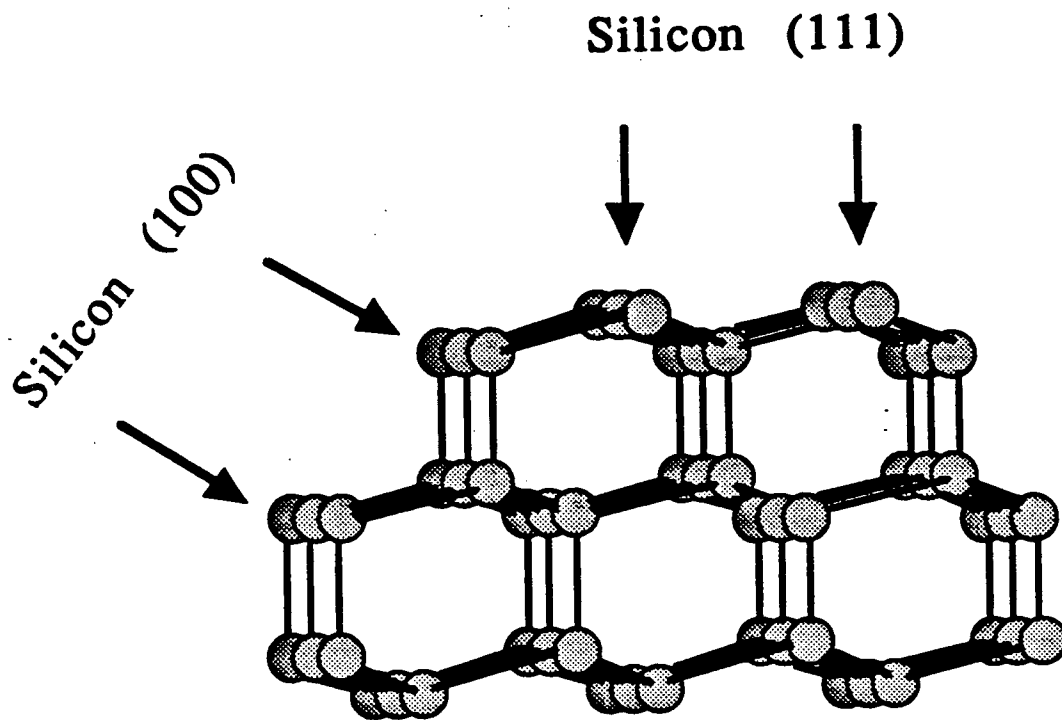
Figure 1.2 (111) and (100) faces of crystalline silicon.

If production of intrinsic silicon with a high resistance is desired, further purification is possible through zone refining. One end of the silicon ingot is heated producing a cross-sectional wafer of molten silicon. Since the impurities have a greater solubility in the molten silicon than in the crystal, they begin to concentrate in the molten zone. The molten zone is then moved along the entire length of the ingot, carrying the impurities to the end of the ingot where they can be removed.

Wafers are cut from the silicon ingot with a diamond-edged saw to a thickness of approximately 0.5 mm. Wafer flatness is very critical in device fabrication and as a result a number of lapping and polishing steps are carried out to produce wafers with thickness variations of less than +/- 25 μm.

1.2.1.1 Defects

Wafers cut from single crystal ingots are not perfect crystals and do contain a number of defects which affect the electrical and chemical properties of the devices made from them. Some of these defects arise during the growth of an ingot from a melt and some are introduced during the subsequent processing steps of the wafers. Defects can be classified as being either point or line defects and are schematically represented in Figure 1.3. There are three classes of point defects; vacancy defects (the absence of an atom from a lattice site Figure 1.3a), interstitial defects (the presence of an atom in a non-lattice or interstitial location Figure 1.3b) and substitutional or antistructural defects (the occupation of a lattice site by a impurity atom Figure 1.3c). Vacancy defects are often referred to as Schottky defects and if a vacancy and interstitial defect are adjacent to one another, they are often called Frenkel defects (Figure 1.3d). Unlike point defects which affect only one lattice site, line defects are propagated in two dimensions throughout the crystal lattice. The two most common line defects are edge and screw dislocations. Edge dislocations arise when there is an additional plane of atoms in the crystal lattice (Figure 1.3e). Screw dislocations propagate themselves through a crystal much like the movement of a screw thread upon rotation (Figure 1.3f).
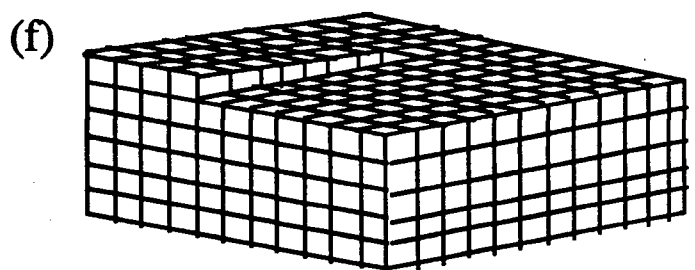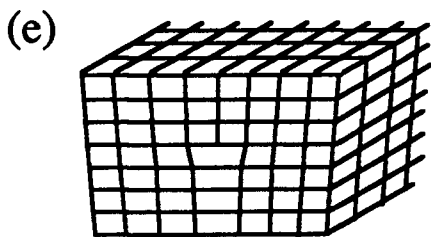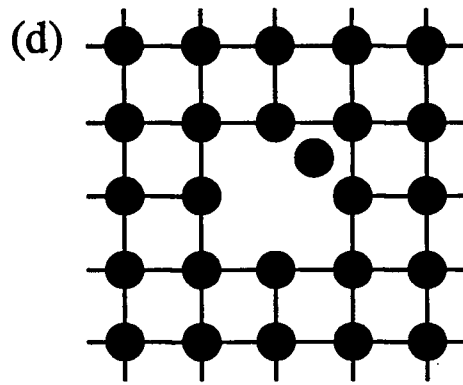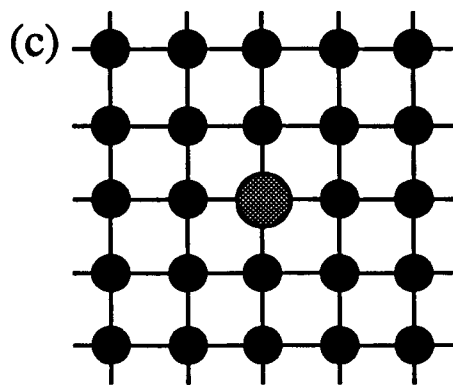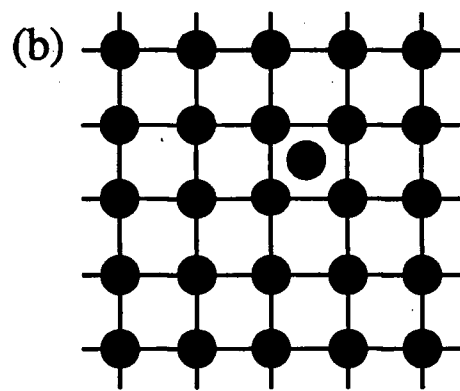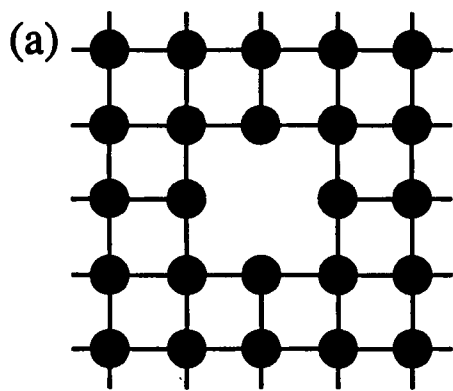
Figure 1.3 Crystal defects and dislocations: (a) vacancy defect, (b) interstitial defect, (c) substitutional defect, (d) Frenkel defect, (e) edge dislocation and (f) screw dislocation.

The detection of defects is most commonly achieved by performing a selective crystallographic wet etch of the wafer surface. The etchant required to delineate the defects is dependent upon the crystallographic face being studied but in general consists of a solution of HF and an oxidizing acid. Tables of the various etching solutions are commonly available[4].

1.2.2 Polycrystalline Silicon Thin Films

Polycrystalline silicon, although not as widely used in device fabrication as its single crystal counterpart, does have many important applications. The main advantage of polycrystalline grown silicon is that deposition temperatures as low as 550 °C can be used compared to the relatively high temperatures of 950-1150 °C required for epitaxial film growth. Epitaxial films are single crystal films which retain the crystal orientation of the substrate lattice on which they are grown. For example an epitaxial film of silicon grown on a silicon (100) substrate would also have a (100) orientation. Some applications of polycrystalline silicon films include the use of heavily doped polycrystalline silicon to construct gate electrodes and interconnects in metal-oxide-semiconductor (MOS) devices, and to construct emitter structures in bipolar devices. Lightly doped polycrystalline silicon films can be used to fabricate high-value load resistors in static memories and to refill trenches in dielectric isolation technologies.

Polycrystalline silicon films are most commonly grown by chemical vapor deposition (CVD). A silicon containing gas, usually SiH_4, is passed over a hot substrate (550 to 750 °C) at pressures ranging from 10^{-4} to 10 Torr where the gas thermally decomposes leaving behind a silicon film. Unlike epitaxial silicon films which have a single crystal orientation, polycrystalline silicon films are composed of grains which may or may not be dominated by a particular crystal orientation. Grains are typically a few hundred nm in diameter, with higher deposition temperatures favouring larger grain size. The interface region between grains is referred to as the grain boundary and is composed of randomly ordered crystal lattices containing many unsaturated bonds. The preferred crystal orientation of the grains is dependent upon both deposition temperature and pressure, as can be seen from the data presented in Figure 1.4. This data, reported by Joubert et al.[5], shows the dominating crystal orientation of polycrystalline silicon grown by

chemical vapor deposition as a function of deposition temperature and silane pressure. The figure can be divided into five regions. At low pressure and high temperature, the films tend to consist of randomly orientated grains. An increase in silane pressure first favours the (100) orientation and then the (110) orientation. A low temperature and high silane pressure favours (311) oriented grains. Finally at low temperatures and higher pressures only amorphous, non-crystalline silicon is deposited.

The doping of the polycrystalline silicon films is usually achieved by ion implantation. An ion beam of the desired dopant atom is formed by ionization of a suitable source material (such as red P(s), PCl_3 or PH_3 for phosphorus atoms) followed by mass filters and ion focussing lenses. These ions are then accelerated to the wafer surface with energies of up to 1MeV, resulting in implantation depths of several microns. The implanted ions at this point do not occupy the proper lattice sites and are considered electrically inactive. There is also considerable damage to the lattice due to the high energy ions that bombard the lattice during implantation. For these two reasons, implantation is followed by high temperature annealing. The annealing process allows dopant atoms to migrate from interstitial sites to lattice sites, thereby becoming electrically active. Annealing also reduces the number of crystal defects introduced by the implantation process.

The introduction of dopants in polycrystalline silicon may also be achieved through diffusion. Wafers are heated to temperatures between 900 and 1300 °C and a dopant source gas is passed over the surface. The temperature and the dose of dopant determines the concentration profile in the silicon.

The material properties of polycrystalline silicon are similar to those of single crystal silicon with two exceptions, namely diffusion and dopant distribution. The diffusion constants for the grain boundary regions are higher than for single crystal silicon located within the grains. The result is that the diffusion of dopant atoms occurs principally in the grain boundary region. Dopant atoms also tend to accumulate in these grain boundary regions producing an inhomogeneous distribution of dopant. This can lead to differences in electrical properties between single crystal and polycrystalline silicon. For a given dopant concentration, the resistivity of polycrystalline silicon is generally higher than for single crystal silicon resulting from dopant atoms being tied up
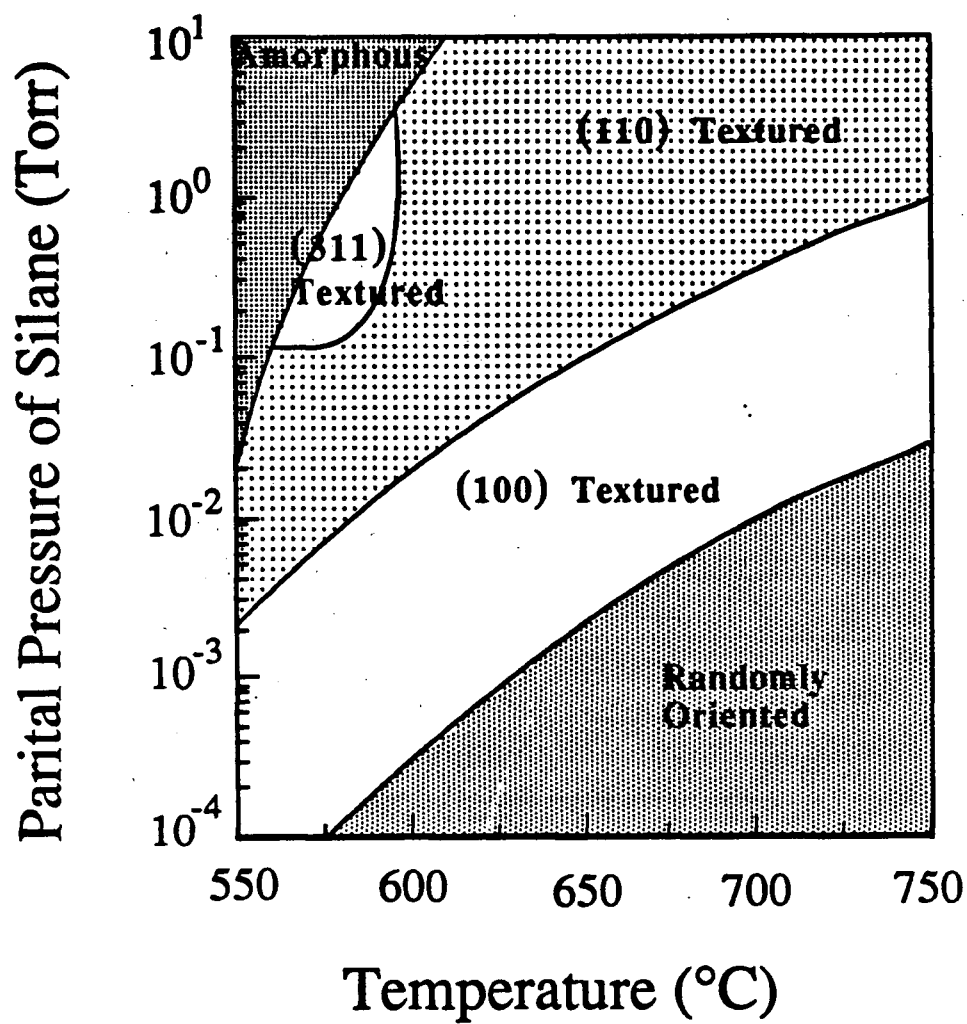
Figure 1.4 Crystal orientations of polycrystalline silicon grown by CVD using silane.

in the grain boundaries. This effect is minimized by annealing polycrystalline silicon films at high temperatures (900 to 1000 °C) which promotes the integration of dopant atoms into the single crystal region of the grains.

1.2.3 Effect of Doping

When silicon is doped with either n- or p-type dopant atoms, even at concentrations as low as a few ppm, a number of changes occur in the electrical behavior of the semiconductor. In order to facilitate a discussion of these changes, one should begin with a brief discussion of semiconductor band theory.

In a solid, the number of atomic orbitals brought together to form molecular orbitals is very large. The energy separation between the resulting levels is very small, giving rise to the formation of two bands. The lower energy valence band is composed of bonding orbitals and the higher energy conduction band is composed of antibonding orbitals as shown in Figure 1.5a. The separation between the two bands is called the band gap and represents the energy required to excite or promote an electron from the valence band to the conduction band. In an intrinsic semiconductor, the fraction of electrons in the conduction band as a function of temperature can be given by the Fermi-Dirac expression[6],

$$f(E) = \frac{1}{1 + \exp[(E - E_F)/kT]}$$

(1.1)

where E is the energy of the band gap and E_F is the Fermi energy or Fermi level. The Fermi level is defined as the energy level at which the probability of finding an electron is one half. Since the density of states in the valence band and the conduction band are assumed to be equal, the Fermi level is placed mid-way between the two bands in a pure semiconductor.

If a dopant atom is present in the silicon lattice, either intentionally or as an impurity, the position of the Fermi level can be shifted. If the dopant atom is a Group VA element such as phosphorus, the extra valence electron can be removed leaving behind a P^+ in the silicon lattice. A small amount of energy is required to remove this electron (typically <0.1 eV) and hence the

(a)

Conduction Band

E_C .... Donor Level

E_F .... Fermi Level

E_V .... Acceptor Level

Valence Band

(b)

Conduction Band

E_F

Surface State

Occupied States

Valence Band

Semiconductor   Vacuum

(c)

Conduction Band

E_F

Surface State

Occupied States

Valence Band

Semiconductor   Vacuum
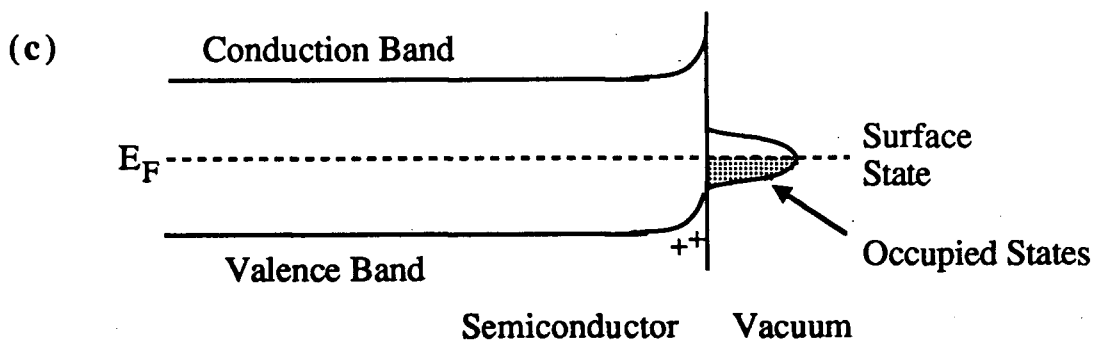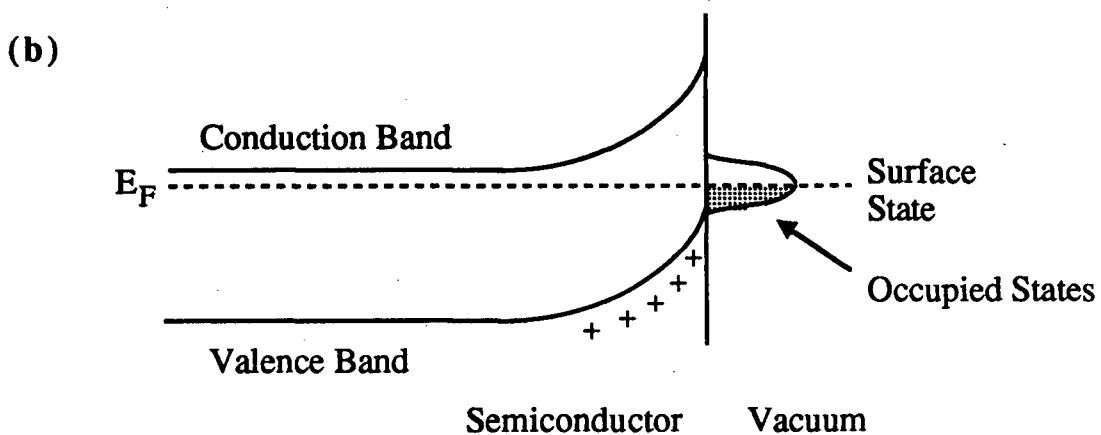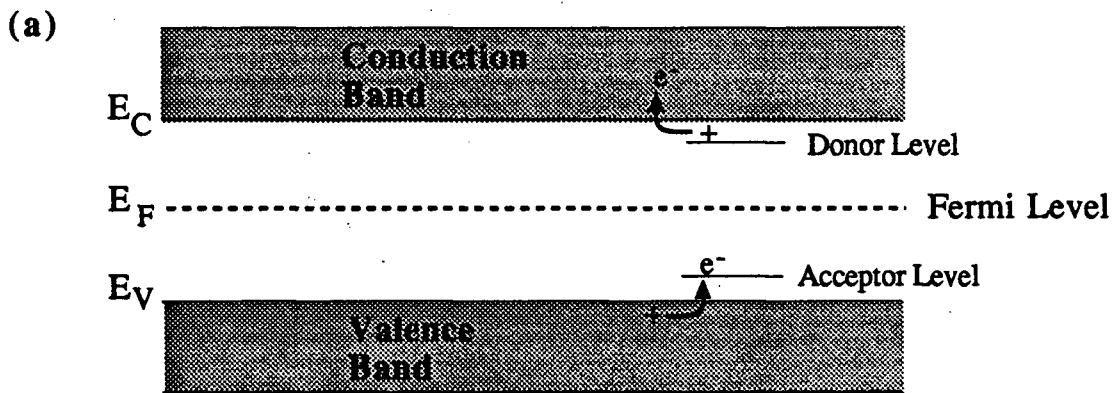
Figure 1.5 (a) Band structure for a semiconductor. Band Bending for n-type (b) and intrinsic (c) material.

position of this donor state is located just below the conduction band. Because the energy separation between the donor state and conduction band is so small, nearly all the electrons are promoted into the conduction band. If the dopant atom is a Group IIIA element, then an acceptor state is created which is located only slightly above the valence band. Once again the energy separation is very small (typically <0.1 eV) and an electron is easily promoted from the valence band to the acceptor level at room temperature, leaving a hole free in the valence band to conduct current. In a real intrinsic semiconductor at room temperature, the number of electrons in the conduction band is given by the number of impurity atoms donating electrons, and not by the of number of electrons thermally exited from the valence band.

The diagram of the valence and conduction bands given in Figure 1.5a is only true for the bulk of the semiconductor. At the surface of the semiconductor the Fermi level is controlled by the energies of the surface states associated with defects or adsorbates. For a solid in equilibrium, the position of the Fermi level is constant and it is the energy bands themselves that are perturbed at the surface. This results in what is known as band bending. In n-type silicon, where the Fermi level is located just below the conduction band, there is a large degree of band bending (Figure 1.5b) as electrons migrate into surface states, leaving behind a depletion region containing holes. In intrinsic silicon, the Fermi level is located midway between the top of the valence band and the bottom of the valence band (Figure 1.5c). The degree of band bending is less than in n-type silicon and the resulting depletion layer is smaller. One would not expect to see any depletion layer in the case of p-type silicon.

1.3 Etching

Etching of semiconductors is performed to either remove material uniformly over a large area, in the case of wafer thinning and polishing, or to locally transfer a pattern made by resist lithography to the underlying layer. Etching may be achieved by either wet or dry processes. Wet etching, although the older and less expensive process, is giving way to dry etching processes which allow for a more efficient transfer of the small geometries required in the fabrication of micron and sub-micron device structures. Dry etching processes also eliminate the need to handle

and dispose of large amounts of corrosive chemicals and waste. The following discussion will therefore emphasis dry etching processes to reflect this shift away from wet etching processes.

1.3.1 Wet Etching

In the early days of microelectronic fabrication, wet etching was used exclusively in all etching processes. The most common etchants employed were mixtures of HNO_3 and HF in water or acetic acid which work by first oxidizing the silicon to SiO_2 and then dissolving the oxide in the HF. The resulting etch profiles were isotropic, that is the etching occurred equally in all directions, leading to an undercutting of the mask (Figure 1.6a). If the width of the mask is large compared to the etch depth, then the undercutting may be inconsequential. However as the ratio of mask width to etch depth decreases, isotropic etching can be disastrous resulting in a complete undercutting and lifting off of the mask. In contrast, anisotropic etching occurs preferentially in one direction. In device fabrication, it is often desired to etch perpendicular to the surface, producing a profile with vertical walls and no undercutting (Figure 1.6b). It is difficult to obtain vertical etch walls in wet etching, although some control over etching direction can be obtained through crystallographic etching. Using the fact that certain crystallographic planes have a higher density of silicon atoms, a preferential etch in a particular direction is possible. For example, either a hydrazine in water mixture, or KOH in water or isopropanol etches faster in the [100] direction than in the [111] direction where the planes are closely packed, resulting in V-shaped trenches. It is the isotropic etching characteristic of wet processes which has limited its application today principally to the area of wafer polishing.

1.3.2. Dry Etching

Dry etching encompasses a wide range of etching environments which may contain both chemically reactive neutral species as well as charged ions. The presence of ions, which can be accelerated perpendicular to the surface by electric fields, allows for more directional control over the etching process resulting in anisotropic etch profiles.

(a)

Mask

Silicon

Isotropic Etching

(b)

Mask

Silicon
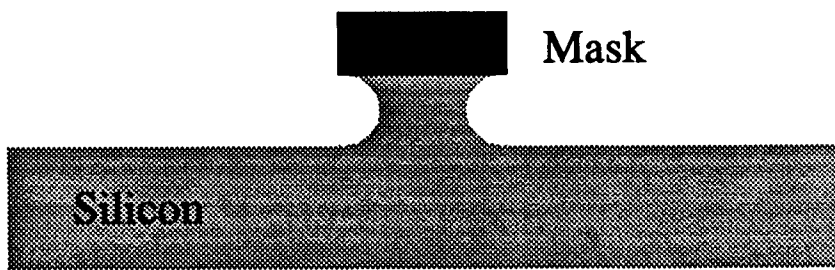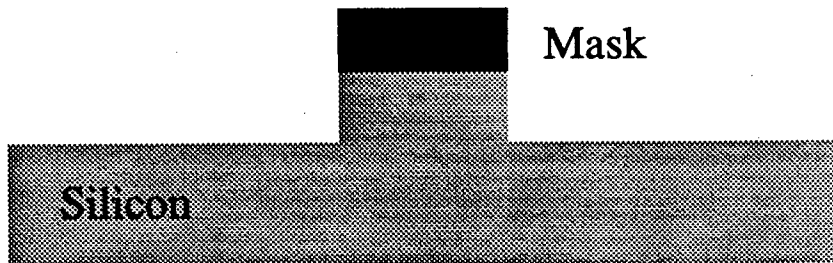
Anisotropic Etching

Figure 1.6 Isotropic and anisotropic etch profiles.

The relative contribution of ions to reactive chemical species in the etching process has given rise to a number of classifications. At one end of the spectrum is ion milling and ion sputtering. These processes rely entirely on the physical sputtering of the surface by heavy charged ions, usually Ar^+. In the case of ion sputtering, ions are produced in an argon discharge and accelerated to the cathode upon which the wafer being etched is placed. In ion milling, electron beam ionization is used to produce argon ions which are then accelerated by an electric field to the substrate surface. The advantage of ion milling over ion sputtering is that the ion energy and ion density can be independently controlled. Both, however, expose the surface being etched to high energy ions which can significantly increase the number of crystal defects and thereby affect the quality of devices subsequently produced. A second major drawback is that both ion milling and ion sputtering show poor selectivity in their removal rate of different materials, making it difficult to find suitable masks for pattern transfer. Thirdly, as the etch depth increases, the sputtered material may become redeposited on the side walls of the features being etched, thereby limiting the etch depth.

One way to avoid some of these problems is to use lower energy ions in the presence of a reactive gas. This configuration, known as plasma assisted etching or reactive ion etching, utilizes the directionality of the ions to accelerate chemical etching perpendicular to the surface being etched. The result is cleanly etched surfaces, essentially vertical walls with little undercutting of the mask, and minimal crystal damage to the etched surface. Plasma-assisted etching also yields a more selective etch, providing sufficient removal rate while limiting the damage to the mask and hence ensuring accurate pattern transfer.

Various mechanisms have been proposed to explain the interaction of neutral and ion species with the silicon substrate resulting in anisotropic etch profiles. Whether or not one or more of these mechanisms dominates is dependent upon the chemical species present, as well as the pressure and temperature at which the etching is carried out. The first mechanism is one whereby the chemical etch rate is limited by product desorption. The ions bombarding the surface assist in product desorption, thus increasing the etch rate[7]. A second possibility is that the ion bombardment of the surface provides energy to surface species which promotes the formation of

17

product[8,9,10]. Thirdly ion bombardment induces damage to several atomic layers of the silicon lattice, allowing for easier penetration of the reacting species resulting in an increase in the rate of formation of volatile products[11]. Lastly, depending upon the type of plasma gas used, species of radicals can be formed in the plasma which recombine on the silicon surface, forming a protective mask and hence preventing further etching[12]. Ions bombarding the horizontal surface prevent the build up of this layer whereas lateral walls not exposed to the ions are passivated.

Although much work has been done on various reactive ion etching systems, a full understanding of the etching process is far from complete. The etching environment contains many charged and neutral species produced in the discharge and understanding the role played by these individual species in the presence of ion bombardment of the surface is difficult. The easiest way to understand the chemistry of the etching species is to study them in the absence of ion bombardment.

1.3.2.1 Chemical Etching

In the absence of ion bombardment of the silicon surface, only chemical etching occurs. Although chemical etching is not widely employed in microelectronic fabrication due to its typical isotropically etched profiles, it is often employed to study the fundamental chemistry of the etching processes found in more complex systems. The advantages are that only a limited number of chemical species are present compared to those often present during reactive ion etching, and the physical effect of ion bombardment can be excluded. The kinetics of pure chemical etching are also of interest to those developing direct writing techniques using laser and ion beams. Many of the processing steps required in the fabrication of devices can be avoided by using direct writing techniques to transfer patterns to the semiconductor surface. This is achieved by exposing selected areas of the surface to either a photon or ion flux in the presence of a reactive gas, such as chlorine. The photons or ions enhance the etching in the exposed areas resulting in pattern transfer to the silicon surface. Knowing how the surface not exposed to these beams will react at various gas pressures and temperatures will therefore be important.

18

In an effort to elucidate the mechanisms of chemical etching, three approaches are commonly taken in the collection of experimental data. The first involves studying the surface of silicon under high (10^{-6} to 10^{-8} Torr) or ultra high (10^{-8} to 10^{-11} Torr) vacuum conditions after exposure to an etchant. Various techniques are used to probe the surface such as x-ray photoelectron spectroscopy, Auger emission spectroscopy, and thermal desorption spectroscopy to name a few. Very little of the surface is etched and the measurements are sensitive only to those surface species stable after exposure is complete. It is perhaps more appropriate to refer to this as an adsorption reaction. A second approach is to probe the dynamics of the reaction using molecular beam and laser techniques. Measurements are made under high vacuum conditions and molecular beams can be employed to provide a large flux of reactants at the surface while maintaining a low background pressure. Once again the amount of material removed is small and the term etching may not be applicable. Thirdly, kinetic studies can be performed on the etching process by studying the effect of macroscopic variables on the rate of reaction. Typically these variables include the concentration of the reactants and the reaction temperature, with the resulting reaction rate, or etch rate, approaching microns per minute. The present study adopts this third approach. It should be noted that these kinetic studies, performed at gas pressures in the range of milliTorr or Torr, may also lead to a better understanding of the "pressure gap" often observed in gas-solid chemical reactions upon going from high to low pressures[13].

In the following pages, a brief literature review will be given of chemical etching of silicon by the halogens fluorine, chlorine and bromine. The studies discussed represent some of the more relevant works reported on the kinetics of chemical etching.

1.3.2.1.1 Fluorine Etching

Of all the halogens employed in the etching of silicon, fluorine has been the most widely studied. The first reported study of the reaction of F_2 with silicon was by Kuriakose and Margrave[14] in 1964. The reaction was studied at temperatures between 75 and 900 °C and at F_2 partial pressures of 2.8 to 52.5 Torr in He. The reaction order with respect to fluorine partial pressure was observed to range from 0.6 to 1.0. Above 150 °C, the reaction was characterized by

an activation energy of 5.4 kJ mol^{-1} while below this temperature a value of 50 kJ mol^{-1} was determined. More recently, activation energies of 33 and 38 kJ mol^{-1} have been determined for the etching of silicon by F_2[15,16,17]. The silicon fluorides SiF_2 and SiF_4 have been identified as the only products from this reaction[17,18]. Similar studies have also been performed on fluorine atom etching whereby the atoms are produced through the dissociation of F_2 either thermally or in a plasma discharge. Reaction products have been identified as SiF_2 and SiF_4, with activation energies for their production of 9 and 14 kJ mol^{-1} respectively[19]. Flamm et al.[20] also reported a comparable activation energy for the etching of silicon by F atoms of 10.4 kJ mol^{-1}. Surface studies have revealed F_2 dissociatively adsorbs on the silicon surface, producing 1 to 1.5 monolayers of SiF_2-like species [18,21]. In contrast to the limited adsorption of F_2, a much greater uptake of F atoms into several monolayers was reported, suggesting an ability of the atoms to diffuse into the silicon lattice.

Various chemical species have been employed to provide reactive fluorine species at a silicon surface. Perhaps the most widely used has been XeF_2. At room temperature XeF_2 is a crystalline solid with a vapor pressure of approximately 5 Torr. The etch rates measured for XeF_2 etching are $\sim 10^4$ times faster than those obtained for F_2 etching[22]. These etch rates have been found comparable to those obtained for F atom etching, although it has been suggested direct comparison of results obtained with the two etchants should be done with caution[23]. Reaction products from XeF_2 etching of silicon have been identified as SiF_2 and SiF_4[24,25], with activation energies for their production of 28 and 23 kJ mol^{-1} respectively[26]. Surface studies have indicated the reaction proceeds with a build up of a corrosion or reaction layer[27] similar to that observed in F atom etching. Species present on the surface after exposure were identified to be SiF, SiF_2 and SiF_3, with no evidence for the existence of unreacted interstitial fluorine[28]. Other fluorine containing species such as ClF_3, BrF_3, BrF_5, IF_5 and NF_3 have also been employed to provide a source of F atoms in silicon etching [17,29,30].

20

1.3.2.2.2 Chlorine Etching

Unlike fluorine, chlorine does not spontaneously react with silicon. At room temperature Cl_2 will adsorb onto a silicon surface and studies employing photoemission spectroscopy have revealed the presence of binding sites with one, two and three chlorine atoms bonded to silicon atoms on a Si(111) 7x7 surface[31,32,33]. Upon annealing to 400°C, however, silicon species bonded to only one chlorine atom were observed[34]. A recent scanning tunnelling microscope study by Boland and Villarrubia[35] yielded similar findings. A silicon (111) surface exposed to Cl and then annealed at 400 °C produced a surface composed mainly of SiCl, with only a small amount of $SiCl_2$ and $SiCl_3$. A second exposure of Cl at room temperature converted many of the SiCl species into the more highly coordinated silicon chlorides.

At temperatures greater than approximately 300 °C, surface reactions between Cl_2 and silicon will lead to formation of volatile products. There have been a number of studies which have examined the products of this reaction under varying conditions. Florio and Robertson[36] in 1969 identified $SiCl_4$ as the only reaction product resulting from the exposure of silicon (111) to $4x10^{-8}$ Torr of Cl_2 at 580 °C. The activation energy for the desorption process was found to be 146 kJ mol^{-1}. Madix and Schwarz[37] examined the same reaction at Cl_2 pressures between 10^{-5} and 10^{-6} Torr and temperatures of between 770 and 1500 K. Using a modulated Cl_2 molecular beam with a phase sensitive mass spectrometer, they found $SiCl_2$ to be the only reaction product under these conditions. The activation energy for the formation of product was 165 kJ mol^{-1}. Their results also indicated a first order dependence on Cl_2 pressure at temperatures above 1050 K. More recently, Sander et al.[38] have investigated the reaction products desorbing from a silicon surface exposed to a Cl_2 flux of $5x10^{16}$ molec cm^{-2} s^{-1} at temperatures of 300 to 1000 K. (A flux of 10^{16} molec cm^{-2} s^{-1} is equivalent to a pressure of approximately 10^{-4} Torr.) At temperatures between 425 and 800 K, essentially all silicon atoms left the surface as $SiCl_4$ while at temperatures between 800 and 1000 K, $SiCl_2$ took over as the dominant reaction product. No reaction was observed at temperatures below 425 K.

In a thermal desorption spectroscopy study of the reaction of Cl_2 with silicon by Jackman et al.[39], the collection of thermal desorption spectra identified the presence of two desorption

peaks, α and β, coinciding at temperatures of 450 and 950 K respectively. In thermal desorption spectroscopy, a silicon sample is exposed to a known amount of Cl_2 at room temperature. The temperature of the sample is then ramped and the species desorbing from the surface are detected by mass spectrometry as a function of temperature. The species desorbing from the α state were found to be almost exclusively $SiCl_4$, with $SiCl_2$ and $SiCl_4$, along with possibly limited amounts of SiCl and Cl, desorbing from the β state. The activation energies for desorption from the α and β states were 115 and 235 kJ mol^{-1} respectively. The conclusion drawn from these studies regarding reaction products is that at low reaction temperatures, the higher coordinated $SiCl_4$ is favoured. As the temperature is increased, a greater proportion of the silicon leaves the surface as the lower coordinated $SiCl_2$.

Aoto et al.[40] have studied the stable chemisorbed species present on silicon (100) and (111) surfaces after exposure to both Cl_2 and Ar^+ ions (i.e. after ion-assisted etching). Using surface techniques of Auger electron spectroscopy, x-ray photoelectron spectroscopy, low-energy electron energy loss spectroscopy and reflection high-energy electron diffraction, it was concluded that the surface is composed of SiCl, $SiCl_2$ and $SiCl_3$. The more highly coordinated $SiCl_3$ was found to exist in a surface layer extending 4 Å from the surface, while SiCl was present in a layer extending 6 Å from the surface. In the presence of ion bombardment, SiCl dominated and only after high Cl_2 exposures (3×10^8 Langmuir or 1 Torr for 300s) is $SiCl_3$ observed on the surface.

Ogryzlo et al.[41] have studied the Cl_2 etching of variously doped polycrystalline silicon films at temperatures between 300 and 500 °C and at pressures between 0.3 and 10 Torr. The etch rate was found to increase non-linearly with increasing pressure and tended towards a saturation limit, although this limit was not reached within the pressure range studied. The etch rates were also found to increase with increasing dopant concentration. An activation energy of 56 kJ mol^{-1} was determined for the three heavily doped polycrystalline silicon wafers. A mechanism was proposed whereby Cl_2 is dissociatively adsorbed onto silicon in a non-reversible step, followed by a re-ordering of the surface to produce a volatile product.

The etching of various single crystal and polycrystalline n-type silicon wafers by Cl atoms has been reported by Ogryzlo et al[42]. The enhancements in etch rates for n-type silicon were found

to vary with crystallographic orientation, with enhancements being greater for n-type silicon (111) than for n-type silicon (100) at the same dopant concentration. The temperature dependence of the etch rate revealed activation energies of between 17.2 and 19.7 kJ mol^{-1} for all wafers. Although differences in the etch rate of up to 3 orders of magnitude were observed for the various samples, these differences were attributable to changes in the Arrhenius preexponential factor of the rate constants only. The activation energy was found to remain the same for all samples studied.

1.3.2.2.3 Bromine Etching

Bromine, like chlorine, does not spontaneously react with silicon at room temperature. It will however dissociatively adsorb on a silicon surface. Transmission channelling using a 2.5 MeV He$^+$ ion beam has been used to study the chemisorption of bromine on a silicon (111) surface[43] and has found that Br preferentially adsorbs at an on-top position, that is directly over a silicon atom in the top monolayer of the crystal.

Jackman et al.[44] recently investigated the reaction of Br_2 with silicon (100) using thermal desorption spectroscopy. The thermal desorption spectra (that is the plot of ion signal versus sample temperature) collected after various Br_2 exposures indicated the presence of two desorption peaks, α and β, coinciding at temperatures of 500 and 770 K respectively. The activation energies for desorption from these states were determined to be 119 and 186 kJ mol^{-1} respectively. The species desorbing from the α state consisted mainly of the higher brominated silicon bromides, $SiBr_3$ and $SiBr_4$, as well as Br and Br_2. The species desorbing from the β state were a mixture of $SiBr_2$ and Br atoms with the relative amount of $SiBr_2$ increasing with increasing Br_2 surface coverage. The conclusion to be drawn from this study regarding reaction products is that at any given temperature, the products may contain various silicon bromides, as well as Br and Br_2, with lower temperatures favouring more strongly coordinated silicon bromides.

In the same study, Jackman et al. also examined the surface of silicon after Br_2 exposure at 300 K using Auger electron spectroscopy. Surface techniques such as Auger electron spectroscopy and x-ray photoelectron spectroscopy require that the measurements be made under ultra high vacuum conditions (~10^{-10} Torr) which makes *in situ* studies of etching reactions difficult to

perform. Thus these surface studies detect only stable chemisorbed surface species, which may or may not be representative of the true reaction intermediates present on the surface during the etching reaction. The signal intensity from bromine was found to saturate after an exposure of 9×10^{14} molec cm^{-2} and was believed to result from a saturation of the Auger probe depth, estimated to be equivalent to ~3 surface layers. This result at room temperature would indicate the build up of a corrosion layer, similar to that observed in fluorine etching of silicon[45]. In contrast, an x-ray photoelectron spectroscopy study performed on n-type silicon (111) samples etched in a HBr reactive ion etching reactor[46], found the presence of only a monolayer of bromine on the silicon surface. The bromine was contained in $SiBr$, $SiBr_2$, $SiBr_3$ and $SiBr_4$ species, with a greater concentration of the lower brominated species. A ratio of the bromine and silicon peak intensities indicated a bromine to silicon ratio of 2.3:1. It is likely that the surface bombardment by ions during etching encourages only a monolayer coverage of bromine in contrast to the multilayer coverage observed in the study by Jackman et al.[44] One can only speculate whether or not these room temperature surface studies are indicative of the surface during exposure to Br_2 at elevated temperatures.

There has been only one reported investigation of the etching of silicon by Br_2. In 1982 Sveshnikova et al.[47] reported a study of the Br_2 etching of silicon (100) and (111) at temperatures between 490 and 550°C. The authors found that at low pressures the etch rate increased non-linearly with increasing pressure, but reached a limiting value at pressures between 5 and 15 Torr depending upon reaction temperature. A mechanism was proposed in which the first step in the reaction is the reversible adsorption of Br_2 on the reacting surface, and the pressure independence results when the surface is saturated with adsorbed Br_2.

1.4. Fabrication of a Device

Although the use of etching for device fabrication is not central to this study, a brief discussion of the steps involved in the fabrication of a simple device may aid the reader in having a better understanding of some of the requirements of the industry. As an example, the processing steps required for the fabrication of a typical metal-oxide-semiconductor (MOS) transistor[48] are

outlined in Figure 1.7. The first step is the thermal oxidation of a p-type single crystal silicon substrate followed by the deposition of a silicon nitride film (Figure 1.7a). The oxide layer will help to protect the silicon surface during subsequent processing steps and the silicon nitride film acts as a mask during selective oxidation as it prevents the diffusion of oxidant molecules from reaching the underlying silicon. A photoresist is then laid down and the mask pattern is transferred to the underlying silicon nitride film (Figure 1.7b). Wet etching of silicon nitride is difficult and hence this step is usually achieved using a fluorine containing plasma. The regions exposed by the nitride mask are then implanted to form p^+-type regions (the + superscript indicates heavily doped material) forming channel stops for the device. The next step is removal of the photoresist and thermal oxidation of the exposed silicon regions (Figure 1.7c). As the oxygen becomes incorporated, the oxide layer extends both above and below the original surface. This is followed by the removal of the silicon nitride, commonly achieved with phosphoric acid (Figure 1.7d). The next step requires the growth of the gate oxide. Since the quality of this oxide is critical to the performance of the transistor, the previous oxide is removed and a new oxide is grown under very carefully controlled conditions (Figure 1.7e). A gate is then formed by depositing a polycrystalline silicon film by CVD followed by doping with phosphorus to lower its resistance thus forming n^+-silicon (Figure 1.7f). A silicon nitride film is deposited, patterned and the underlying n^+-type polycrystalline silicon is etched to produce a gate structure on the surface (Figure 1.7g). The source and drain are now formed by ion implantation which produces two n^+-type silicon regions (Figure 1.7h). A field oxide is formed by depositing a phosphosilicate glass followed by patterning and etching to expose the source and drain (Figure 1.7i). Metal contacts are made to the gate, source and drain by deposition of aluminium followed by patterning to yield the proper contact points (Figure 1.7j). Finally, the entire device is covered with a passivating layer, usually a silicon oxide or silicon nitride film, and patterned to allow bonding to the contacts.

It is evident from this example of a routinely fabricated transistor that many complex and divergent processing steps are required in the fabrication of microelectronic devices. The importance of understanding the wide ranging chemistries involved in these processing steps is obvious.

(a)

(b)

(c)

(d)

(e)

(f)

(g)

(h)

(i)

(j)

	Silicon
	Oxide
	CVD Oxide
	Polycrystalline Silicon
	Aluminum
	Photoresist
	Silicon Nitride
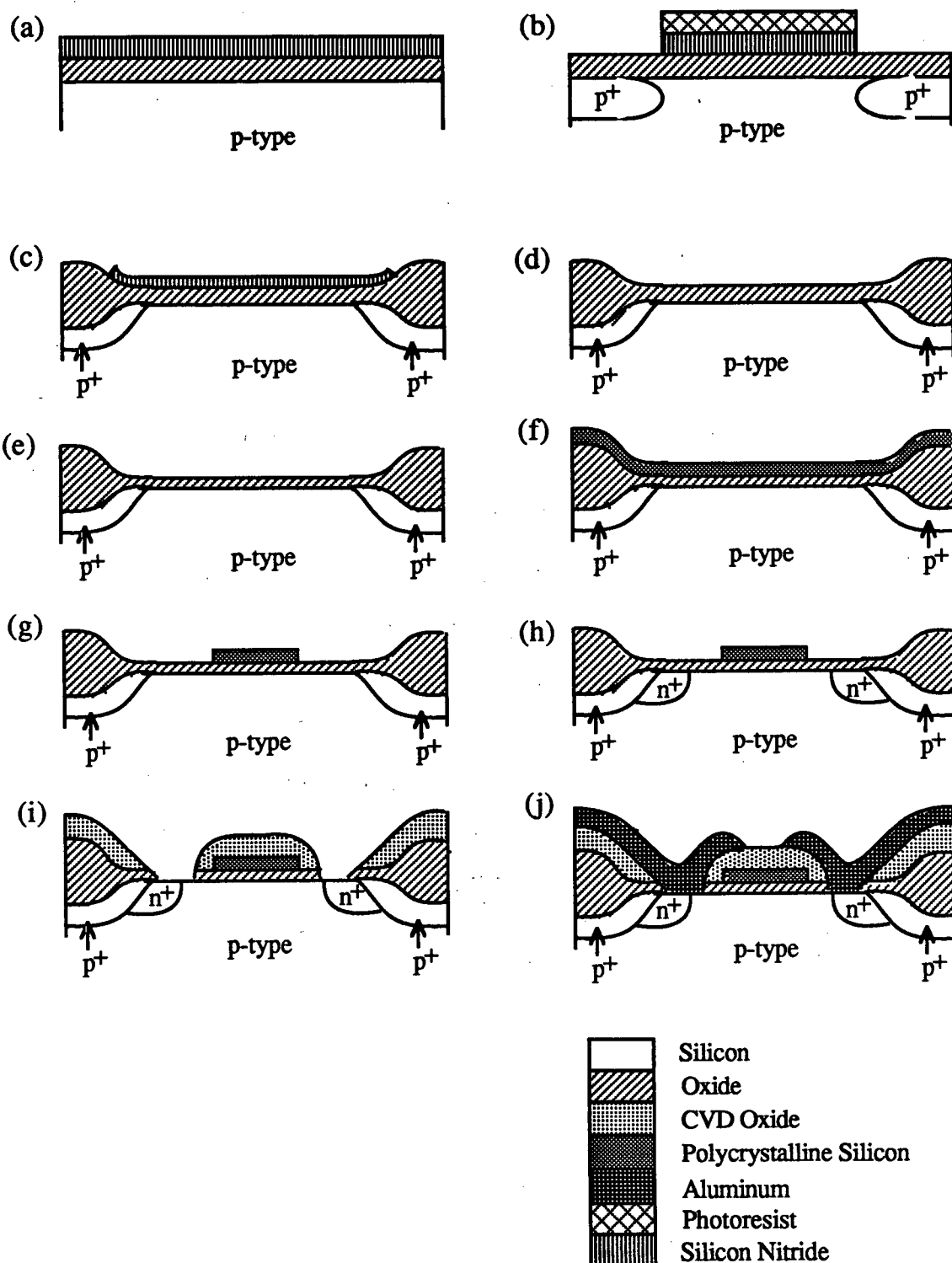
Figure 1.7 Processing steps in the fabrication of a MOS transistor.

1.5 Mechanisms for Gas-Solid Etching Reactions

Although the work contained in this thesis is specific to the etching of silicon by bromine and chlorine, there are five general steps which are common to all gas phase etching. They are:

1. Diffusion of etchant to the surface.

2. Absorption of the etchant on the surface.

3. Formation of a product molecule from one or more surface adsorbed species.

4. Desorption of product from the surface.

5. Diffusion of product away from surface.

In most etching systems it is possible to ensure steps 1 and 5 are not rate controlling by employing sufficient gas flows and choosing appropriate temperatures and etchant pressures. Hence these two steps seldom influence the observable kinetics of the reaction. The remaining three steps play a more critical role in the etching process and a brief discussion of each is warranted.

1.5.1. Adsorption

The adsorption of a gaseous molecule on a surface is a complex process in itself and as such has received considerable attention from physicists and chemists. It is not the intention of the author to try to address the complexities of this process in this thesis, but rather to review the fundamentals as they pertain to the etching of semiconductors.

A gaseous molecule approaching a surface undergoes a weak interaction with the surface as a result of van der Waals' forces. This process is referred to as *physisorption* and the resulting bond enthalpy is usually less than 40 kJ mol^{-1}. The adsorption is reversible resulting in an equilibrium between the surface adsorbed species and the bulk gas molecules. Since the interaction is weak, the internal bonds of the adsorbed molecule are not broken. Once physisorbed, a molecule may form strong chemical bonds with surface atoms through *chemisorption*. The molecule may remain intact and become molecularly chemisorbed, as is often observed with CO, or may be dissociatively chemisorbed, as is often observed with O_2. Whether an adsorbed molecule

experiences molecular physisorption, molecular chemisorption or dissociated chemisorption depends upon the species involved and the resulting bonds that are formed. A simple model for understanding these three possibilities was introduced in 1932 by Lennard-Jones[49]. Imagine a molecule AB with zero potential energy approaching a surface as represented in the potential energy diagram in Figure 1.8. The potential energy of the molecule dips negative as it becomes physisorbed to the surface. Also included in the energy diagram is a line which represents the potential energy of atoms A+B. At infinite distance, their potential energy is positive and corresponds to the bond energy of AB. As the atoms A and B approach the surface, their energy is lowered slightly by van der Waals' interactions, and then more dramatically as each become chemically bonded to surface atoms. Whether a molecule becomes physi- or chemisorbed depends on the relative positioning of the two energy curves and their cross-over points. In Figure 1.8a the barrier between the physisorbed and chemisorbed energy wells is below the zero of energy. Once the molecule is physisorbed it spontaneously dissociates forming chemisorbed species A and B. If the barrier is positive, as in Figure 1.8b, then molecular physisorption occurs at low temperatures and as the temperature is raised, some molecules will pass over the barrier and become dissociatively chemisorbed. The physisorbed species in this case is a precurser to the chemisorbed state. If the energy curve for A+B lies well above the energy curve for AB as in Figure 1.8c, then chemisorption occurs without dissociation of AB.

1.5.2 Product Formation

The most widely studied group of gas-solid reactions have been those classified as "heterogeneous catalysis". In these reactions, a surface provides a two dimensional space for the adsorption of gas molecules thus increasing the probability of their collision and subsequent reaction. Mechanisms formulated for such heterogeneous catalysis processes can be equally applicable in etching reactions. For the reaction

$$A + B \xrightarrow{\text{surface}} \text{Products} \tag{1.2}$$

(a)

Potential Energy

A+B

AB

Reaction Coordinate

(b)

Potential Energy

A+B

AB

Reaction Coordinate

(c)

Potential Energy

A+B

AB

Reaction Coordinate
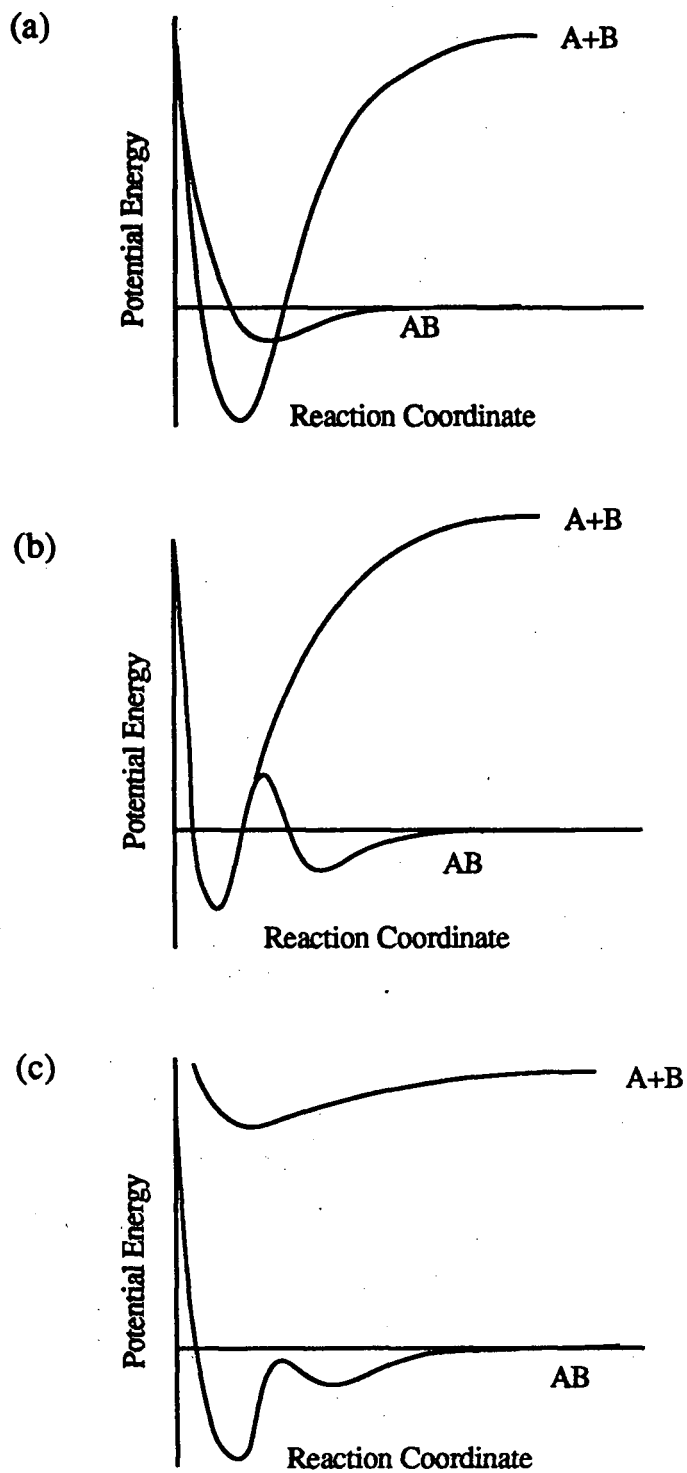
Figure 1.8 Lennard Jones curves for physi- and chemisorption of molecule AB.
(a) dissociative chemisorption, (b) physisorption and (c) molecular chemisorption

which is catalyzed by a surface, two mechanisms have been proposed. In the first, adsorption of molecule A is followed by a collision with molecule B directly from the gas phase, leading to product formation and desorption. This is referred to as the Eley-Rideal[50] mechanism. In the second mechanism, adsorption of both molecules A and B is required before the reaction can occur. This concept was originally proposed by Langmuir[51] and Hinshelwood[52] and is now referred to as the Langmuir-Hinshelwood mechanism. Differentiating between the two mechanisms has been difficult using traditional kinetic measurements. However, the introduction of molecular beam relaxation spectroscopy has helped to elucidate the two mechanisms. By preadsorbing molecule A on the surface, followed by a modulated beam of molecule B impinging on the surface, a modulated flux of product from the surface can be detected. If preadsorption of B is not required, then there should be no phase shift between the modulated beam of B and product flux from the surface. These results would lend support for a Eley-Rideal mechanism. If on the other hand a phase shift is observed, then preadsorption of B would appear required and the results would be suggestive of a Langmuir-Hinshelwood mechanism. Such experiments have been successful in demonstrating that both pathways do exist. The conditions under which one of these mechanisms dominates are difficult to predict and some reactions are found to proceed by both mechanisms depending upon the catalyst employed. For example, the oxidation of CO to CO_2 on an indium-doped ZnO catalyst is found to proceed through an Eley-Rideal mechanism[53] whereas a Langmuir-Hinshelwood mechanism has been found for the same CO oxidation process on Pt(111)[54].

1.5.3 Desorption

Once product is formed on the surface, desorption is the final process required in the etching reaction and can be viewed as the reverse process of physisorption discussed above. The molecule is located at the bottom of the physisorption energy well shown in Figure 1.8b and must overcome this barrier to desorb. The energy required to kick the molecule out of the well is provided by the random thermal motion of the lattice atoms about their equilibrium position.

If product desorption were rate limiting in a etching reaction, one would expect to observe a saturation in the etch rate as the reactant pressure is increased at constant temperature. The reaction

would then become zero order with respect to etchant pressure and the observed activation energy for the process would be indicative of the desorption step.

1.5.4 The Pressure Gap in Gas-Solid Reactions

For the traditional approach to gas-solid reactions it has been assumed that much of the energy required for reaction of adsorbed species and subsequent desorption from the surface is provided by the surface itself in the form of phonons or lattice vibrations. One shortcoming of this approach has been its inability to account for the absence of reactivity at low pressures. An example is the dissociative adsorption of CH_4 on a Ni surface which occurs readily at pressures greater than 1 Torr, but is not observed at pressures less than 10^{-4} Torr[55]. Ceyer[13] has proposed that many gas-solid reactions are aided by collisions from gas phase molecules. The energy transferred from a gas molecule colliding with a physisorbed species on the surface may be sufficient to either force the species over the dissociative chemisorption energy barrier or over the energy barrier for desorption. Ceyer has likened the effect of the incoming gas molecules to that of a hammer; the larger the hammer, the larger the amount of energy transfer to the adsorbed species. This effect has been demonstrated for the dissociated adsorption of CH_4 on a Ni surface by using molecular beams of Ar, Ne and Kr[56]. Decreasing the pressure of a reaction occurring at constant temperature, although not affecting the energy distribution of gas phase molecules, will lower the absolute number of molecules colliding with the surface which have sufficient energy to bring about reaction. This will result in a decrease in the observed rate of that surface process. The implications of such a mechanism are that high vacuum studies of surface reactions, whether they be heterogeneous catalysis, chemical vapor deposition or semiconductor etching, may yield different kinetics and dynamics than observed at higher pressures. It is therefore important to examine gas-solid reactions, such as the etching of silicon, not only under high vacuum conditions, but also at higher pressures where the collisions of gas phase molecules with surface species may provide additional reaction pathways.

31

1.6 Purpose of Study

The objective of this study is the determination of the orders and rates of the reaction of chlorine and bromine atoms and molecules with intrinsic and doped silicon. By determining the rate constants for these reactions as a function of temperature the energetic requirements of the rate controlling steps can be obtained. This information will aid in the identification of the reactions involved in these steps. A determination of the pressure dependence of the reaction could help to establish the nature of those rate controlling steps. The variation of the reaction rate with dopant concentration could also contribute to our understanding of the etching mechanism. Finally, a comparison of the reactivity of Br and Br_2 relative to Cl and Cl_2 would be useful for an assessment of the relative merits of these etching gases.

Chapter 2. Experimental

2.1 Apparatus

Silicon etching was performed in one of two flow reactors, one dedicated to molecule etching experiments, the second to atom etching experiments, and follow a general design previously employed for etching studies in our laboratory[57,58]. The two types of etchants required unique experimental conditions which follow a general reactor design.

2.1.1 Reactor for Br_2 and Cl_2 Etching Reactions

A schematic of the reactor design employed to study the etching of silicon by molecular bromine and chlorine is presented in Figure 2.1. The reactor consisted of a 40 cm length of quartz tube with an inner diameter (ID) of 25 mm. Originally this section was constructed of Pyrex, but this limited the maximum etching temperature to below 530 °C. The Pyrex was replaced with quartz in an effort to obtain a wider temperature range over which measurable etch rates could be produced. The quartz reactor tube was integrated into the remaining Pyrex system with the aid of quartz-Pyrex graded seals. Pyrex was employed whenever possible because of its chemical resistance to Br_2 and Cl_2. Items such as pressure gauges, fittings, etc., exposed to the gaseous etchants were constructed out of stainless steel and monel. The attack of these surfaces by Br_2 and Cl_2 appeared to be negligible in the absence of H_2O. O-rings used in fittings were made from neoprene and teflon. Although the teflon o-rings were resistant to attack by Cl_2 or Br_2, they showed little elasticity and were found to require frequent replacing as they became compressed. The valves used to throttle the pump, as well as the valve on the Br_2 reservoir were constructed from teflon.

The system was pumped by a cryostatic pump backed by a rotary pump (Sargent Welch Model No. 1400) permitting the system to be pumped down to a base pressure of a few milliTorr prior to the etching of each sample. The cryostatic pump prevented either halogen from entering the rotary pump, as well as any back diffusion of hydrocarbon vapors. The pumps were isolated from the remaining system by two teflon stopcocks with maximum orifices of 4 and 10 mm. These stopcocks permitted fine and coarse throttling of the pump.
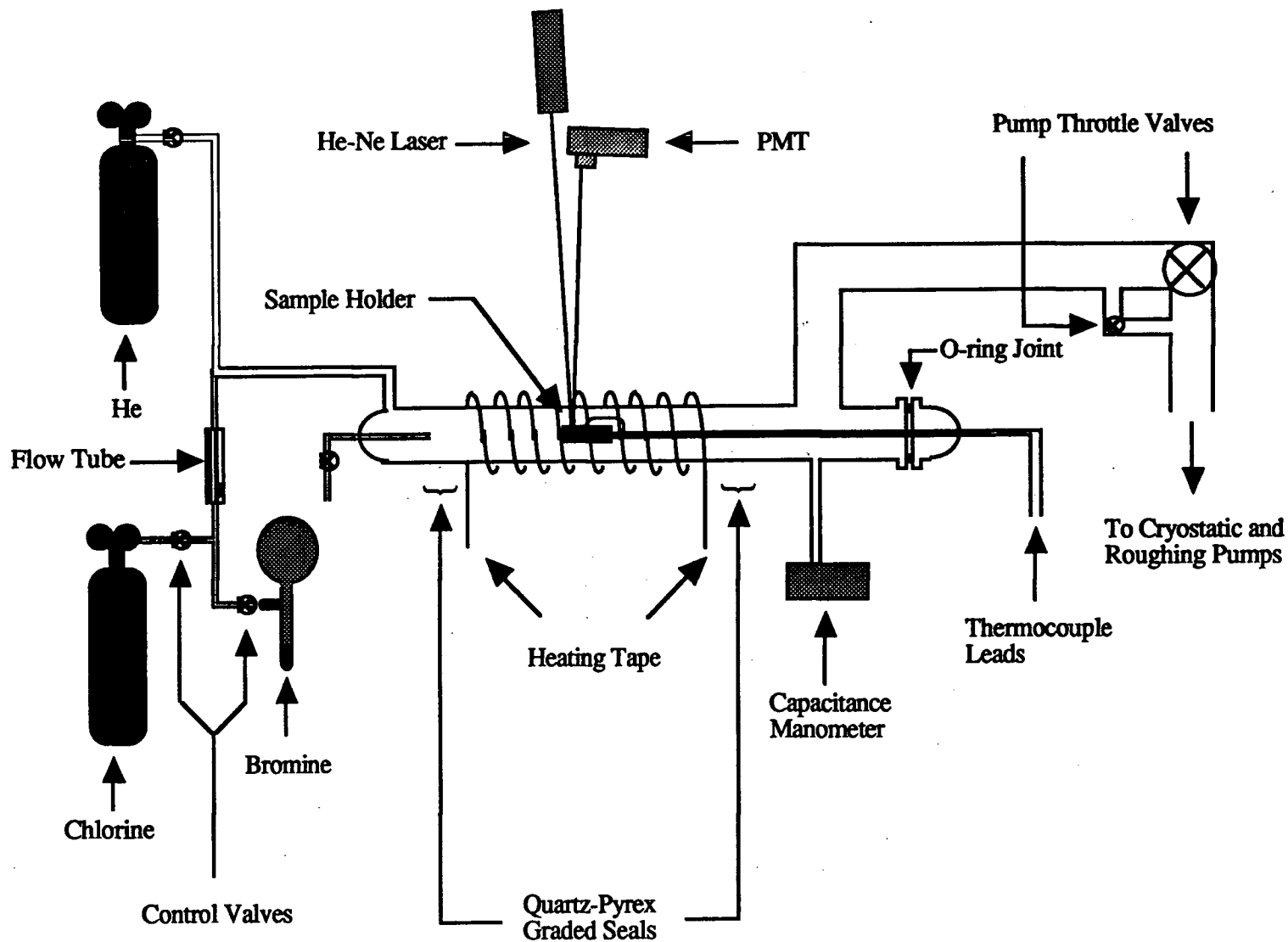
Figure 2.1 Apparatus for Cl_2 and Br_2 etching of silicon.

Gas pressures were measured using a capacitance manometer (MKS Model 220BHS) with a pressure range of 10^2 to 10^{-2} Torr. Pressures measured with this gauge were checked against 2 other similar gauges to ensure the accuracy of the measurements. A cold cathode pressure gauge (HPS Model 421) was used to check the absolute base pressure in the system.

Relative Br_2 and Cl_2 gas flows were measured using a flow tube (Matheson R615A) complete with glass float. The absolute gas flows were determined by calibrating the flow tube for each gas by monitoring the pressure rise in the system observed upon closing the throttles to the pumps. Using this pressure rise and the ideal gas law, the gas flow was calculated.

The reactor was also equipped with a He gas line. The He was used to bring the system up to atmospheric pressure after completing an etching experiment and to provide a positive pressure of inert gas while loading and unloading samples. This was done in an effort to avoid the introduction of air or moisture into the system.

2.1.2 Reactor for Br and Cl atom Etching Reactions

There were a number of criteria in reactor design which had to be met in order to facilitate atom etching experiments. In general they were (1) the incorporation of a microwave discharge to produce atomic species from the dissociation of either Br_2 and Cl_2, (2) minimal distance between the discharge region and the sample, as well as higher gas flows to ensure rapid transport of atoms from the discharge region to the sample, and (3) facilities for monitoring and measuring atom concentrations. These considerations led to the following reactor design.

The gas delivery and pumping systems, as well as the pressure measuring devices were the same as those used in the molecular etching reactor described above and have been omitted from the schematic of the atom etching reactor presented in Figure 2.2. The discharge tube consisted of an 11.5 mm quartz tube located upstream from the sample holder. Quartz was required to withstand the high temperatures associated with the microwave discharge. The quartz tube was connected to the remaining Pyrex system with stainless steel o-ring fittings (Cajon, Model Ultratorr). Joining two glass tubes together with these fittings results in a gap approximately 1 cm wide between the two ends allowing direct exposure of the gas to the inner stainless steel surface

35
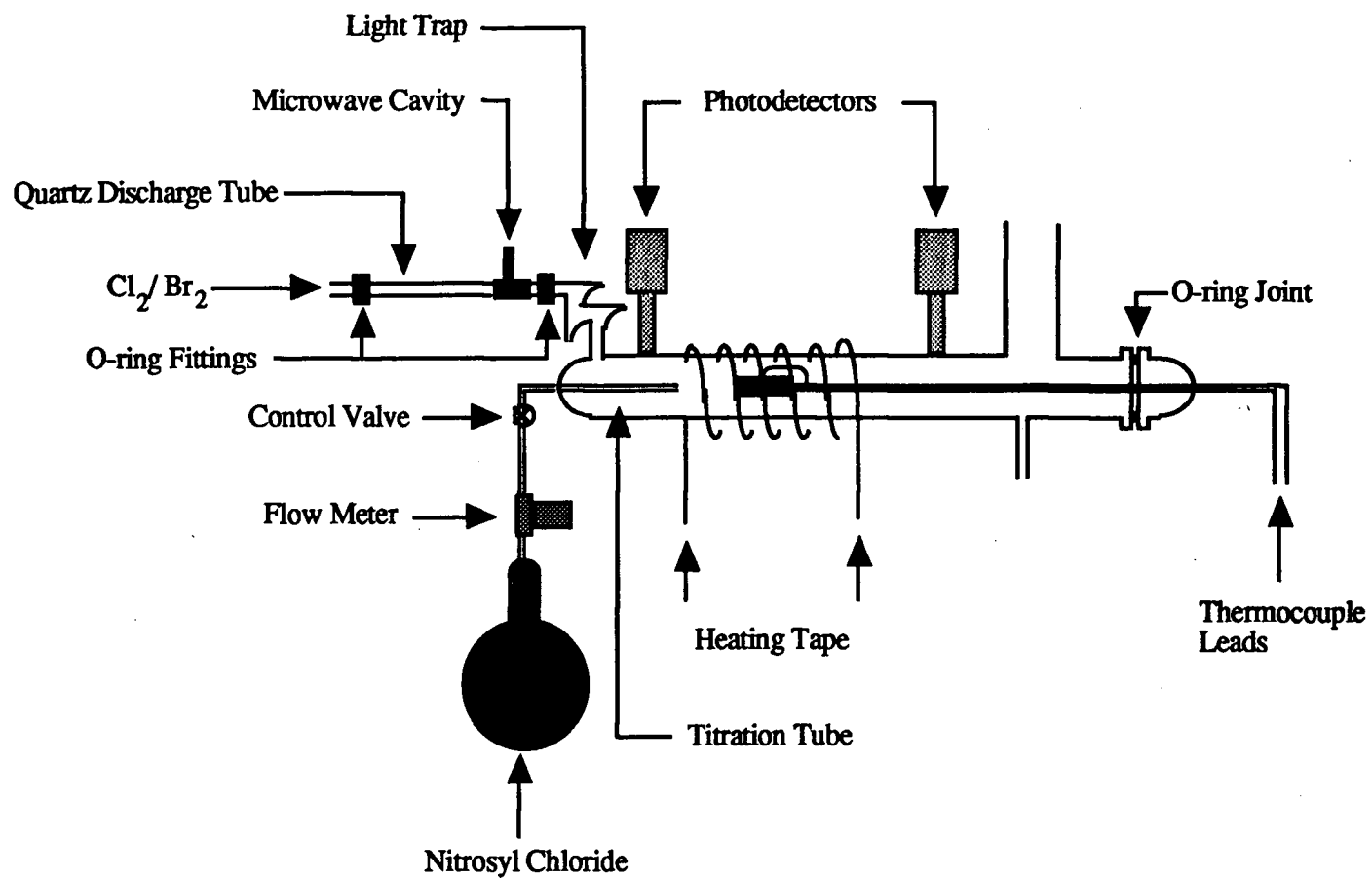
Figure 2.2 Appartus for Cl and Br etching of silicon.

of the fitting. When the gas flowing through the fitting contains highly reactive species such as Br or Cl atoms, the metal surface could either react with the atoms or provide a suitable surface for the atoms to recombine. In either case this could significantly reduce the atom concentrations observed downstream. In order to prevent exposure of these atoms to the stainless steel surface of the downstream fitting, the end of the Pyrex tube was reduced in diameter slightly such that it could pass through the center of the fitting and be brought up flush with the quartz tube.

The more reactive atomic species were expected to significantly reduce the temperature necessary to obtain an etching reaction and hence only Pyrex was required in the construction of the main reactor tube. A titration tube located at the upstream end of the main reactor tube and extending 6 cm downstream was incorporated to facilitate the determination of absolute atom concentrations by the NOCl titration (discussed in section 2.5.3). The flow of NOCl used in the titration experiments was measured with a flow meter (Sierra Trak Model 821S2-04). Also required in the monitoring and determination of atom concentrations were two silicon photodiodes located at positions 8 cm upstream and downstream from the sample holder. The photodiodes were covered with red filters which limited the transmission of light to wavelengths longer than 600 nm. To prevent light emitted from the discharge region from reaching the photodetectors, a light trap was incorporated between the discharge tube and the main reactor tube. The sample holder was located at a total distance of 20 cm downstream from the discharge cavity. This position was found sufficiently remote from the plasma to prevent charged ions from reaching the sample, yet close enough to provide rapid transport of atoms produced in the discharge to reach the sample. Heating of the reactor tube was achieved by wrapping a 7 cm long region centered about the sample holder with heating tape connected to a Variac.

2.1.3 Sample Holder

There were difficulties in finding suitable materials from which to construct a sample holder. The holder had to withstand the extremely reactive environment resulting from several Torr of either Br_2 or Cl_2 at temperatures up to 600 °C. Metals such as stainless steel and monel, although inert to these halogens at room temperature, readily react at elevated temperatures. The

surface upon which the sample is placed should be flat and polished to ensure good thermal contact with the sample. It was also desirable to use a relatively large mass for the holder in comparison to the sample being etched so that any heat generated in the sample and transferred to the holder would result in a negligible temperature rise. The holder also had to maintain a vacuum within the reactor, while being removable for quick loading of samples. A mechanism for applying pressure on the sample to hold it in place and ensuring good thermal contact with the holder was also required.

The original prototype holder, based on previous designs used in this laboratory[57], consisted of a platform constructed from a 10x30x0.5 mm piece of single crystal silicon wafer attached with a high temperature ceramic cement to a 4 mm quartz tube support. A thin SiO_2 layer (up to a few hundred nm thick) was thermally grown on the wafer to prevent attack by bromine or chlorine. A chromel-alumel thermocouple was placed inside the quartz tube to record the temperature. The quartz tube was epoxied (Torr Seal) to a 25 mm diameter Pyrex o-ring joint which allowed quick loading and unloading of samples. The epoxy seal was located outside the heated region and was resistant to attack by the two halogens at room temperature. After a number of early experiments, this holder was found to be unsuitable for a number of reasons. Repeated heating cycles from room temperature to temperatures of 500 or 600 °C rapidly destroyed the adhesive bond between the underside of the wafer platform and the ceramic cement. The porous nature of the ceramic cement also raised concerns about the possibility that O_2 and H_2O were being absorbed each time the holder was removed from the system to load a sample. As the cement degassed under vacuum, the introduction of O_2 and H_2O could encourage the growth of an inhibiting oxide layer on the sample being etched. Finally, the cement was observed to discolor after repeated exposures at high temperatures, suggesting a reaction with the halogen gases may be occurring. For these reasons, an improved holder design was felt to be imperative.

The sample holder design finally chosen is presented in Figure 2.3. An 18x14x9 mm block of silicon was machined from a single crystal ingot. Two 4 mm holes were bored lengthwise through the block. One surface of the block was polished to a mirror finish. This was the surface on which the sample would be placed. A thin, protective, SiO_2 layer was thermally grown on the

Quartz Spring

Silicon Block with
Surface Oxide

4 mm Quartz Tube

Epoxy Seal

Thermocouple
Leads

25 mm O-ring Joint
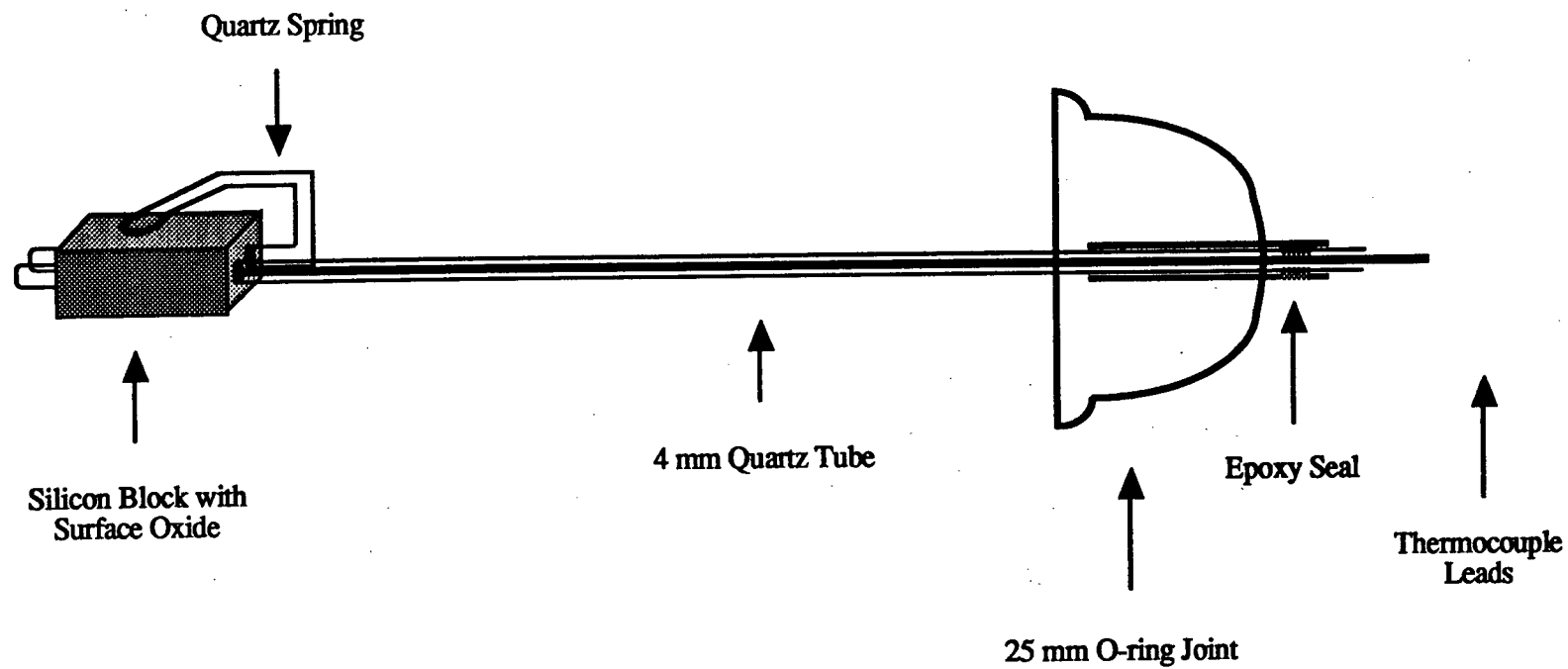
Figure 2.3 Sample holder used in molecular and atomic chlorine and bromine etching of silicon.

surface by heating the block to 1000 °C while passing H_2O vapor over the surface. The block was supported by a 4 mm quartz tube through which passed a chromel-alumel thermocouple connected to a readout (Omega Model 115 KC) for measuring temperature. Epoxy (Torr Seal) was used to provide a vacuum seal between the quartz tube and the o-ring joint as indicated in the figure. Samples to be etched were held in place by a quartz spring attached to the quartz support tube.

2.2 Chemicals

2.2.1 Single Crystal Silicon (100)

Wafers of single crystal intrinsic silicon (100), 0.5 mm thick and 100 mm in diameter, were obtained from AT&T Bell laboratories. The wafers were cleaned according to the procedure outlined in section 2.3 and stored in protective containers. The containers protected the wafers from contact with dust particulate but could not be considered air tight.

2.2.2. Polycrystalline Silicon

Polycrystalline silicon films are generally not available as an over the counter product. When they are required in industry, they are deposited by in house facilities. The intention was originally to develop a deposition process within our laboratory so that films meeting our specifications and grown under identical conditions could be provided. The films would then be doped with phosphorus to desired levels by ion implantation at a facility in the Department of Electrical Engineering. After the establishment of such a deposition facility in our laboratory failed to materialize, wafers were obtained from two sources, AT&T Bell Laboratories in Murray Hill, New Jersey and Bell Northern Research in Ottawa. The thicknesses of the polycrystalline films and the dopant concentrations were determined according to the procedure given in sections 2.2.1.1 and 2.2.1.2 and are listed in Table 2.1. Also included in the table is a code number for each wafer which will be used to identify them. The experimental conditions under which these 5 films were grown could not be ascertained. The only information available was that the silicon films were grown on single crystal silicon wafers covered with a thermally grown gate oxide layer (the term gate oxide refers to the thin oxide layer, not more than 10 or 20 nm thick, grown on

Table 2.1 Polycrystalline silicon wafers used in etching studies.

Wafer Number	Source	Dopant Concentration	Film Thickness
BN1	Bell Northern	intrinsic	350 nm
BN2	Bell Northern	5×10^{18} atoms cm^{-3}	420 nm
BN3	Bell Northern	5×10^{19} atoms cm^{-3}	510 nm
AT1	AT&T Bell	intrinsic	650 nm
AT2	AT&T Bell	8×10^{19} atoms cm^{-3}	650 nm

silicon to produce the gate in metal-oxide-semiconductor (MOS) devices). All n-type samples were doped with phophorus.

2.2.2.1 Determination of Film Thicknesses

The film thicknesses were determined by laying down a striped photoresist mask on top of a thin (<50 nm) SiO_2 film thermally grown on top of the polycrystalline silicon film. The striped pattern was transferred to the oxide layer by wet etching with a 5% HF aqueous solution. The sample was then etched in the reactor with Br_2 to remove the silicon layer. The sample was then removed and the height of the steps were measured using a Tencor profilometer (discussed further in section 2.6).

2.2.2.2 Determination of Dopant Concentrations

The dopant concentrations were measured using the four point probe method. The measurement was made by bringing an array of four equally spaced tungsten carbide electrodes in contact with the surface to be measured. A current of a few milliamperes is passed through the two outermost electrodes and the resulting voltage drop across the inner two electrodes is measured. The calculated surface resistance is then multiplied by the film thickness to yield a value in units of ohm cm. Conversion tables for each type of dopant atom are available which then relates the film resistance to a dopant concentration.

2.2.3 Bromine

In the initial experiments, reagent grade Br_2 (Aldrich 99.5%) was employed. The purity of the Br_2 was further improved by refluxing it over KBr for one hour followed by distillation. This was then followed by a second hour of refluxing over P_2O_5 and finally the fraction that distilled over at 59 °C (boiling point of Br_2) was collected. The bromine was then placed in a 5 liter glass bulb complete with a cold finger. The bromine was degassed by immersing the finger into a $CO_{2(s)}$-ethanol bath which solidified the Br_2 (freezing point of -7.2 °C). The bulb was simultaneously pumped in an effort to remove all non-condensable gases. This process was

42

repeated for a total of three times. Partway through the etching studies, sealed ampules of 99.99+% pure Br_2 (Aldrich) were obtained and used in all subsequent experiments. The high purity Br_2 was loaded into the clean 5 liter glass bulb under nitrogen. Any trapped non-condensables (presumably only N_2) were removed using the process described above.

2.2.4 Chlorine

A cylinder of *high purity* Cl_2 (Matheson) was used in all Cl_2 etching experiments without any further purification. The purity of the chlorine was believed to be 99.99% and was considered suitable for etching studies. However it was not discovered until later that this was the lowest grade of Cl_2 sold by Matheson with a quoted purity of 99.5%. In hind sight the author would recommend a higher grade be used in view of the scatter in data observed when using Br_2 with the equivalent purity.

2.2.5 Nitrosyl Chloride

The NOCl used to titrate Cl and Br atoms was prepared in the laboratory by reacting Cl_2 with an excess amount of NO. An evacuated 12 liter glass vessel was filled with 300 Torr Cl_2. NO was introduced into the bulb to a total pressure of 800 Torr. The pressure in the bulb began to fall immediately as the reaction

$$2NO + Cl_2 \longrightarrow 2NOCl \tag{2.1}$$

proceeded. An additional 200 Torr of NO was added once the total pressure in the bulb fell below 600 Torr to ensure an excess of NO. The vessel was allowed to sit for several days. The excess NO was removed by pumping the gas mixture through a u-tube immersed in a slurry of ethyl bromide held at -119 °C by additions of liquid N_2. The excess NO, which is still gaseous at this temperature, is pumped away while the NOCl, which has a melting point of -65 °C, solidifies and remains in the trap.

2.3 Wafer Cleaning

As a precautionary measure all wafers were put through the following cleaning cycle, sometimes referred to as an RCA wash. Each wafer was placed first in a boiling solution of $NH_4OH:H_2O_2:H_2O$ (1:1:5) for 10 min, rinsed in distilled H_2O, and dipped in a 5% aqueous HF solution. The wafer was then placed in a boiling solution of $HCl:H_2O_2:H_2O$ (1:1:6) for another 10 minutes, rinsed in distilled H_2O and then dipped in the HF solution. The H_2O_2 oxidizes organic material that may be present on the surface, and the NH_3 is effective in removing heavy metals by forming strong complexes with them. The oxidizing nature of the two solutions leads to the formation of a thin oxide layer on the surface which is then removed along with contaminants during the HF dip.

The surface that remains after a HF dip has drawn considerable attention in recent years. In growing epitaxial silicon films on a silicon substrate, complete removal of SiO_2 from the surface prior to deposition is critical. Traditionally high temperature annealing (~1100 °C) has been used to remove surface contaminants such as O and C, but this is giving way to low temperature processes, many of which involve treatments with dilute HF[59,60,61]. The silicon surface after HF treatment has been studied using polarized internal reflection spectroscopy and it was found that the surface silicon atoms were terminated with hydrogen yielding mono-, di- and trihydride species[62]. A thermal desorption spectroscopy and x-ray photoelectron spectroscopy study have revealed appreciable amounts of hydrogen on the surface after an HF dip and that this hydrogen remains stable for at least two weeks in air, thereby passivating the surface against oxidation[63]. A theoretical study by Trucks et al.[64] suggested the reaction proceeds by sequential insertion of HF into Si-Si bonds, eventually resulting in the desorption of SiF_4 and a hydrogen terminated surface.

2.4 Cl_2 and Br_2 Etching

2.4.1 Temperatures and Pressures

The reaction temperatures and etchant pressures were chosen such that an accurately measured etch rate could be achieved. Using laser interferometry, etch rates between a few nm min^{-1} and 1000 nm min^{-1} were the most easily measured. Etch rates higher than 1000 nm min^{-1}

were avoided due to the possibility that the exothermicity of the reaction, (ΔH_f of -663 and -415 kJ mol^{-1} for the reaction of Cl_2 and Br_2 with silicon forming SiX_4), would lead to a runaway in the etch rate. Due to the relatively low Br_2 vapor pressure of approximately 180 Torr at room temperature, operating pressures greater than 50 Torr were not practical. Pressures of either Cl_2 or Br_2 less than 0.1 Torr required high temperatures in excess of 600 °C in order to produce measurable etch rates and hence this set the lower pressure limit. The temperatures were then chosen such that measurable etch rates could be obtained within this pressure range.

Another consideration in choosing a reaction temperature and reactant pressure was to ensure that the rate of reaction was not limited by the arrival rate of reactant on the surface. It is possible to verify this condition with the following calculation to a first order approximation. At a Br_2 pressure of 30 Torr and a temperature of 600 °C, an etch rate of 1000 nm min^{-1} is observed. Assuming Br_2 behaves as an ideal gas, the flux of molecules to the surface is given by[65]

$$z = \frac{P}{(2\pi mkT)^{1/2}}$$

(2.2)

where P is the gas pressure, m is the molecular weight of the gas, k is Boltzmann's constant and T is the temperature. Under the above conditions, this equation yields a Br_2 collision frequency on the surface of

$$z\,(Br_2) = 3 \times 10^{21} \text{ molec cm}^{-2} \text{ s}^{-1}.$$

(2.3)

This can be compared to the flux of Si atoms leaving a surface being etched at a rate of 1000 nm min^{-1},

$$\text{flux (Si)} = 8 \times 10^{16} \text{ atoms cm}^{-2} \text{ s}^{-1}.$$

(2.4)

From this calculation, roughly 10^4 Br_2 molecules collide with the surface for every Si leaving the surface. The large numbers of reactant molecules reaching the surface compared to those being

45

consumed ensure that the reactant molecules are not being diluted by product molecules leaving the surface.

2.4.2 Gas Flows

Gas flows of 12 to 15 sccm (where sccm stands for standard cubic cm per minute, i.e. cm^3 min^{-1} at STP) were chosen for both Cl_2 and Br_2 etching experiments. If the flows were too small, product desorbing from the surface might dilute the concentration of reactant over the surface. For example, at a gas flow of 12 sccm, a temperature of 600 °C and a pressure of 30 Torr, the number of reactant molecules passing through the reactor tube is approximately $5x10^{18}$ molec s^{-1}. Under these conditions, the maximum etch rate expected is 1000 nm min^{-1}. This corresponds to $5x10^{15}$ product molecules leaving the surface every second for an average sized sample of 0.06 cm^2. Even under these extreme conditions, product molecules dilute the reactant stream by only 0.1%.

2.4.3 Etching Procedure

Samples ranging in size from 0.04 to 0.09 cm^2 were cut from the various wafers. Prior to being etched, all samples were dipped in 5% HF solution, dried under a stream of N_2 and then mounted onto the holder while still under the same N_2 stream. The holder was then loaded into the etching reactor while the system was flushed with He. The positive pressure of He helped to prevent air or moisture from entering the system during the loading procedure. The system was pumped down to base pressure and the reactor tube brought to the desired temperature with the heating tape. Once the temperature stabilized, the gas was introduced at a flow of 12 to 15 sccm and the pump throttled to produce the desired pressure. After a little practice, a stable pressure and flow could be obtained in a matter of seconds. Etch rates for the polycrystalline samples were then measured by laser interferometry. In the etching of intrinsic samples, a timer was used to measure the total exposure time which was later combined with the measured etch depth to determine the etch rate. These two techniques for measuring etch rates are discussed further in section 2.6. Once etching was complete, the system was evacuated, cooled and brought to atmospheric pressure with He. The total time required to etch one sample was approximately 30-60 minutes.

2.5 Cl and Br Etching

2.5.1 Temperatures and Pressures

The Cl_2 and Br_2 pressures were chosen such that the maximum partial pressure of atoms could be produced from the microwave discharge. This favoured pressures less than a one or two Torr. Because high gas flows were also required (see section 2.4.2.), the lower pressure limit was determined by the pumping speed of the system. This set the lower pressure limit at approximately 0.5 Torr. The temperature was then adjusted to yield measurable etch rates.

2.5.2 Gas Flows

For Cl and Br atom etching, a high gas flow was required in order to transport the atoms from the discharge to the sample. A long transit time would result in a drop in Cl or Br concentration through atom recombination. A Br_2 flow of 80 sccm was used in all Br atom etching experiments. The relatively low vapor pressure of Br_2 at room temperature, as well as system restrictions, prevented the use of higher flows. At this Br_2 flow, the time required for atoms produced in the discharge to reach the sample was 33 milliseconds. A Cl_2 flow of 160 sccm was used in all Cl atom etching experiments and resulted in a transit time of 17 milliseconds for atoms to reach the sample.

2.5.3 Production of Br and Cl atoms

Microwave discharges have long been used to generate Br and Cl atoms[66]. The molecular halogen to be dissociated can be passed directly through the discharge or diluted in a stream of inert gas such as argon or helium. The advantage of dilution is that a higher degree of dissociation and a higher gas flow can be obtained. The main disadvantage is finding a suitable method for pumping the gas mixture. Once diluted, the halogens can not be efficiently trapped in a liquid nitrogen trap and are then allowed to enter the rotary pump. Needless to say, prolonged exposure of Cl_2 or Br_2 to the pump will eventually lead to its deterioration. In the present study, only the pure halogen gas was passed through the discharge. A 2.45 GHz microwave generator (EMI Model 2000) supplied

47

between 75 and 200 watts of power to a quarter wave cavity. The cavity and the immediate area of the discharge tube were air cooled to prevent overheating.

It has been shown that in the presence of clean quartz walls, essentially no atoms are able to emerge from the discharge region[66]. Coating the walls with an oxy-acid such H_3PO_4, H_2SO_4 or H_3BO_3 has been found to effectively poison the walls of the discharge tube and significantly reduce the rate of wall recombination. In the present study H_3PO_4 was employed for this purpose and applied in the following manner. After cleaning the discharge tube with hot KOH and rinsing thoroughly with distilled H_2O, a small amount of concentrated H_3PO_4 was applied to the discharge region. The acid was dehydrated by heating the tube externally with a hot flame while passing N_2 through the tube. The removal of H_2O was important as its presence in the etching reactor could encourage the formation of an oxide layer on the silicon samples effectively stopping the etching reaction. After the heating process, a thin film of P_2O_5 remained on the surface.

All Pyrex surfaces between the discharge region and the point of etching including the sample holder itself were poisoned by the following procedure. After rinsing the surfaces with hot KOH and then rinsing thoroughly with distilled H_2O, the apparatus was filled with 10% aqueous H_3PO_4 and allowed to stand for 1 hour. After draining this solution, the surfaces were rinsed sparingly with distilled H_2O and then dried.

It was relatively easy to determine whether or not atoms were reaching the downstream sample. The gas phase recombination of Cl and Br atoms is accompanied by a red luminescence emission. By darkening the room and shielding emission originating from the discharge region, the presence of atoms could be easily verified by the appearance of the luminescence afterglow. The observation of a relatively constant glow down the main reactor tube indicated only minimal decay in the atom concentration over that distance. Because the luminescence intensity is proportional to the square of the atom concentration, this rather routine inspection can be sensitive to small changes in atom concentrations.

2.5.4 Monitoring and Determining Cl and Br Atom Concentration

Cl and Br atoms can recombine in the gas phase according to the following reaction

$$X + X + X_2 \xrightarrow{k_r} X_2 + X_2^*$$

(2.5)

where X is either Br or Cl, X_2 is the respective diatomic and k_r is the recombination rate constant. A second Cl_2 or Br_2 molecule is required as a third body in the reaction. The X_2^* molecule produced as a result of the reaction is in an excited triplet state which can then relax to the ground state by emission of a photon. The chemiluminescence is a broadband emission extending from 600 to 1150 nm in the case of the Cl_2 emitter and a similar emission band for the Br_2 emitter although shifted slightly to longer wavelengths. This termolecular reaction is relatively slow at pressures of 1 Torr and does not significantly reduce atom concentrations in the tens of milliseconds it takes the atoms formed in the discharge to reach the sample.

The chemiluminescence of the recombination reaction provided a convenient method of monitoring the atom concentration in the flow reactor. Fixing a photodetector along the main reactor tube 8 cm upstream from the sample holder, and monitoring its output voltage, the microwave power could be adjusted to ensure the same atom concentration was used for each etching experiment. The absolute concentration was determined by titration with NOCl [65,67]. Once the desired atom concentration was achieved, NOCl was introduced until the luminescence intensity monitored by a second photodetector located 8 cm downstream from the sample holder was totally extinguished. The sample holder itself was not in place during the titration experiment. The reaction of NOCl with Cl or Br,

$$NOCl + X \xrightarrow{} NO + ClX$$

(2.6)

occurs rapidly and to completion[68]. The flow of NOCl was decreased in increments and the intensity produced from the atom recombination recorded. A titration curve was constructed by plotting $(intensity)^{1/2}$ (remembering that the atom concentration is proportional to the square root of the intensity) versus NOCl flow (Figure 2.4). An extrapolation of the $(intensity)^{1/2}$ data to the y-axis yields the NOCl flow required to reach the end point in the titration. This flow of NOCl at the
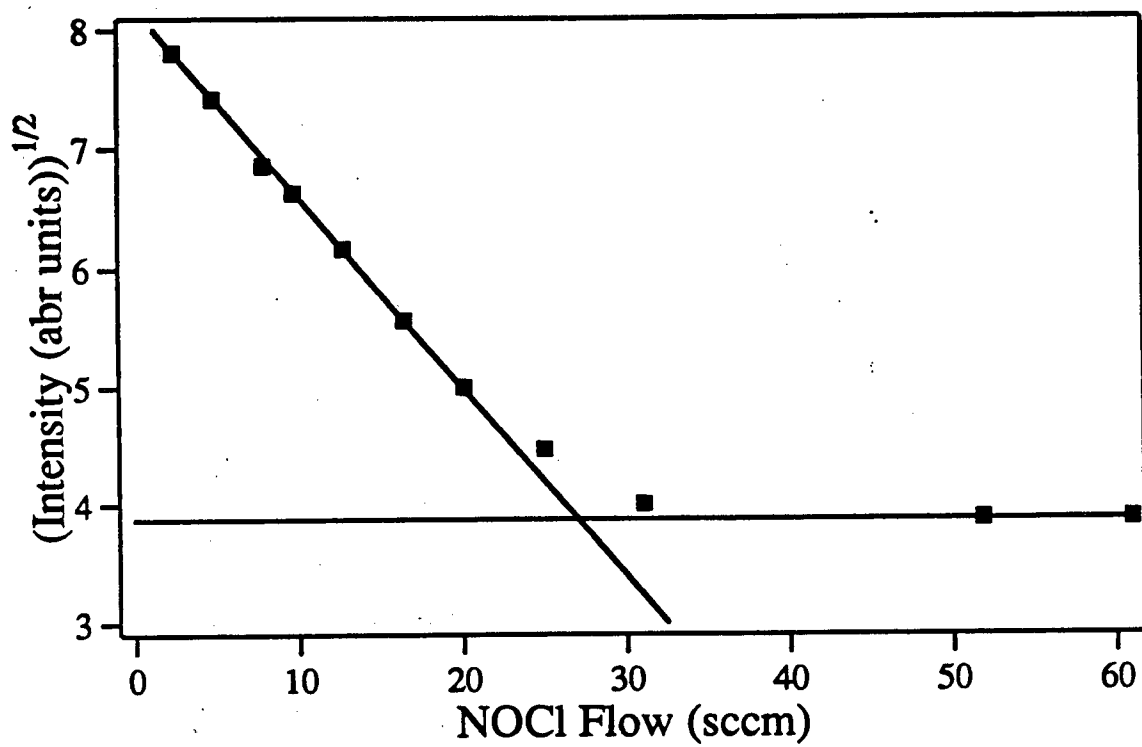
Figure 2.4 NOCl titration curve.

end point is equal to the flow of atoms. The partial pressure of atoms can then be determined from the equation

$$P_X(\pm15\%) = \frac{F_X(\pm10\%)}{F_T(\pm10\%)} P_T(\pm5\%)$$

(2.6)

where P_X is the partial pressure of atoms, P_T is the total pressure (atoms and molecules), F_X is the flow of atoms (from the titration experiment) and F_T is the total flow. The relevant uncertainties in these parameters are indicated in parenthesizes.

2.5.5 Etching Procedure

The procedure followed in the atom etching experiments was essentially the same one used in molecule etching experiments discussed in section 2.4.3. Once the sample was loaded and the temperature stabilized, a flow of either Cl_2 or Br_2 was established and the pump throttled to yield the desired pressure. At the lower temperatures employed for atom etching, the molecules did not produce a measurable etch rate (< 0.5 nm min^{-1}). Hence any etching observed could be attributed to atoms only. The microwave discharge was then initiated and the generator power adjusted to produce the desired atom concentration. The etching was terminated by extinguishing the plasma.

2.6 Etch Rate Measurements

Two techniques were used in measuring etch rates, profilometry and interferometry. Profilometry is a mechanical technique that was employed to measure the etch rates of the silicon (100) samples. A SiO_2 mask was first grown on the surface by thermal oxidation and then patterned to yield alternating stripes of oxide and silicon (100) surface. After etching the samples with halogen atoms or molecules, the mask was removed by a HF wash leaving step features on the surface where etching occurred. The fine stylus of a profilometer is then traversed across the surface and the step heights are measured, producing a trace of the surface as shown in Figure 2.5. The depth of the etch is then divided by the total etching time to give an etch rate. The major source of error is the determination of etch depth which is often made difficult by the uneven etched

51

12/20 02:05
ID #
VERT.   5kA
 L -1.160kA
 R -2.280kA
    -1.120kA
Avg-1.025kA
TIR 2.530kA
Ra 1.065kA
HORIZ 2000um
 L   160.0um
 R 1840.um
    1680.um
Area 167.77
SCAN MENU 1
 um   s/um

2000 .2 1
 400   1 5
  80   5 25
SCAN t= 8sec
      DIR —>
STYLUS 18mg
  60 1600um LEVEL

TENCOR INSTRUMENTS
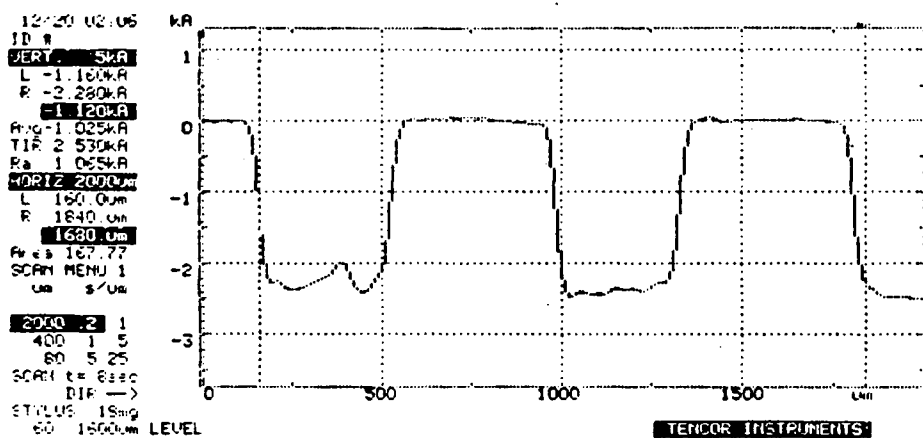
Figure 2.5 Profilometry trace of a silicon (100) sample, masked with SiO_2 and etched with Br_2.

surface. Typical variations in etch depths are estimated at ±10%, resulting in a similar uncertainty in the measured etch rates. The etch rates were found to be constant, i.e. within experimental error, over time.

The second technique was laser interferometry and was used to measure the etch rates of all polycrystalline silicon samples. The laser beam of a 0.5 mW HeNe laser was reflected off the surface of the sample being etched (Figure 2.6). Part of the laser beam (beam B) is reflected off the top silicon surface, while part (beam A) passes through the polycrystalline film with a thickness d and is reflected off the underlying gate oxide layer. Because the beam diameter of 0.5 mm is so much larger than the thickness of the films being etched (<1 μm), the overlap of the two reflected beams is almost 100 %. The reflected beams are directed to a photodetector, in this study a photomultiplier tube, and the output voltage monitored on a chart recorder. As the film is etched, the additional distance travelled by beam A relative to beam B decreases and the two reflected beams go in and out of phase with each other resulting in a sinusoidal wave pattern. A maximum in the reflected intensity will occur each time the decrease in distance travelled corresponds to the wavelength of the laser beam (632.8 nm), i.e.

$$\lambda = 2n\Delta a \quad . \tag{2.7}$$

Since the extra distance travelled by beam A is through silicon and not air, the index of refraction, n, must also be included. If the beam is approximately perpendicular to the surface, i.e. $\theta \approx 0°$, then $d \approx a$ and the etch rate, in nm min^{-1}, can be given by

$$\text{Etch Rate} = \frac{\lambda}{2nt} \tag{2.8}$$

where t is the time measured between two adjacent maxima. A typical interferogram resulting from the etching of a polycrystalline film is shown in Figure 2.7. The index of refraction of silicon is wavelength dependent[69] and has a value of 3.85 at 632.8 nm. The index of refraction exhibits a slight temperature dependence[70] ranging from a value of 3.85 at room temperature to 4.15 at
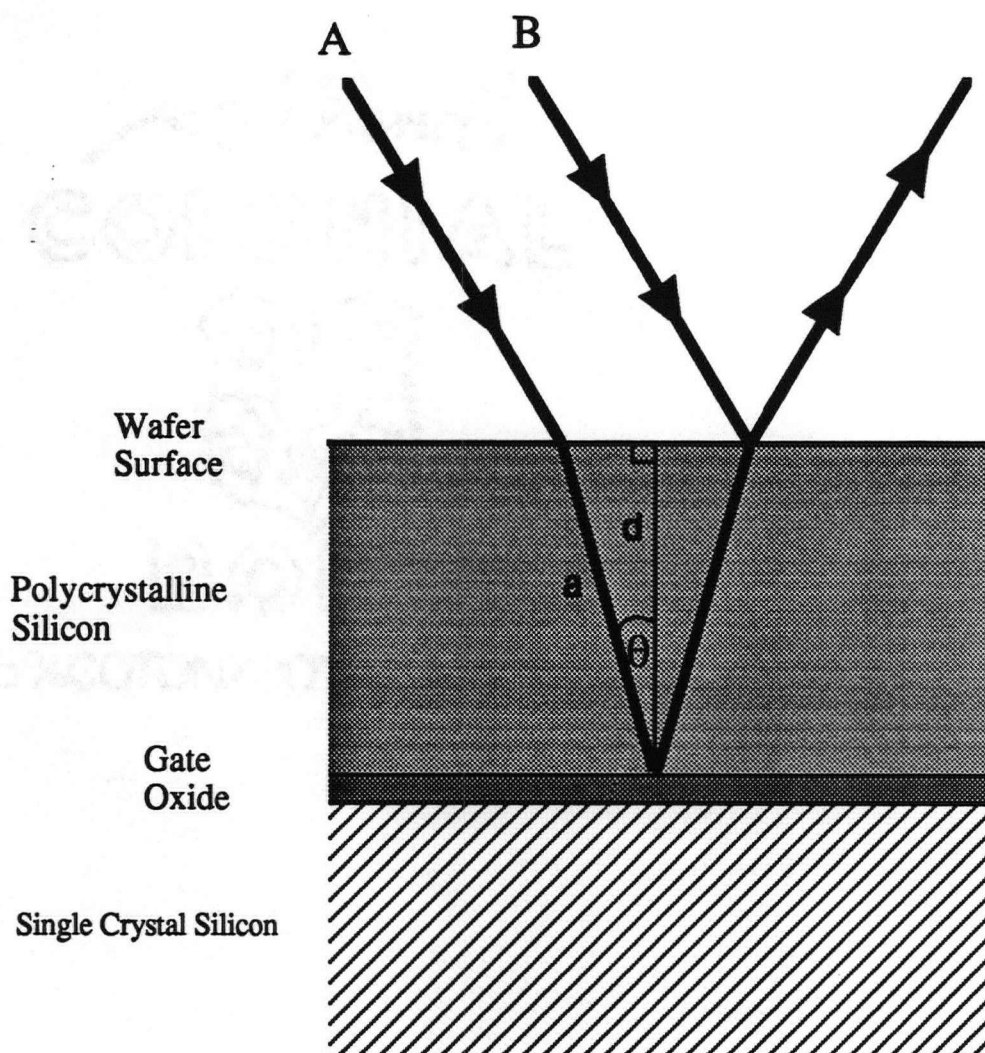
Figure 2.6 Laser interferometry determination of polycrystalline silicon etch rates.
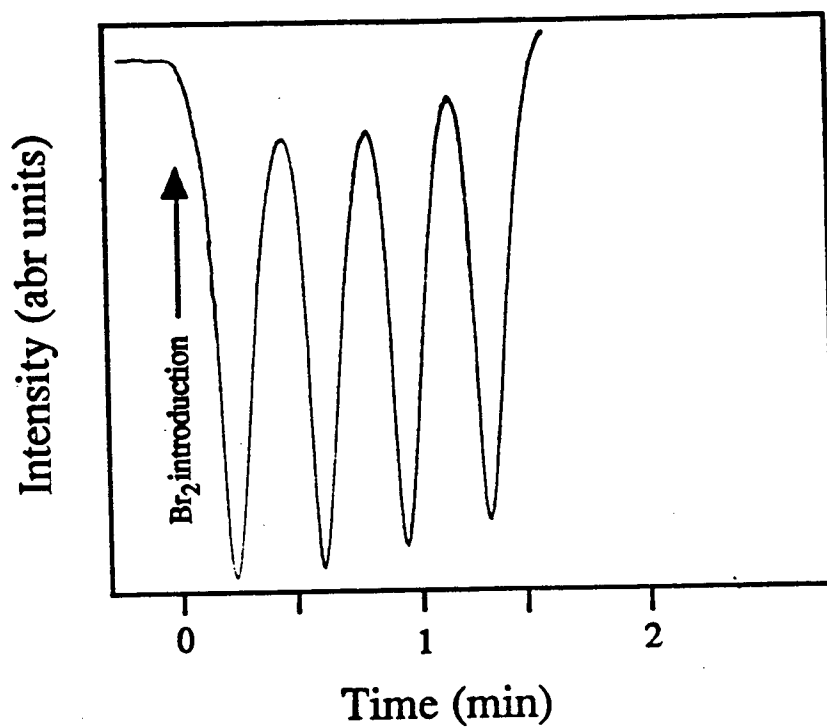
Figure 2.7 Interferogram resulting from the etching of intrinsic polycrystalline silicon (BN1 wafer) by Br_2.

600 °C. The appropriate values of refractive index were determined and used in equation (2.8) to calculate etch rates. This *in situ* method of measuring etch rates is accurate to within ± 5%. The only significant source of uncertainty being that associated with the determination of the time, t, obtained from the distance between adjacent maxima in the interferogram.

2.7 Curve Fitting and Plotting

All plotting of data and subsequent curve fitting was performed on a Apple Macintosh personal computer using the software package Igor version 1.1 by WaveMetrics.

Chapter 3. Results

3.1 Overview

The original mandate of this study was an examination of bromine etching of silicon and this emphasis is reflected by the large collection of experimental data presented in this thesis. Included in this data set are etch rates measured for a number of single crystal and polycrystalline wafers, some of which were doped with n-type dopants. The results obtained from this study, especially the pressure dependence of the Br_2 reaction with silicon, were somewhat surprising in light of previous studies on Br_2 and Cl_2 etching of silicon[47,41] and strongly suggested etching experiments using Cl_2 should be performed and the results compared. To this end a modest number of Cl and Cl_2 etching experiments were performed on intrinsic and n-type polycrystalline silicon films (BN1 and BN2 wafers respectively) and are included in this chapter.

Finally there will be a brief discussion of experiments that were attempted, but had to be abandoned. The inability to produce results from these experiments, although discouraging, had a limited effect on the overall study. In some cases the information sought after, such as the determination of reaction products, has since appeared in the literature. Including a brief discussion of these experiments may serve to point the direction of future experiments.

3.2 Br_2 Etching Results

The following experimental results were collected over a three year period during which the etching apparatus and procedure underwent many changes. These changes were made in an effort to achieve a higher degree of reproducibility in the etch rate data leading to more accurately determined quantities such as rate constants and activation energies. In an effort to demonstrate why and how these changes were made, the experimental results will be presented in chronological order.

3.2.1 Intrinsic and n-type Polycrystalline Silicon (AT1 and AT2 Wafers)

The etching of intrinsic polycrystalline silicon (AT1 wafer) was studied by measuring the etch rate as a function of Br_2 pressure and temperature. Establishing the pressure dependence of

the reaction allows for the determination of the reaction order with respect to the etchant Br_2 and the temperature dependence allows for the determination of an activation energy. The etch rates were measured at temperatures of 500, 510 and 520 °C. An all Pyrex reaction tube was used in these early studies and temperatures above 530 °C were not employed as to avoid possible collapse of the reaction tube. This resulted in a rather narrow experimental temperature range yielding maximum etch rates of approximately 200 nm min^{-1}. Br_2 pressures in these studies were varied from 0.25 to 30 Torr. The etch rates measured in these experiments are plotted versus Br_2 pressure (Figure 3.1). Examination of this data indicates a non-linear increase in etch rates with increasing pressure. The etch rates tend towards a saturation limit at high pressures, although this saturation is not realized within the pressure range studied. Assuming the reaction rate is proportional to the Br_2 pressure, then an expression for the etch rate can be written as

$$\text{Etch Rate} = k(P_{Br_2})^n \quad , \tag{3.1}$$

where k is a rate constant and n is the order of the reaction with respect to Br_2 pressure. A plot of ln (etch rate) versus ln (Br_2 pressure) should be linear with a slope equal to n, the order of the reaction with respect to Br_2. The experimental data when presented in this manner does yield linear plots with slopes equal to approximately 0.5 (Figure 3.2), suggesting a half order dependence on Br_2 pressure. This is further verified by the linear plots of etch rate versus (Br_2 pressure)$^{1/2}$ (Figure 3.3). An empirical rate equation can be written as

$$\text{Etch Rate} = C_1(Br_2 \text{ Pressure})^{1/2} - C_2 \quad . \tag{3.2}$$

The above equation is written with a negative sign preceding C_2 in anticipation of a negative intercept from plots of etch rate versus (Br_2 pressure)$^{1/2}$ using the more accurate etch rate data. A weighted linear least squares fit of the data yields values for the slopes (C_1) and intercepts (C_2) of the three resulting straight lines which are given in Table 3.1. Also included are the errors associated with each, determined from a weighted least squares linear fit of the data. A weighting
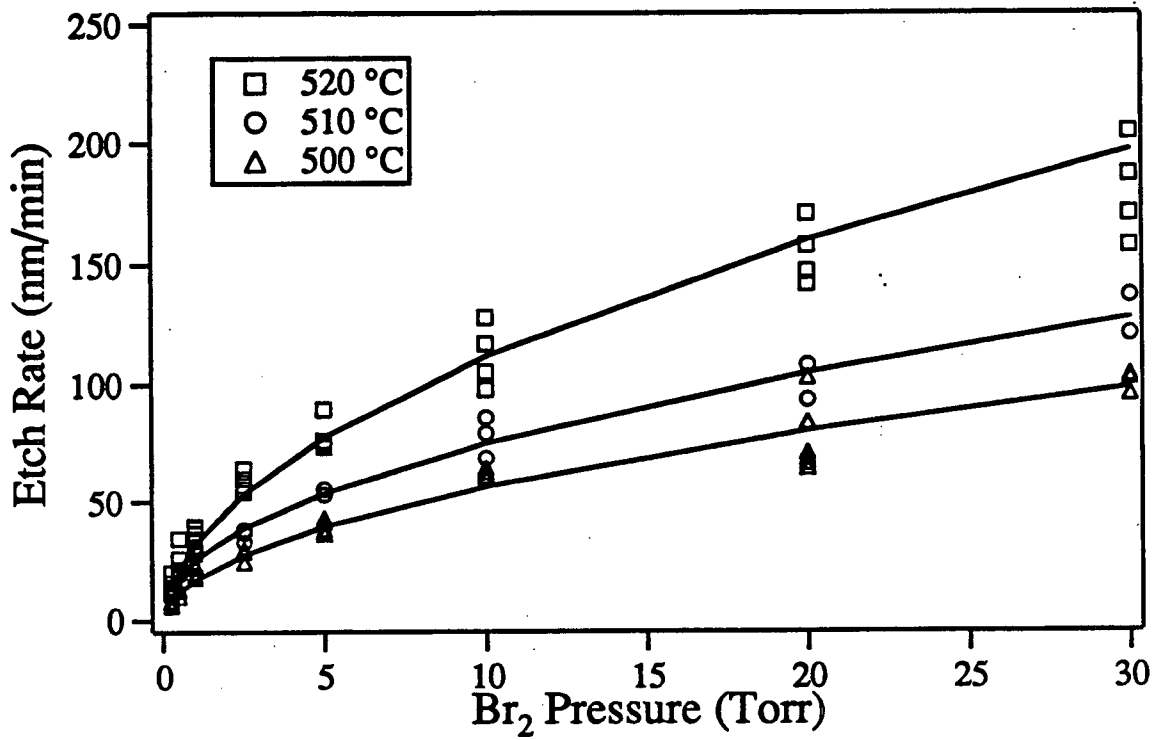
Figure 3.1 Etch rates of intrinsic polycrystalline silicon (AT1 Wafer) versus Br_2 pressure (original data).
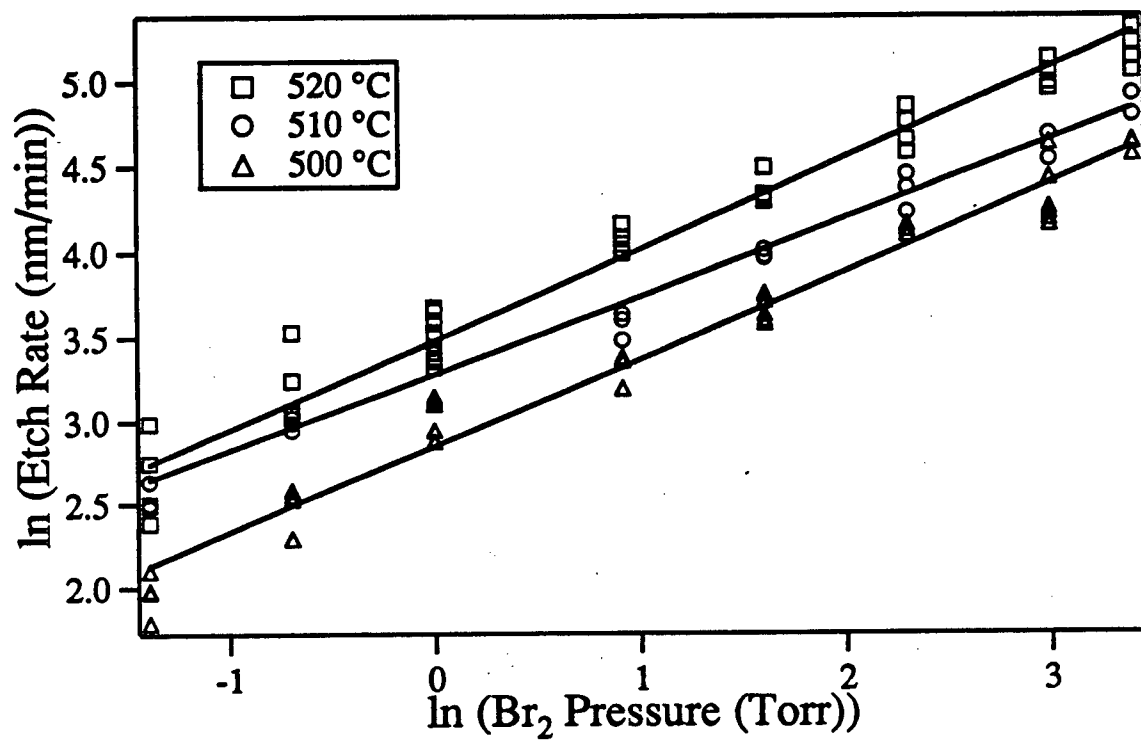
Figure 3.2 ln (etch rate) versus ln (Br$_2$ pressure) for etching of intrinsic polycrystalline silicon (AT1 Wafer) (original data).

Figure 3.3 Etch rates of intrinsic polycrystalline silicon (AT1 wafer) versus $(Br_2$ pressure$)^{1/2}$ (original data).

Table 3.1 Slopes and intercepts from weighted linear least squares fit of etch rate versus (Br_2 pressure)$^{1/2}$ plots presented in Figure 3.3 for the etching of n-type polycrystalline silicon (AT1 wafer, original data).

Wafer	Temperature (°C)	Slope (C_1) nm min^{-1} Torr^{-1}	Intercept (C_2) nm min^{-1}
AT1 (Intrinsic)	500	18.3 ± 0.7	1.5 ± 0.7
	510	22.9 ± 1.1	-2.5 ± 1.1
	520	40.0 ± 1.3	5.2 ± 1.1

factor corresponding to the reciprocal of 15% of the etch rate was assigned to each etch rate. A value of ±15% was obtained from the relative spread in etch rates measured from different samples at the same pressure and temperature. This value is larger than the ±5% uncertainty inherent in the laser interferometry technique used to measure the etch rates. However, it does seems reasonable as it brings the majority of data points onto the line produced from the weighted linear least squares fit. In general the error inherent in the etch rate measurement technique, be it either interferometry or profilometry, was less than the observed scatter. The error in the pressure readings is $< \pm$ 1-3% and can be considered negligible compared to the uncertainty in the etch rates. Hence the weighted linear least squares fit performed on the data assumed error only in the etch rate values.

It was obvious from the results presented in these figures that the experimental data contained a significant degree of scatter. The initial response to this scatter was to collect more data points. This eventually lead to data sets containing 30 to 50 etch rates measured at one temperature and various Br_2 pressures. Although this approach would eventually lead to a statistical average of the data, it did not directly address the origin of the scatter, nor did it eliminate it. There were a number of suspected sources responsible for the scatter including poor thermal contact between the sample and the holder, presence of water in the system, formation of a partial surface oxide layer prior to etching, etc. To determine whether or not any of these possible sources were responsible for the observed scatter, the contribution from each source was drastically increased to see if the scatter changed correspondingly. To this end the following experiments were performed.

In order to examine the importance of good thermal contact with the holder, samples were mounted with a small piece of wafer wedged under one end so that direct contact with the holder was made only along one edge of the sample. The etch rates measured with this sample mounting were found to be no different from those previously observed.

The next possible source of scatter to be considered was the formation of a partial oxide layer on the surface of the silicon sample after the HF dip and prior to being loaded into the reactor. Silicon samples were left open to the atmosphere after the HF dip for up to 15 minutes before being loaded into the reactor. This was considerably longer than the 10 to 15 seconds normally

taken to mount and load samples. Once again no significant difference in the etch rates was observed.

Attention was next directed to the possible presence of H_2O in the system, which might be inhibiting the etching process by encouraging the formation of an oxide layer. A 100 ml bulb complete with a teflon stopcock, was evacuated, partially filled with H_2O and connected to the system. A sample was loaded into the reactor, the system then evacuated, and the temperature raised to 510 °C. Br_2 was introduced at a pressure of 10 Torr and the etching monitored *in situ* with laser interferometry. The stopcock on the H_2O bulb was then opened and the total pressure was allowed to rise to 15 Torr. The etch rate was observed to stop immediately (Figure 3.4a). The experiment was performed again, but this time the amount of H_2O introduced into the system was reduced by partially opening the stopcock for a one second burst. This resulted in a momentary increase in pressure of 0.5 Torr. The etch rate continued unaffected (Figure 3.4b). A minute later, a second similar burst of H_2O vapor was introduced. Initially the etch rate remained unchanged, but within two minutes the interferogram became irregular (Figure 3.4b). It was clear from this experiment that the presence of a fairly large concentration of water was capable of inhibiting the etching reaction completely and that smaller amounts might have an unpredictable effect.

The presence of hydrocarbons on the surface could also affect the etch rate. This possibility was investigated by smearing a HF cleaned sample with pump oil, wiping off the excess with a Kimwipe and then loading it into the reactor. The etch rate measured from the sample was comparable to others previously determined under the same pressure and temperature conditions, suggesting the presence of hydrocarbons on the silicon surface was having little influence on the etch rate.

After failure of the above experiments to clearly identify the source of the scatter, a number of modifications were made to the system resulting in the design presented in Figure 2.1. These included the replacement of metal parts (fittings, tubing, valves, etc.) of the system with ones constructed from inert materials such as Pyrex and teflon. Metal parts that could not be replaced were made from stainless steel or monel. Finally a new sample holder was constructed as
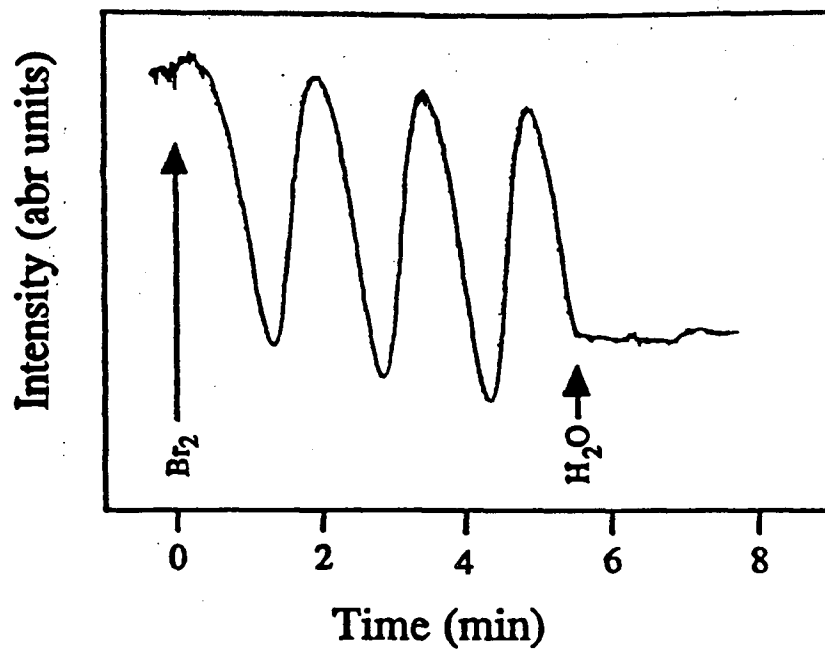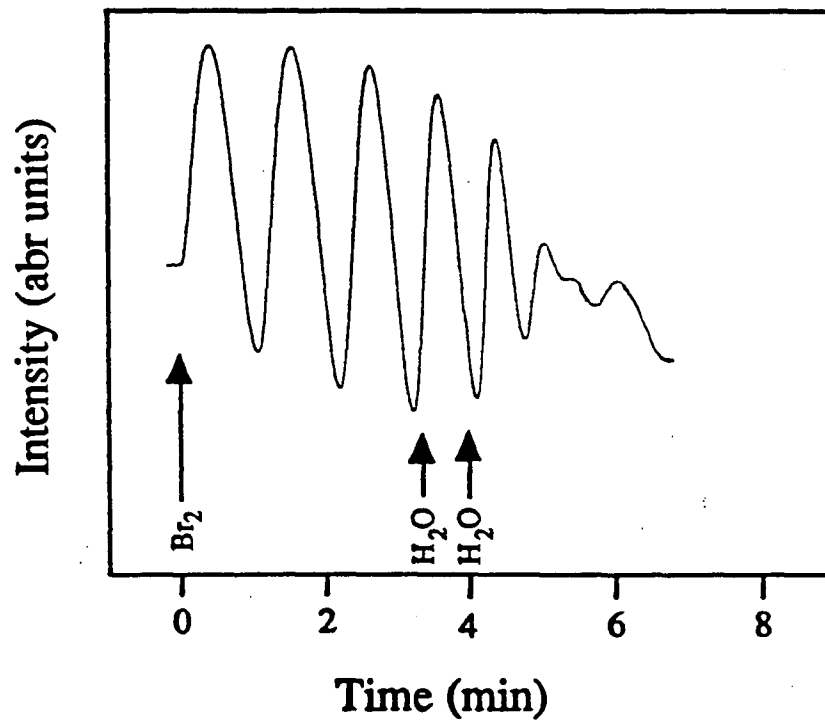
Figure 3.4 Interferogram resulting from the etching of intrinsic polycrystalline silicon (AT1 wafer) by Br_2. H_2O was introduced to observe its effect on the etch rate.

discussed in section 2.1.3. These efforts were modestly rewarded by a reduction of scatter in the etch rates to approximately ±10%.

The pressure and temperature dependence of the etching of intrinsic polycrystalline silicon (AT1 wafer) was repeated, with the above modifications in place. Etch rates were measured at temperatures of 476, 500 and 520 °C, i.e. a somewhat wider temperature range, and at pressures between 0.25 and 30 Torr. The etch rates increase non-linearly with pressure (Figure 3.5) with slopes from a linear least squares fit of a ln (etch rate) versus ln (Br_2 pressure) plot indicating a reaction order of 0.5. Again this is confirmed in the linear variation of etch rate with (Br_2 pressure)$^{1/2}$ (Figure 3.6). The coefficients C_1 and C_2 obtained from a weighted linear least squares fit of the data in Figure 3.6 are given in Table 3.2.

The Br_2 etching of n-type polycrystalline silicon (AT2 wafer) was studied in a similar manner to that described above, namely by measuring the etch rate at Br_2 pressures ranging from 0.25 to 30 Torr and at the three temperatures of 350, 375 and 400 °C. The n-type silicon reacted more readily with Br_2 than did the intrinsic silicon and permitted the use of lower temperatures in obtaining measurable etch rates. The etch rates once again display a non-linear increase with pressure (Figure 3.7). A linear least squares fit of the data in the plot of ln (etch rate) versus ln (Br_2 pressure) yields slopes of approximately 0.5. The half order dependence is again confirmed in a plot of etch rate versus (Br_2 Pressure)$^{1/2}$ (Figure 3.8). Coefficients C_1 and C_2 obtained from the weighted least squares fit of the data are given in Table 3.3.

The interferograms recorded during the etching of the AT2 wafer (Figure 3.9) were markedly different from those obtained in the etching of the intrinsic wafer. As soon as etching begins, the intensity of the reflected laser beam drops drastically and does not recover until all the polycrystalline silicon film is etched. Etch rates were obtained from these interferograms only once the peak to peak heights of the oscillations became constant. The drop in reflectivity during etching is likely due to a roughening of the surface. Factors that contribute to a roughing of the surface may include large grain sizes in the polycrystalline film or a nonuniform concentration of dopant atoms in the grain boundaries. Etching is faster in the grain boundary region where there is a higher concentration of unsaturated bonds and crystal defects. If the silicon is doped, then the

66
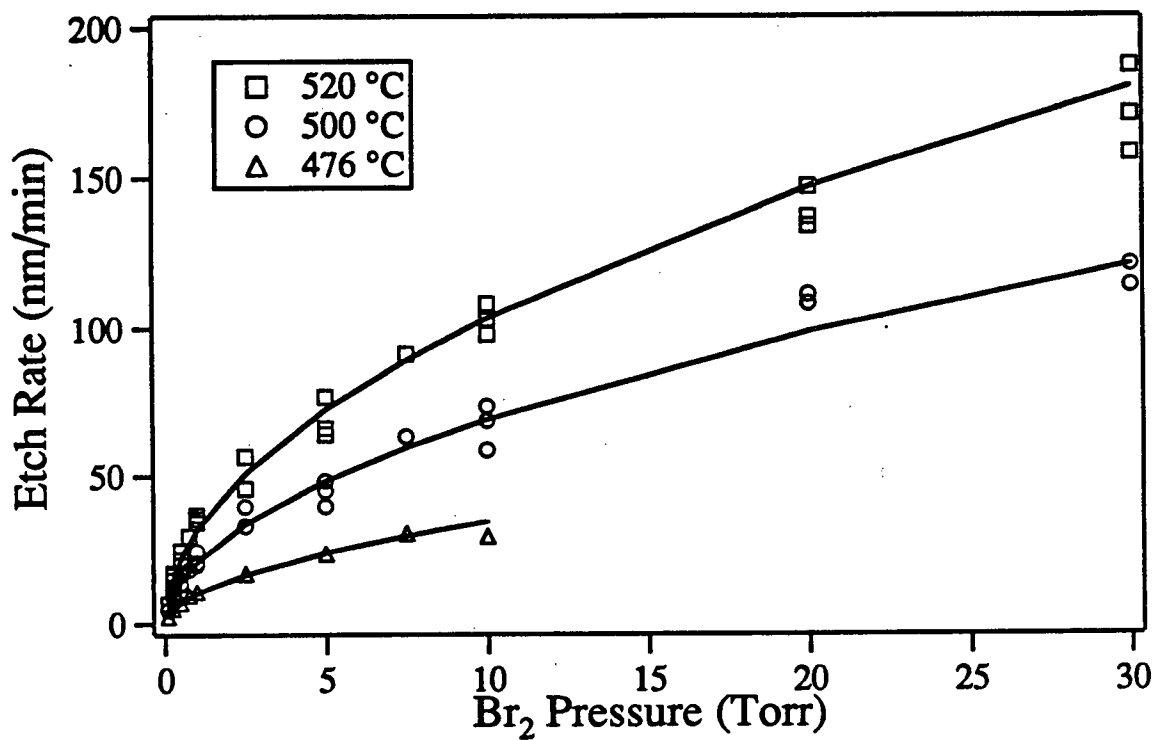
Figure 3.5 Etch rates of intrinsic polycrystalline silicon (AT1 wafer) versus Br_2 pressure.
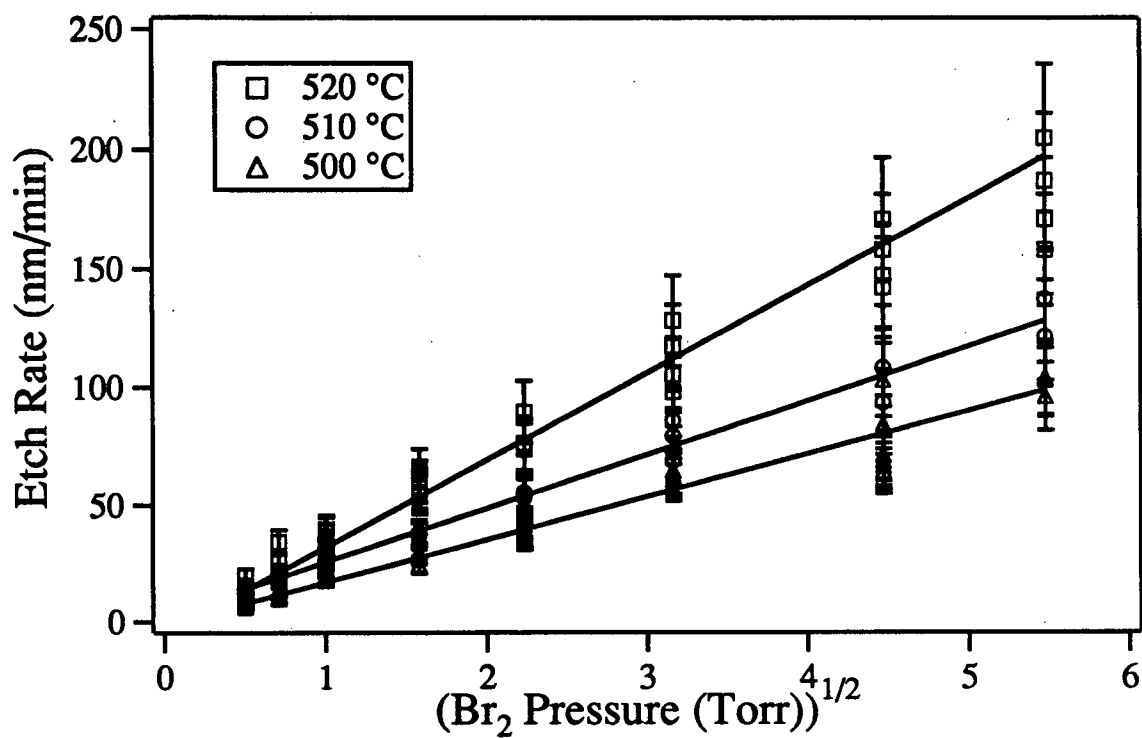
Figure 3.6 Etch rates of intrinsic polycrystalline silicon (AT1wafer) versus $(Br_2 \text{ pressure})^{1/2}$.

Table 3.2 Slopes and intercepts from weighted linear least squares fit of etch rate versus (Br_2 pressure)$^{1/2}$ plots presented in Figure 3.6 for the etching of intrinsic polycrystalline silicon (AT1 wafer).

Wafer	Temperature (°C)	Slope (C_1) nm min^{-1} Torr^{-1}	Intercept (C_2) nm min^{-1}
AT1 (Intrinsic)	476	11.1 ± 0.5	0.9 ± 0.3
	500	22.4 ± 0.6	1.9 ± 0.5
	520	33.2 ± 0.9	1.7 ± 0.7
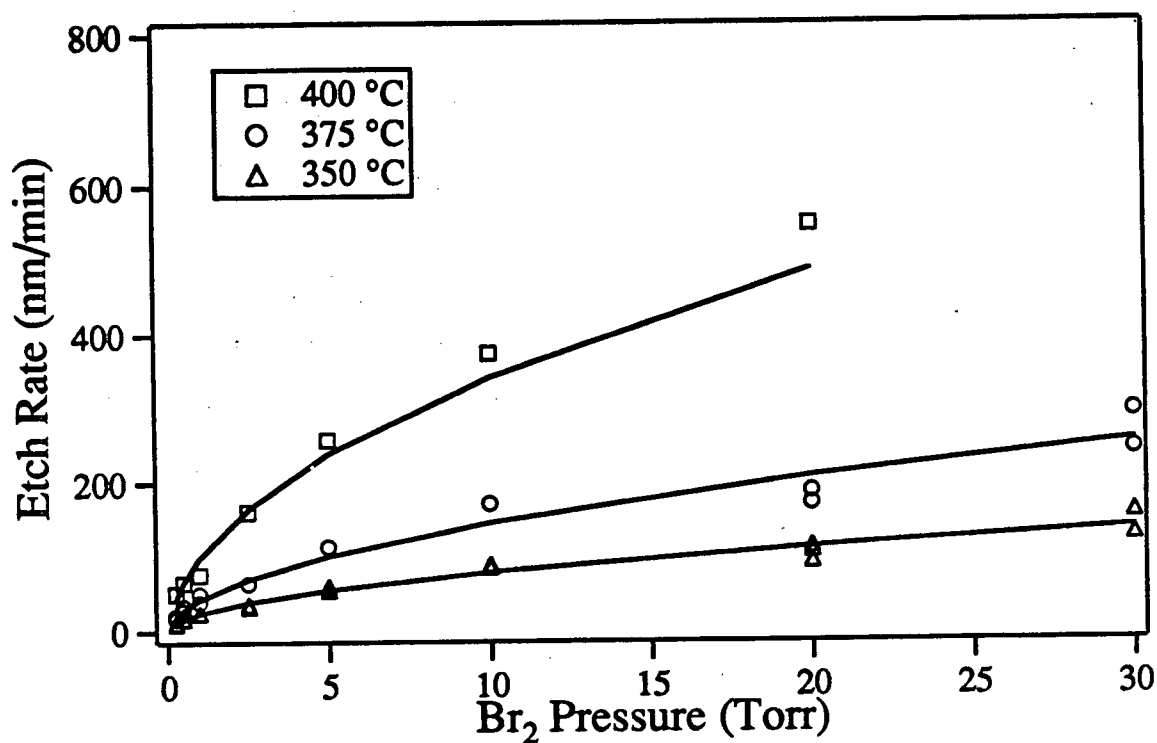
Figure 3.7 Etch rates of n-type polycrystalline silicon (AT2 wafer) versus Br_2 pressure.

Figure 3.8 Etch rates of n-type polycrystalline silicon (AT2 wafer) versus $(Br_2$ pressure$)^{1/2}$.

Table 3.3 Slopes and intercepts from weighted linear least squares fit of etch rate versus (Br_2 pressure)$^{1/2}$ plots presented in Figure 3.8 for etching of n-type polycrystalline silicon (AT2 wafer).

Wafer	Temperature (°C)	Slope (C_1)	Intercept (C_2)
		nm min^{-1} Torr^{-1}	nm min^{-1}
AT2 (n-type)	350	25.4 ± 0.9	1.5 ± 0.9
	375	47.4 ± 1.8	4.6 ± 1.7
	400	112 ± 7	12.5 ± 6.7
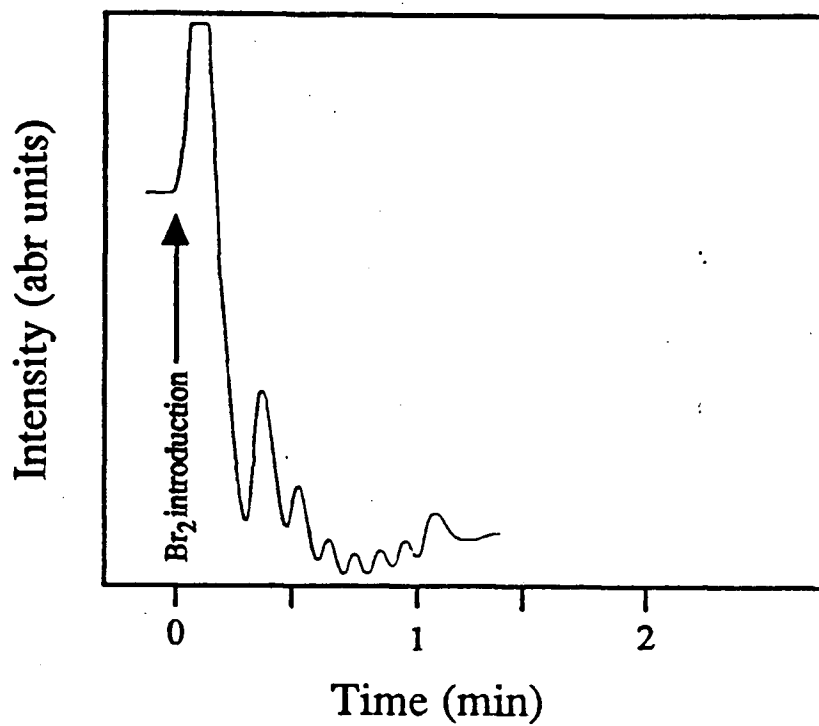
Figure 3.9 Interferogram resulting from the etching of an n-type polycrystalline silicon (AT2 wafer) by Br_2.

accumulation of dopant atoms in these regions would also lead to a fast etch rate. If etching of these regions resulted in surface features with dimensions comparable to the laser wavelength used in the interferometry, then a decrease in reflected laser intensity would be observed.

3.2.2 Silicon (100)

With the quartz reaction tube integrated into the system, higher temperatures were available to study the Br_2 etching of single crystal silicon (100), which from preliminary experiments was observed to etch more slowly than its polycrystalline counterpart. The etch rates were measured exclusively by profilometry and thus first required the deposition of a SiO_2 mask. The oxide was thermally grown in a ceramic oven at 1000 °C over a period of 15 minutes and then patterned with a striped mask with 0.5 mm spacings. The results obtained from these samples were very unusual. The surface after etching was inhomogeneous, containing deeply etched pits and crevices scattered over an otherwise normal looking etched surface. These pits and crevices were filled with a light grey powder which could be easily brushed away. The etch rates in these affected areas were in some cases as high as 30 μ min^{-1}, two orders of magnitude larger than those on the remaining unaffected surface. An investigation of the surface by scanning electron microscopy revealed a large degree of crystallographic etching. An energy dispersive x-ray analysis indicated that only silicon was present on the surface after etching. The origin of this enhancement in etch rate was eventually traced to the ceramic oven (borrowed from another research group) which had been used to grow the oxide. An investigation into the oven's history revealed that it had been used to sinter samples containing arsenic and phosphorus and had obviously become contaminated with these elements. The arsenic and phosphorus were subsequently being annealed into the silicon wafer as the oxide was grown, resulting in high levels of dopants in selected areas. The etching was significantly faster in these affected areas resulting in the deep pits and crevices.

Thermal oxidation of silicon samples was subsequently carried out in an oven consisting of a resistively heated 1.5 inch diameter quartz tube. The problems encountered with the ceramic oven appeared to be eliminated, but it did draw attention to the possibility of contamination through processing, especially at high temperatures, in less than ideal conditions. A request was made to

74

have a striped silicon nitride mask laid down on a silicon (100) wafer in the Department of Electrical Engineering, but the request failed to be filled in time to be used in these studies. While awaiting the arrival of this wafer, a limited number of etching experiments were performed on silicon (100) after which the emphasis of the study was shifted to polycrystalline silicon samples.

The etch rates of the silicon (100) samples were measured at six temperatures ranging from 520 to 580 °C and at Br_2 pressures ranging from 0.25 to 30 Torr. As in the etching of polycrystalline silicon, the etch rates of silicon (100) when plotted versus Br_2 pressure increase non-linearly with increasing pressure (Figure 3.10). Presenting the data as ln (etch rate) versus ln (Br_2 pressure) yields linear plots with slopes of approximately 0.5. As with the previous polycrystalline work, the etch rates follow the empirical rate law given in equation (3.2) and vary linearly with the square root of the Br_2 pressure (Figure 3.11). The coefficients C_1 and C_2 obtained from the weighted linear least squares fit are given in Table 3.4.

3.2.3 Intrinsic and n-type Polycrystalline Silicon (Wafers BN1, BN2 and BN3)

At this point in time, high purity Br_2 (99.99%) was obtained and employed throughout the remaining Br_2 etching studies. Etching was continued on a set of three wafers, one intrinsic (BN1) and two n-type wafers (BN2 and BN3), obtained from Bell Northern Research. Switching to this second set of wafers was done for a number of reasons. Etching of the first n-type sample (AT2 wafer) was accompanied by a dramatic decrease in reflectivity, as shown in the interferogram in Figure 3.9, raising concerns regarding the quality of the polycrystalline film. Comparing these results with ones measured using other n-type polycrystalline silicon wafers would indicate if the loss of reflectivity was a property of all n-type films or unique to this wafer only. Measuring the etch rates of a second intrinsic polycrystalline wafer obtained from a second source would give some indication whether or not the results obtained from one polycrystalline film could be applied to other films obtained from different sources. The AT1 and AT2 wafers were both received with a photoresist mask on the surface and there was some concern this mask was not being completely removed by the cleaning procedure, leading to scatter in the etch rate data. Finally, in order to
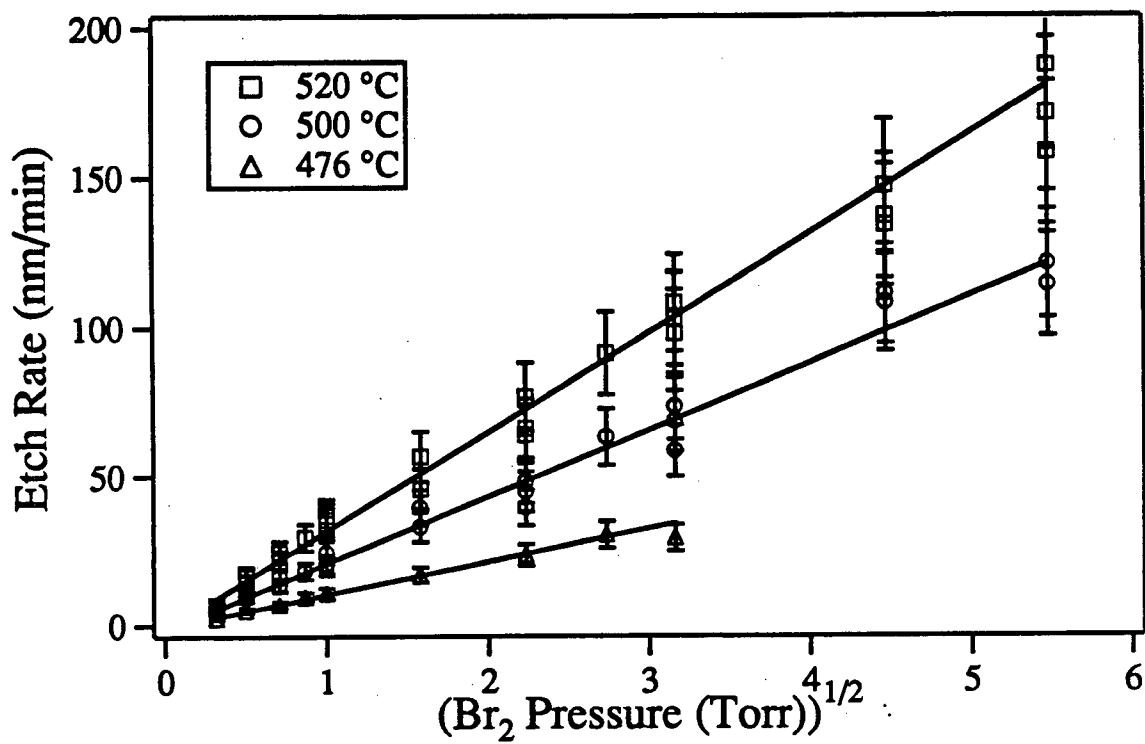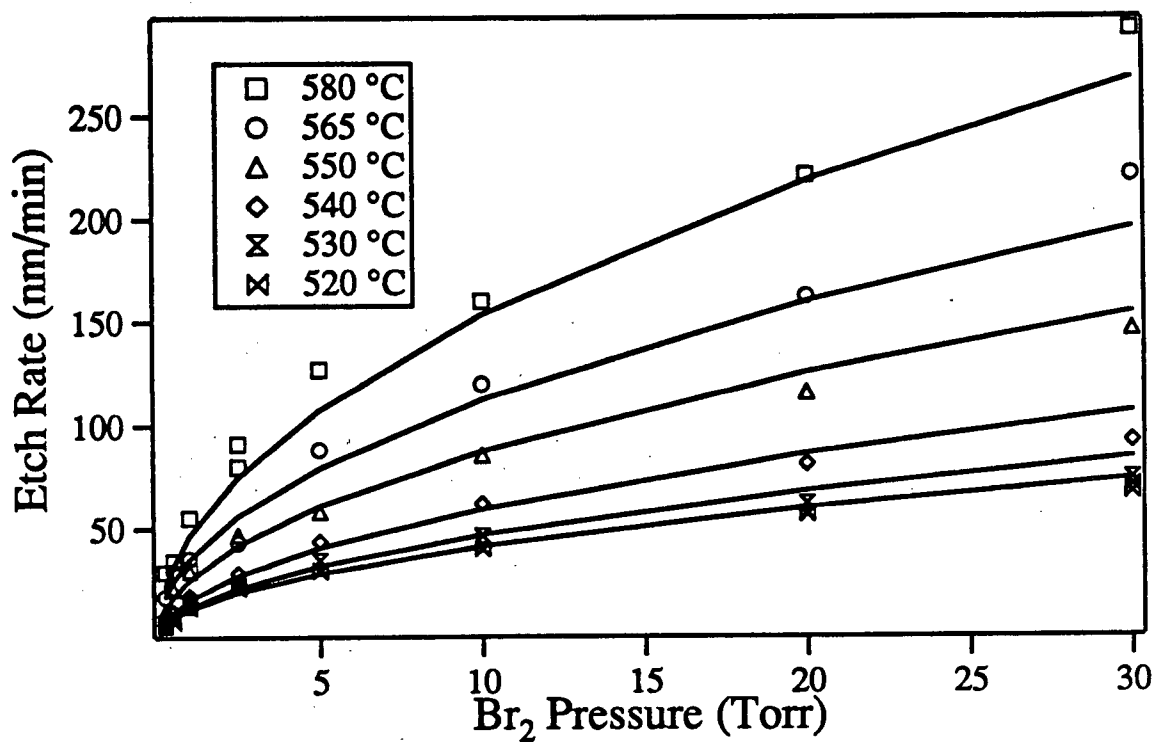
Figure 3.10 Etch rates of intrinsic silicon (100) versus Br_2 pressure.
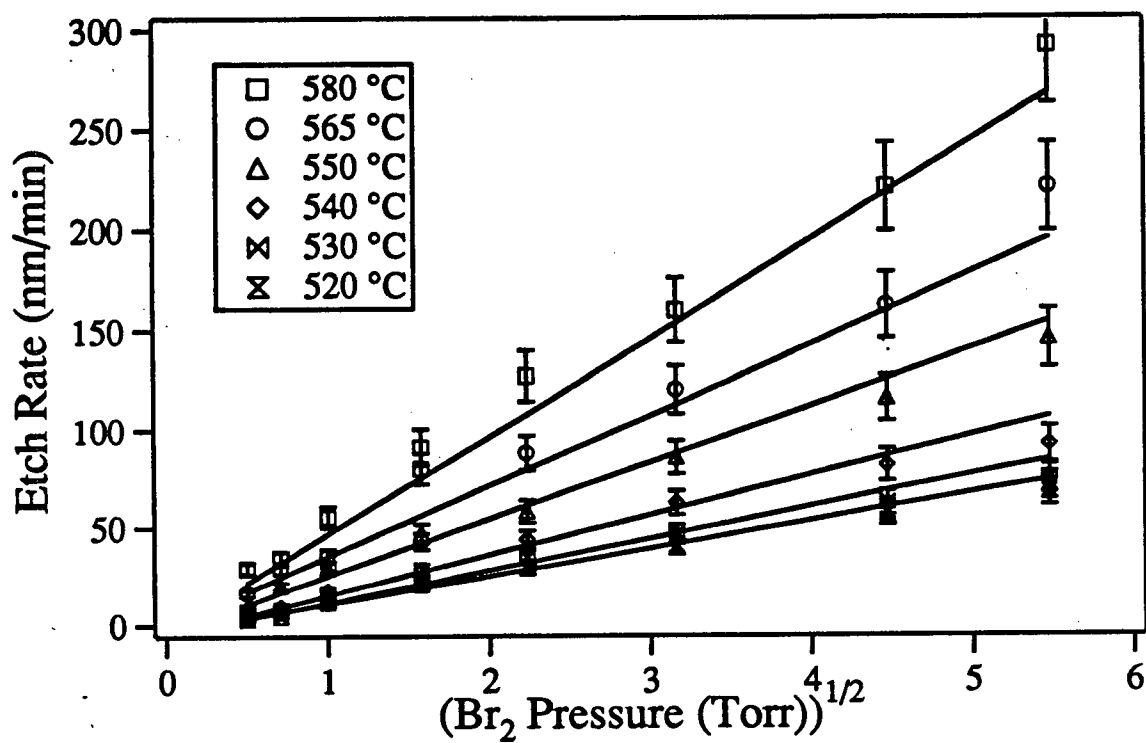
Figure 3.11 Etch rates of intrinsic silicon (100) versus $(Br_2 \text{ pressure})^{1/2}$.

Table 3.4 Slopes and intercepts from weighted linear least squares fit of etch rate versus $(Br_2$ pressure)$^{1/2}$ plots presented in Figure 3.11 for etching of silicon (100).

Wafer	Temperature (°C)	Slope (C_1) nm min^{-1} Torr^{-1}	Intercept (C_2) nm min^{-1}
Silicon (100)	520	14.2 ± 0.5	3.7 ± 0.4
	530	16.3 ± 0.7	5.0 ± 0.5
	540	20.5 ± 0.9	5.5 ± 0.6
	550	28.4 ± 1.3	9.0 ± 0.9
	565	35.9 ± 2.1	1 ± 2
	580	49.6 ± 2.9	3 ± 3

investigate the effect of n-type dopants on the etch rate, it was desirable to etch wafers with various levels of doping. Although the range in dopant concentration among these three wafers (AT2, BN2 and BN3) was not ideal, it did provide a limited range.

The etch rates measured using the high purity Br_2 and the new set of wafers were very reproducible and scatter in the data was reduced to ±5%, close to the uncertainty inherent in the determination of etch rates by interferometry. It is difficult to say whether or not the improvement was due solely to the high purity Br_2. Reproducibility in most experiments tends to improve with time as the system and procedure are continuously improved. It is felt, however, that the higher purity Br_2 was at least partially responsible for reducing scatter in the data.

The etch rates of intrinsic polycrystalline silicon (wafer BN1) were measured at Br_2 pressures ranging from 0.1 to 30 Torr and temperatures of 540, 570 and 600 °C. The quartz tube reactor permitted the use of higher temperatures than those possible in the initial study of intrinsic polycrystalline silicon (AT1 wafer). This resulted in etch rates ranging from a few nm min^{-1} up to 800 nm min^{-1}. The increase in etch rate with increasing pressure (Figure 3.12) is consistent with that observed with previous wafers. Linear least squares fit of ln (etch rate) versus ln (Br_2 pressure) data yielded slopes of approximately 0.5. The half order dependence is confirmed in the plot of etch rate versus (Br_2 pressure)$^{1/2}$ (Figure 3.13). The slopes (C_1) and the intercepts (C_2) obtained from a linear least squares regression of this data is given in Table 3.4. The intercepts are all negative and increase in magnitude with increasing temperature. This is in contrast to the previous plots where intercepts, although often negative, did not display a consistent temperature dependence and appeared to be simply random fluctuations brought about by the larger errors in the etch rate data.

Etch rates for n-type polycrystalline silicon (BN2 and BN3 wafers) were measured at Br_2 pressures ranging from 0.1 to 30 Torr and at temperatures of 360, 385 and 410 °C. Both wafers display a similar etch rate dependence on Br_2 pressure (Figures 3.14 and 3.15 for BN2 and BN3 respectively). The order of the reaction with respect to Br_2 pressure is calculated from the slopes of ln (etch rate) versus ln (Br_2 pressure) plots and was found to be consistently equal to 0.5 for both
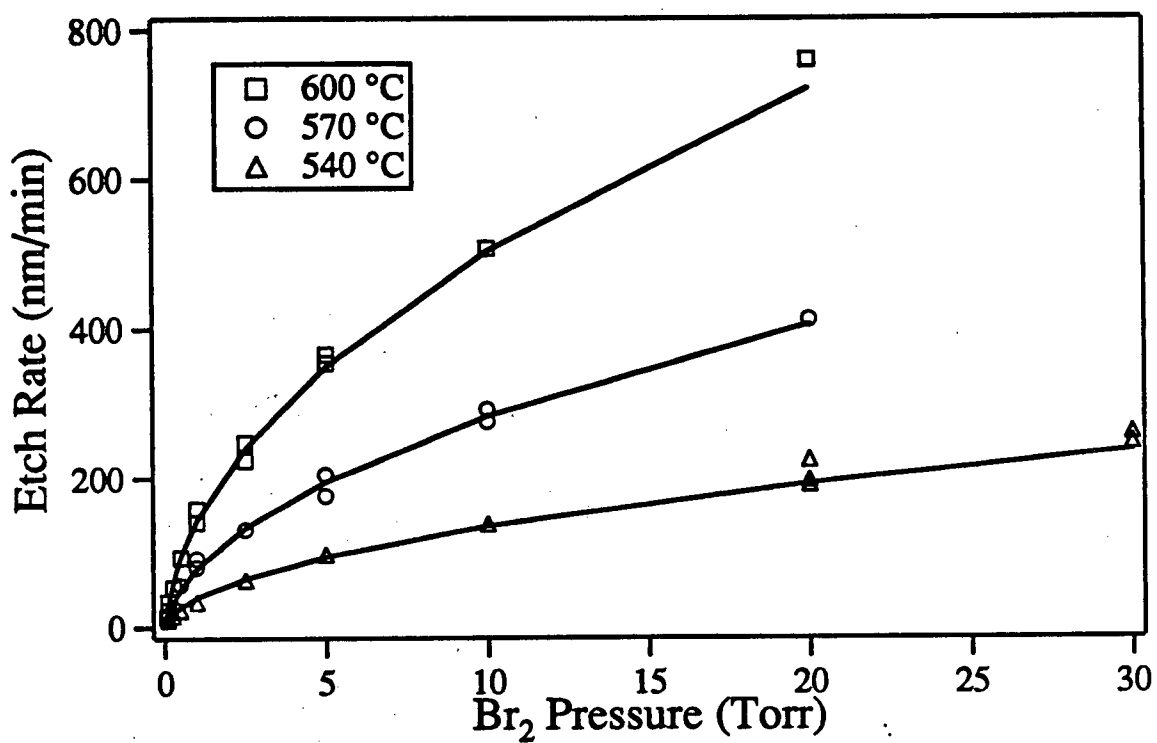
Figure 3.12 Etch rates of intrinsic polycrystalline silicon (BN1 wafer) versus Br_2 pressure.
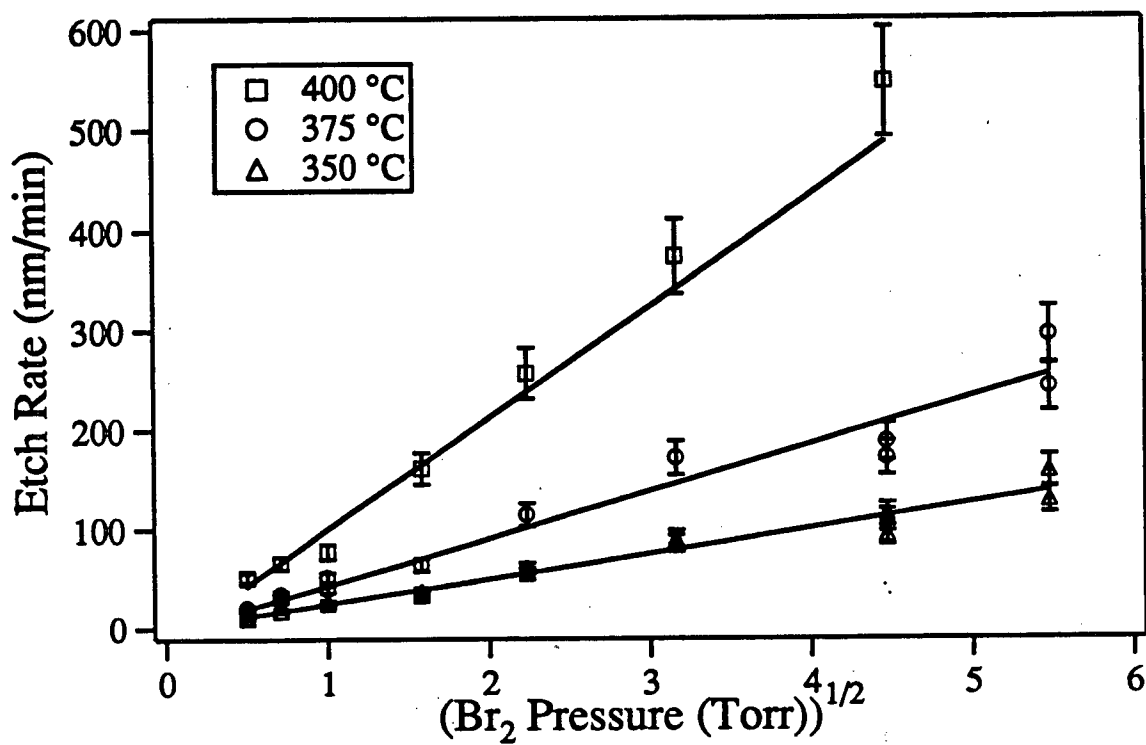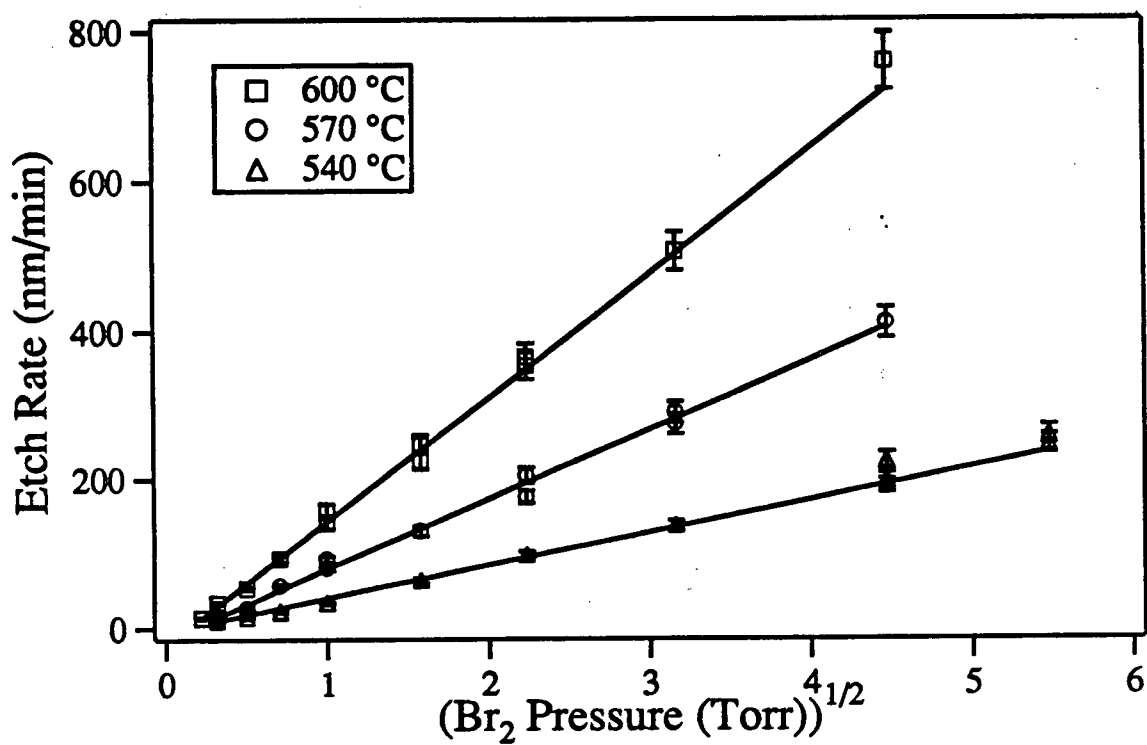
Figure 3.13 Etch rates of intrinsic polycrystalline silicon (BN1 wafer) versus $(Br_2$ pressure$)^{1/2}$.

Table 3.5 Slopes and intercepts from weighted linear least squares fit of etch rate versus (Br_2 pressure)$^{1/2}$ plots presented in Figure 3.13 for etching of intrinsic polycrystalline silicon (BN1 wafer).

Wafer	Temperature (°C)	Slope (C_1) $nm\ min^{-1}\ Torr^{-1}$	Intercept (C_2) $nm\ min^{-1}$
BN1 (intrinsic)	540	44.0 ± 0.7	5.0 ± 0.4
	570	94.2 ± 1.8	16.3 ± 1.0
	600	167 ± 3	25.0 ± 1.0
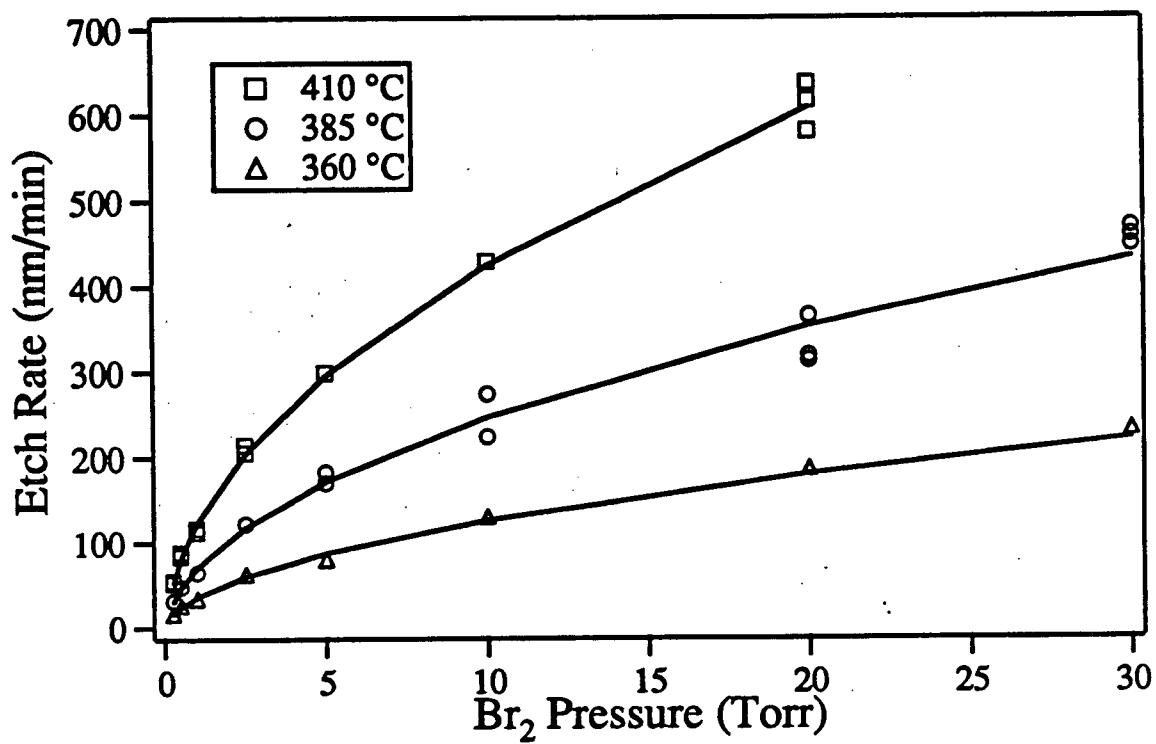
Figure 3.14 Etch rates of n-type polycrystalline silicon (BN2 wafer) versus Br_2 pressure.
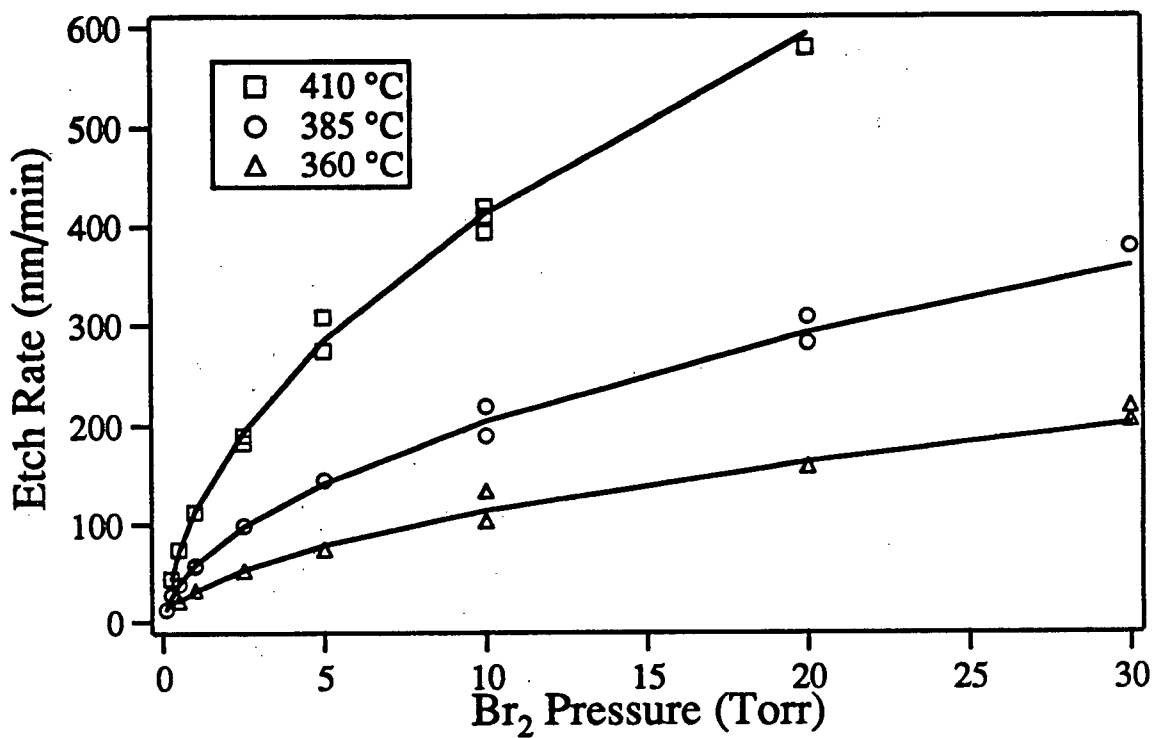
Figure 3.15 Etch rates of n-type polycrystalline silicon (BN3 wafer) versus Br_2 pressure.

wafers. The weighted linear least squares fit of the data in plots of (etch rate) versus (Br$_2$ pressure)$^{1/2}$ (Figures 3.16 and 3.17) yields slopes and intercepts which are given in Table 3.6. The intercepts are all negative and increase in magnitude with increasing temperature, consistent with the results obtained from etching intrinsic polycrystalline silicon (BN1 wafer).

It is worth noting that the interferogram obtained from the etching of the BN3 wafer (Figure 3.18) is similar in appearance to the one obtained for the AT2 wafer. The intensity drops off significantly as the etching begins and as a result etch rates were only determined from the last two or three oscillations where the changes in intensity are more consistent. This is again indicative of a roughening of the surface brought about by either large grain sizes in the polycrystalline film or high concentration of dopant atoms in the grain boundary regions.

3.2.4 Etch Rates of Polycrystalline Silicon at 1.0 Torr Br$_2$

Etch rates presented above for polycrystalline silicon wafers were measured at only three temperatures. Ideally one would prefer to make these measurements at several more temperatures in order to have a more accurate determination of the temperature dependence of the etching process. This was unfortunately not practical to do because of the time required to collect the additional data. In an effort to obtain the temperature dependence over a larger range of temperatures, a compromise was made by measuring etch rates for all five wafers at 1 Torr Br$_2$ and at various temperatures. An Arrhenius temperature dependence is assumed for these etch rates, i.e.

$$\text{Etch Rate} = A \exp^{-(E_a/RT)} \tag{3.3}$$

where A is a temperature independent preexponential factor, R is the gas constant and E_a is the activation enthalpy for the etching process. These etch rates are plotted as ln (etch rate) versus 1/T (Figure 3.19). The etch rates for the AT1 and AT2 wafers were measured using the lower purity Br$_2$ and prior to optimization of the etching reactor. This is reflected in the scatter in the these data sets. The activation enthalpies and preexponentials from a weighted linear least squares fit of the data, including their respective error, are given in Table 3.7.
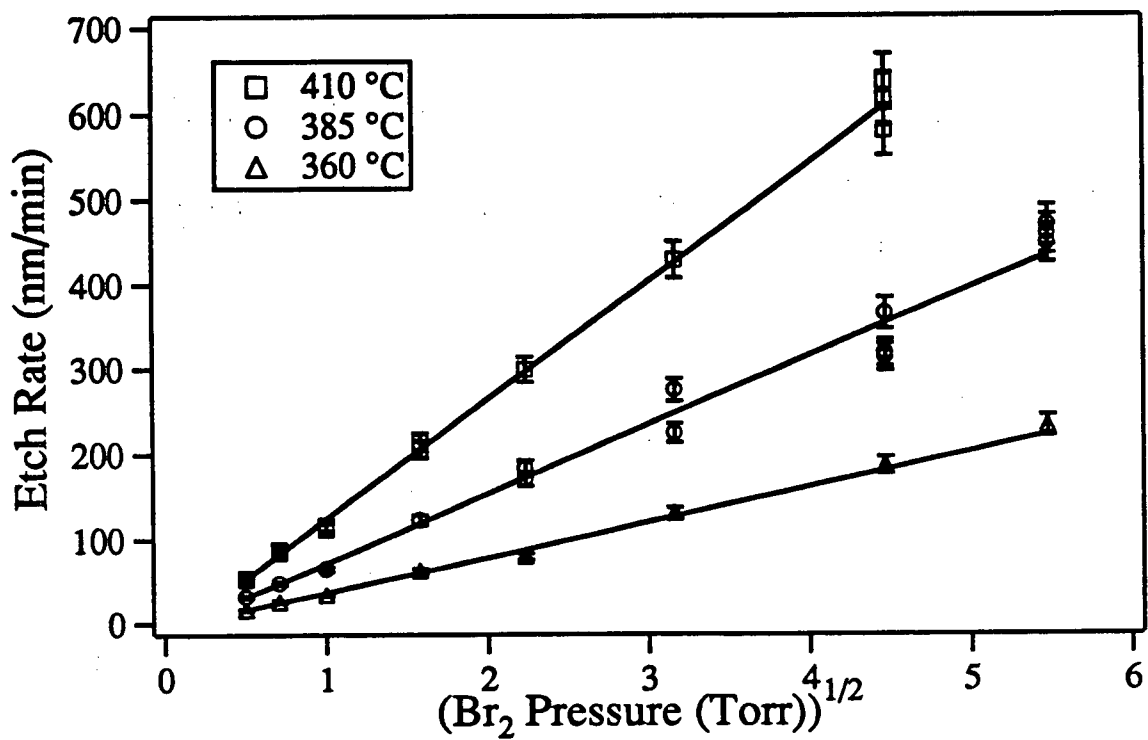
Figure 3.16 Etch rates of n-type polycrystalline silicon (BN2 wafer) versus $(Br_2 \text{ pressure})^{1/2}$.
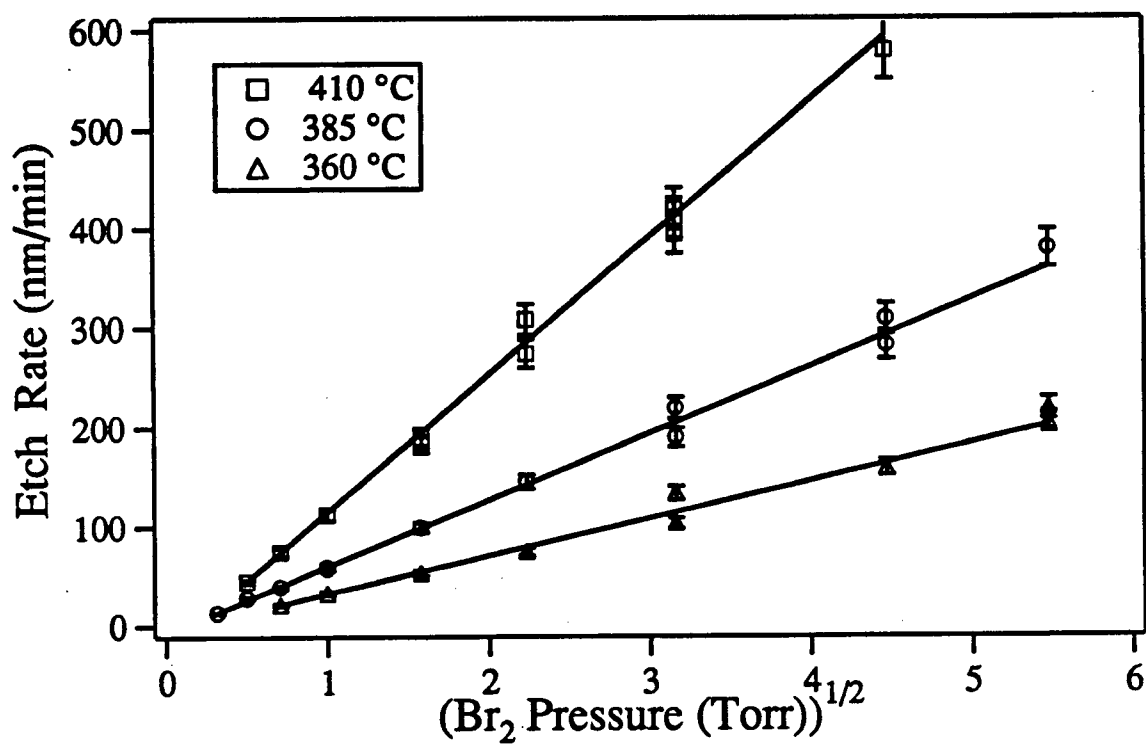
Figure 3.17 Etch rates of n-type polycrystalline silicon (BN3 wafer) versus $(Br_2 \text{ pressure})^{1/2}$.

Table 3.6 Slopes and intercepts from weighted linear least squares fit of etch rate versus $(Br_2$ pressure$)^{1/2}$ plots presented in Figures 3.16 and 3.17 for etching of n-type polycrystalline silicon (BN2 and BN3 wafers).

Wafer	Temperature (°C)	Slope (C_1) nm min^{-1} Torr^{-1}	Intercept (C_2) nm min^{-1}
BN2 (n-type)	360	41.3 ± 1.1	4.5 ± 1.0
	385	81.0 ± 1.4	9.6 ± 1.7
	410	139 ± 3	16.1 ± 3.0
BN3 (n-type)	360	38.0 ± 1.0	5.9 ± 1.3
	385	67.3 ± 1.2	8.3 ± 0.8
	565	138 ± 2.7	24.3 ± 2.6
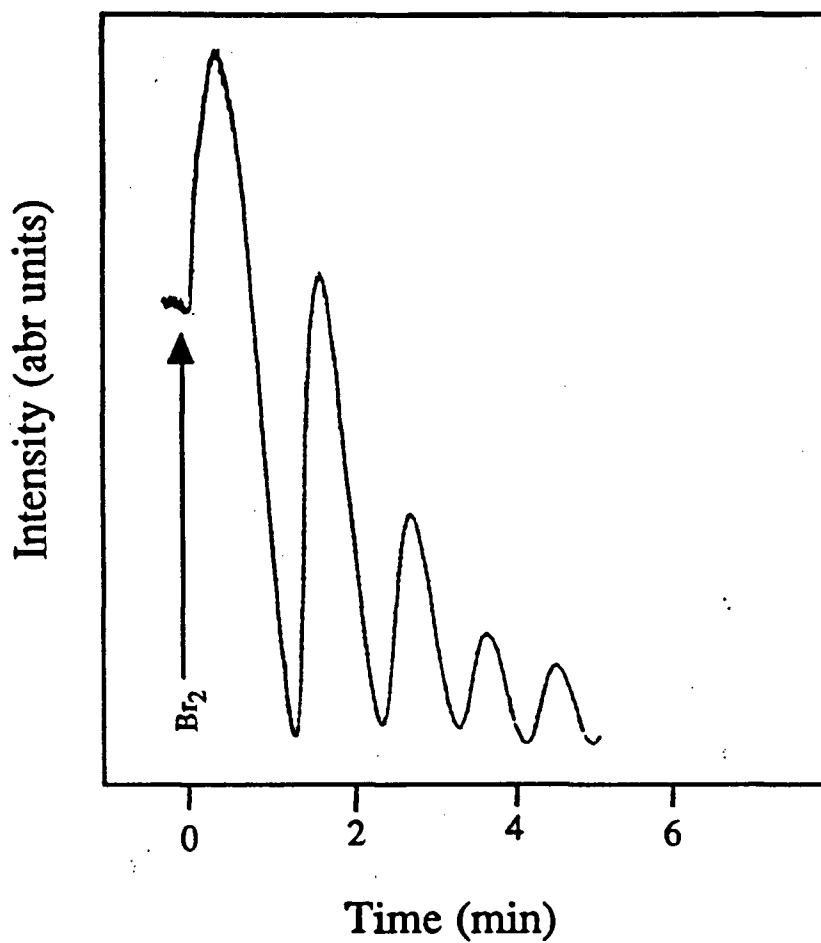
Figure 3.18 Interferogram resulting from the etching of n-type polycrystalline silicon (BN3 wafer) by Br_2.
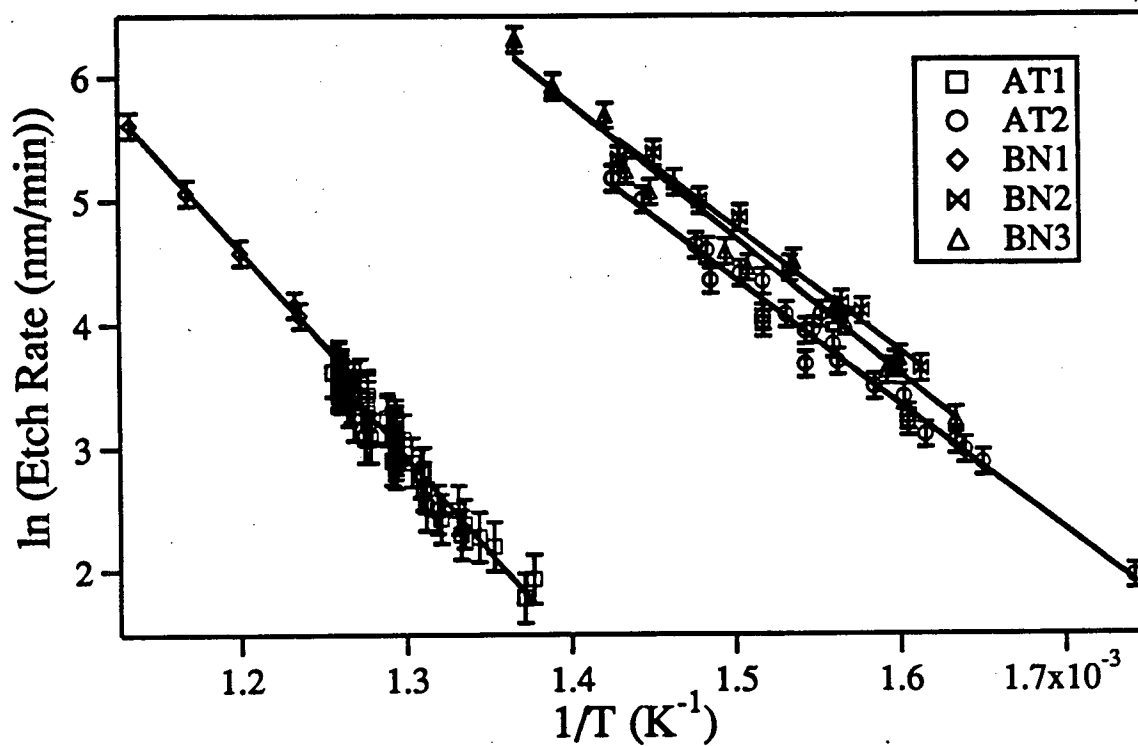
Figure 3.19 ln (etch rate) versus 1/T measured for various intrinsic and n-type polycrystalline silicon wafers at a Br_2 pressure of 1 Torr.

Table 3.7 Activation enthalpies and preexponentials factors from weighted least squares fit of the ln (etch rate) versus 1/T data presented in Figure 3.19 for etching of intrinsic and n-type polycrystalline silicon by 1.0 Torr Br_2 .

Wafer	Activation Enthalpy kJ mol^{-1}	Preexponential Factor nm min^{-1}
AT1 (intrinsic)	129 ± 8	$10^{10.1 \pm 0.5}$
AT2 (n-type)	85 ± 2	$10^{8.5 \pm 0.2}$
BN1 (intrinsic)	125 ± 7	$10^{10.3 \pm 0.4}$
BN2 (n-type)	83 ± 4	$10^{8.6 \pm 0.4}$
BN3 (n-type)	91 ± 3	$10^{9.2 \pm 0.2}$

3.3 Br Etching Results (BN1 and BN2 Wafers)

It is difficult to produce a wide range of measurable Br atom concentrations and, as a result, an accurate determination of the order of the reaction with respect to atom concentration was difficult. The pressure dependence was investigated by measuring the etch rate of n-type polycrystalline silicon (BN2 wafer) at two Br atom partial pressures, 0.20 and 0.08 Torr. Since the intensity is proportional to the square of the atom concentration, this change in pressure by a factor of 2.5 corresponds to approximately a factor of 6 change in intensity. The etch rates were measured at these two partial pressures and at temperatures between 140 and 270 °C. The results are presented in an Arrhenius plot as ln (etch rate) versus 1/T (Figure 3.20). The lines drawn through the two data sets are calculated from a weighted linear least squares regression. The errors in the etch rates are estimated to be ±15%, and this value is also used to calculated the weighting factors for the linear regression. The order of the reaction, n, is given by

$$n = \frac{\ln (\text{etch rate})_{P=0.20} - \ln (\text{etch rate})_{P=0.08}}{\ln (0.20) - \ln (0.08)} \tag{3.4}$$

where ln (etch rate) values are determined from the linear least squares fit of the two data sets. The two lines are not exactly parallel and as a result the value of n will vary depending on the temperatures at which the two values of ln (etch rate) are calculated. These values range from n=0.8 at 140 °C to n=1.1 at 230 °C. Taking the reaction to be first order with respect to Br partial pressure, an expression for the etch rate can now be written including the first order pressure dependence, i.e.

$$\text{Etch Rate} = k\, P_{Br} \quad . \tag{3.5}$$

The value of k is calculated for each etch rate and plotted as ln(k) versus 1/T (Figure 3.21), assuming an Arrhenius temperature dependence for k. A weighted least squares linear regression of this data yields the rate constant expression for n-type polycrystalline silicon (BN2 wafer)
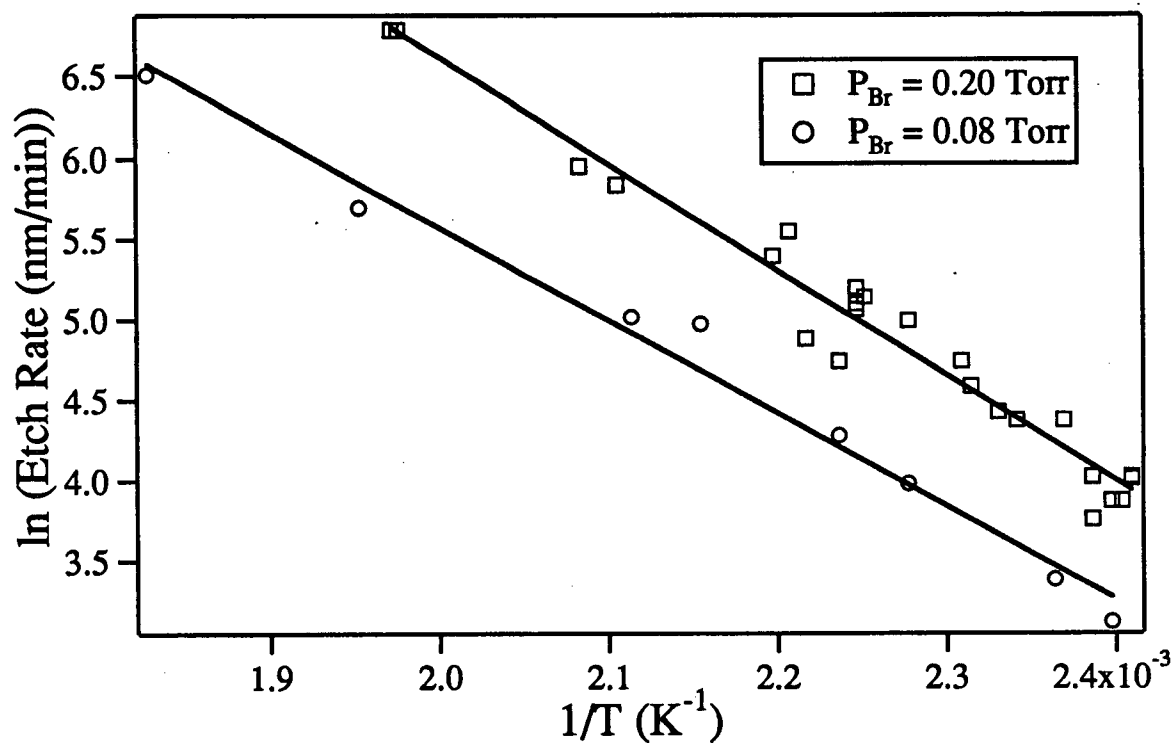
Figure 3.20 ln (etch rate) versus 1/T for etching of n-type polycrystalline silicon (BN2 wafer) measured at two Br partial pressures.
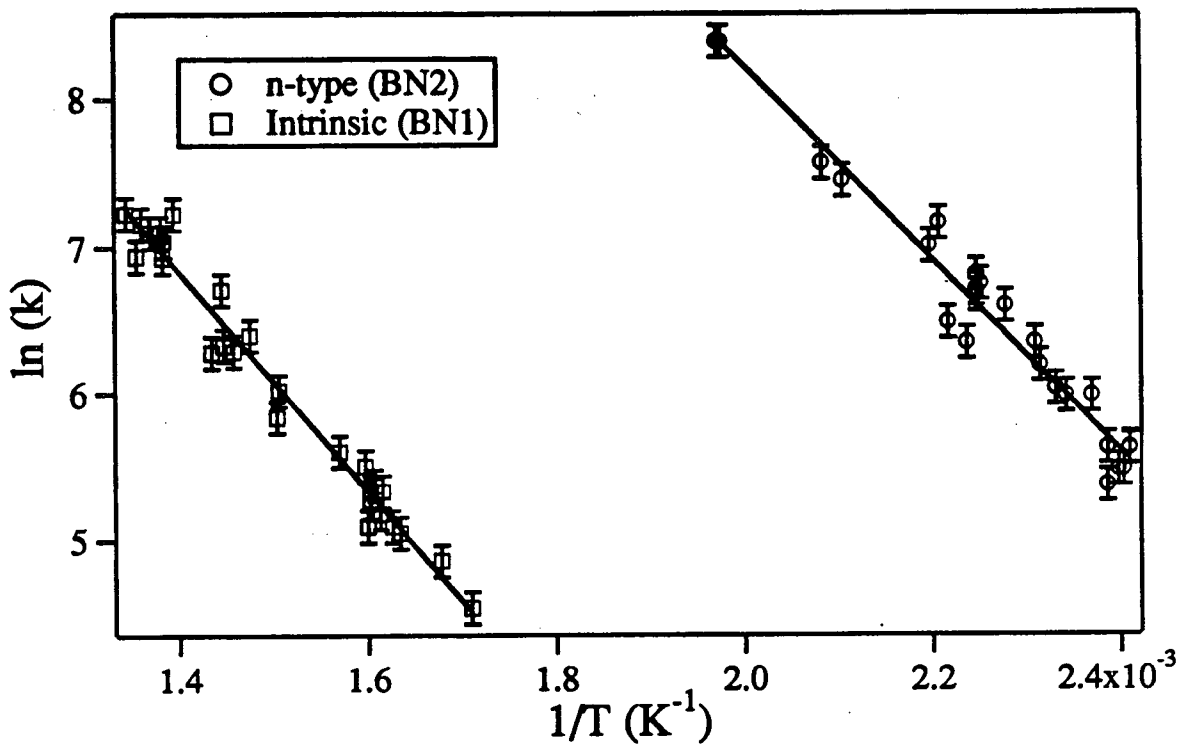
93

Figure 3.21 ln (k) versus 1/T for etching of intrinsic (BN1 wafer) and n-type (BN2 wafer) polycrystalline silicon at a Br atom partial pressure of 0.2 Torr.

$$k = 10^{9.3\pm0.3} \text{ nm min}^{-1} \text{ Torr}^{-1} \exp^{-(55\pm2 \text{ kJ/mol})/RT} \qquad . \qquad (3.6)$$

The relative Br concentration is monitored by measurement of the chemiluminescence intensity and is accurate to within $\pm10\%$. Calibration to an absolute partial pressure, however, requires a titration with NOCl. The titration introduces an error of approximately $\pm15\%$ in the partial pressure, and this error must be included in the preexponential factor given in equation (3.6).

The Br atom etching of intrinsic polycrystalline silicon (BN1 wafer) was measured at an atom partial pressure of 0.20 Torr and at temperatures ranging from 310 to 470 °C. Values for the rate constant k are calculated using equation (3.4) and plotted as ln (k) vs 1/T (Figure 3.21). The Arrhenius expression for the rate constant k is given by

$$k = 10^{7.5\pm0.2} \text{ nm min}^{-1} \text{ Torr}^{-1} \exp^{-(63\pm1.0/RT)} \qquad . \qquad (3.7)$$

3.4 Cl_2 Etching Results

3.4.1 Intrinsic and n-type Polycrystalline Silicon (BN1 and BN2 Wafers)

An experimental investigation into Cl_2 etching of intrinsic silicon was carried out in a manner similar to that described earlier using Br_2 as the etchant. The pressure and temperature dependence of the etching reaction was studied by measuring etch rates at Cl_2 pressures ranging from 0.1 to 50 Torr and at temperatures of 510, 540 and 570 °C. The resulting etch rates measured under these conditions are plotted as a function of Cl_2 pressure (Figure 3.22). The data displays significant scatter and this in general was observed with all the Cl_2 etching studies, especially at these high temperatures. Since the etching reactor and wafers are identical to those used in the Br_2 etching studies previously discussed and in view of the improvement in reproducibility observed upon switching to the high purity (99.99+%) Br_2, the low purity Cl_2 appears the most likely source of the scatter in the results. A linear least squares fit of the ln (etch rate) versus ln (Cl_2 pressure) data yields slopes of approximately 0.5 (Figure 3.23). The half order dependence is confirmed in a plot of etch rate versus (Cl_2 pressure)$^{1/2}$ (Figure 3.24). The slopes and intercepts resulting from a weighted linear least squares fit of the data (weighting factor based on an error of
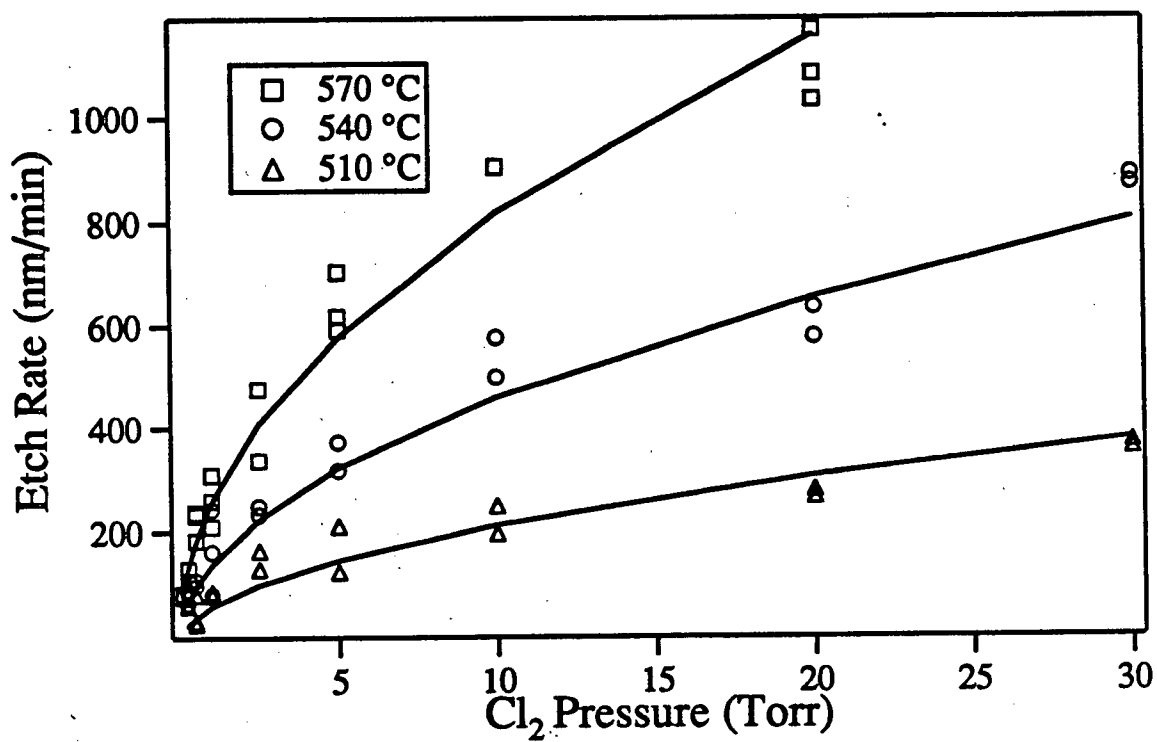
Figure 3.22 Etch rates of intrinsic polycrystalline silicon (BN1 wafer) versus Cl_2 pressure.
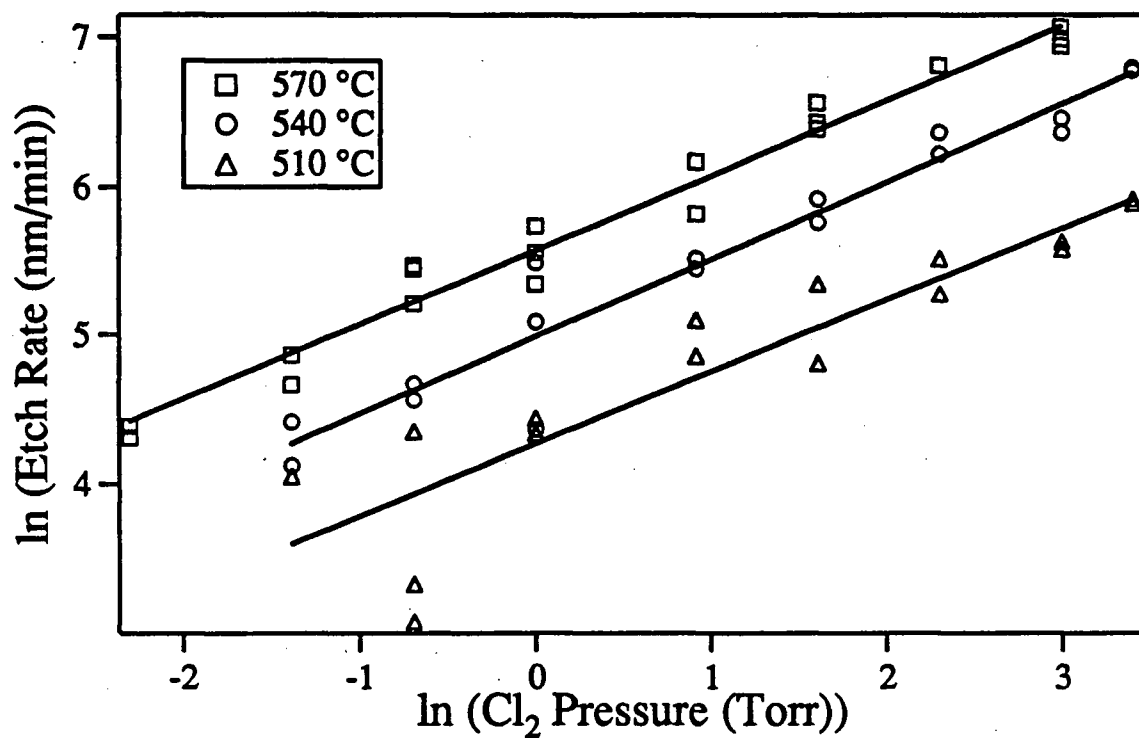
Figure 3.23 ln (etch rate) versus ln (Cl_2 pressure) for etching of intrinsic polycrystalline silicon (BN1 wafer).
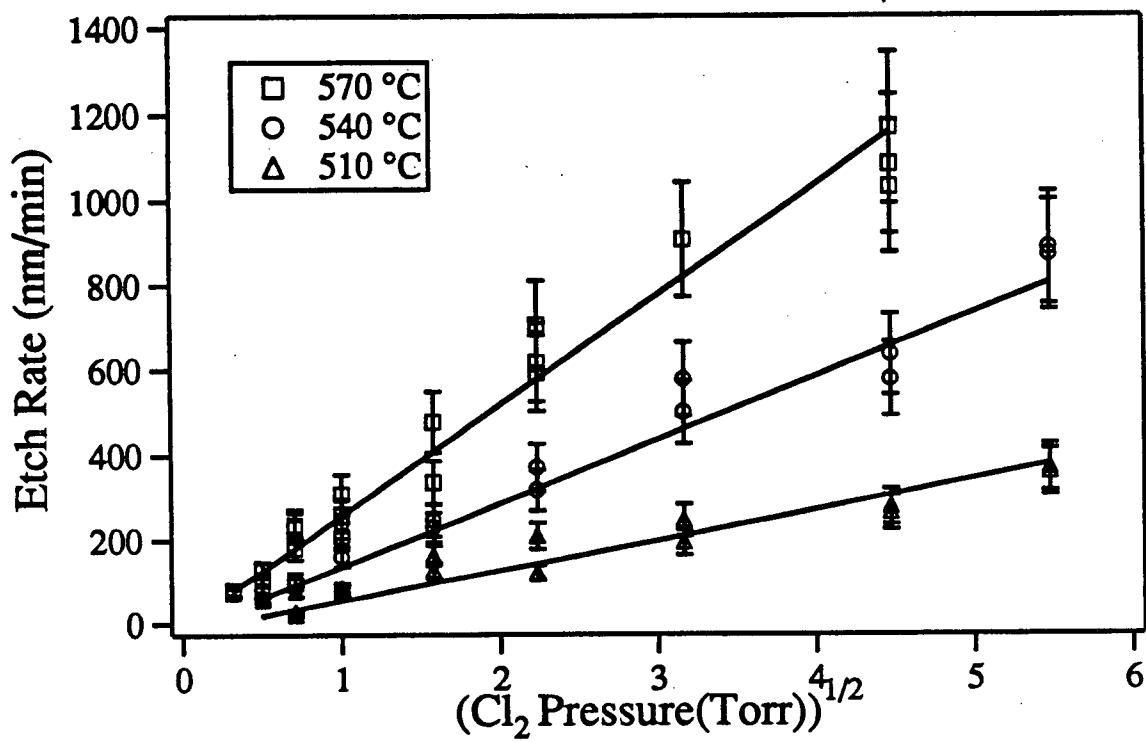
Figure 3.24 Etch rates of intrinsic polycrystalline silicon (BN1 wafer) versus $(Cl_2$ pressure$)^{1/2}$.

±15% in the etch rates) are given in Table 3.8. Because of the relatively large scatter in the data, the intercepts do not appear to display a consistent temperature dependence.

Cl_2 etching of n-type polycrystalline silicon (BN2 wafer) was studied at pressures between 0.1 and 50 Torr and at temperatures of 385, 410 and 435 °C. Cl_2, like Br_2, reacted more rapidly with n-type silicon than with intrinsic silicon and this permitted the use of lower temperatures in performing the etching experiments. The etch rates when plotted against Cl_2 pressure (Figure 3.25) display less scatter than observed in the results for the intrinsic sample obtained at higher temperatures. The reason for this reduction is not readily apparent. A linear least squares fit of the ln (etch rate) versus ln (Cl_2 pressure) data yields slopes of approximately 0.5. The half order pressure dependence is again confirmed from the linear plots of etch rate versus (Cl_2 pressure)$^{1/2}$ (Figure 3.26). A weighted linear least squares fit of the data yields the slopes and intercepts presented in Table 3.9. With scatter of approximately ±10% in the data, the intercepts are determined more accurately and do appear to show a temperature dependence, becoming increasingly negative with increasing temperatures.

3.4.2. Etch Rates of Polycrystalline Silicon at 1.0 Torr Cl_2

The temperature dependence of the reaction was examined further by measuring etch rates at 1.0 Torr Cl_2 and at temperatures between 530 and 690 °C for intrinsic polycrystalline silicon (BN1 wafer) and silicon (100), and between temperatures of 380 and 480 °C for n-type polycrystalline silicon (BN2 and BN3 wafers). The results are presented in an Arrhenius plot as ln (etch rate) versus 1/T for the two intrinsic wafers (Figure 3.27) and the two n-type wafers (Figure 3.28). A weighted linear least squares fit of the data yields activation enthalpies and preexponential factors which are presented in Table 3.10. Also included are the respective errors based on an uncertainty in the etch rates of ±10%.

3.5 Cl Etching Results

The problems encountered in determining reaction order with respect to Br partial pressures were also encountered in the Cl study, namely the difficulty in producing a wide range in atom

Table 3.8 Slopes and intercepts from weighted linear least squares fit of etch rate versus (Cl_2 pressure)$^{1/2}$ plots presented in Figure 3.24 for etching of intrinsic polycrystalline silicon (BN1 wafer).

Wafer	Temperature (°C)	Slope (C_1) $nm\ min^{-1}\ Torr^{-1}$	Intercept (C_2) $nm\ min^{-1}$
BN1 (intrinsic)	510	72 ± 4	18 ± 4
	540	150 ± 9	14 ± 9
	570	260 ± 13	5 ± 9
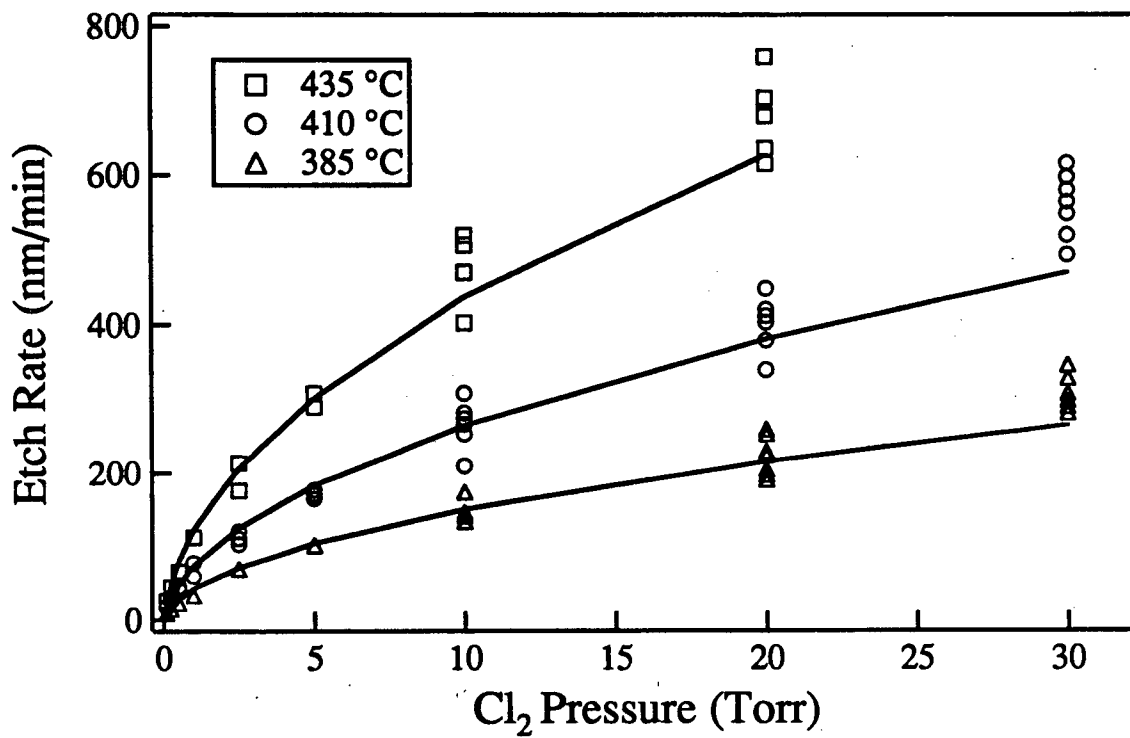
Figure 3.25 Etch rates of n-type polycrystalline silicon (BN2 wafer) versus Cl_2 pressure.
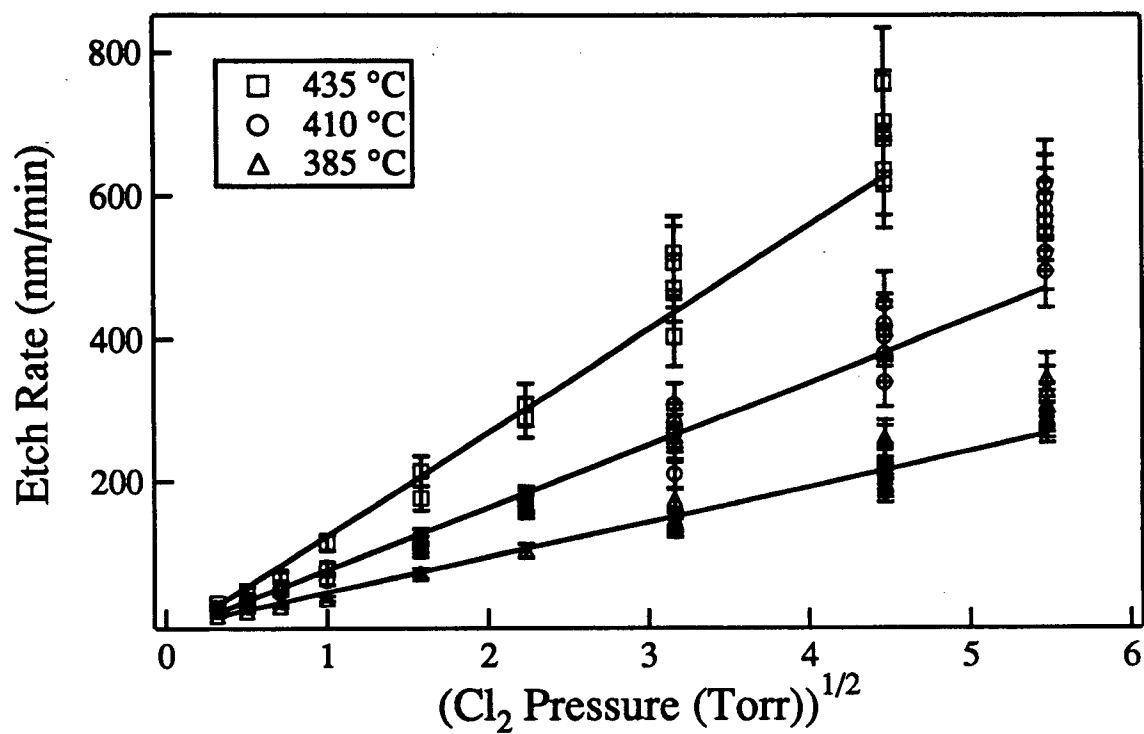
Figure 3.26 Etch rates of n-type polycrystalline silicon (BN2 wafer) versus $(Cl_2 \text{ pressure})^{1/2}$.

Table 3.9 Slopes and intercepts from weighted linear least squares fit of etch rate versus (Cl_2 pressure)$^{1/2}$ plots presented in Figure 3.26 for etching of n-type polycrystalline silicon (BN2 wafer).

Wafer	Temperature (°C)	Slope (C_1) nm min^{-1} Torr^{-1}	Intercept (C_2) nm min^{-1}
BN2 (n-type)	385	50.2 ± 1.1	-9.0 ± 0.9
	410	88.7 ± 1.9	-15.8 ± 1.6
	435	146 ± 4	-24.4 ± 3.0
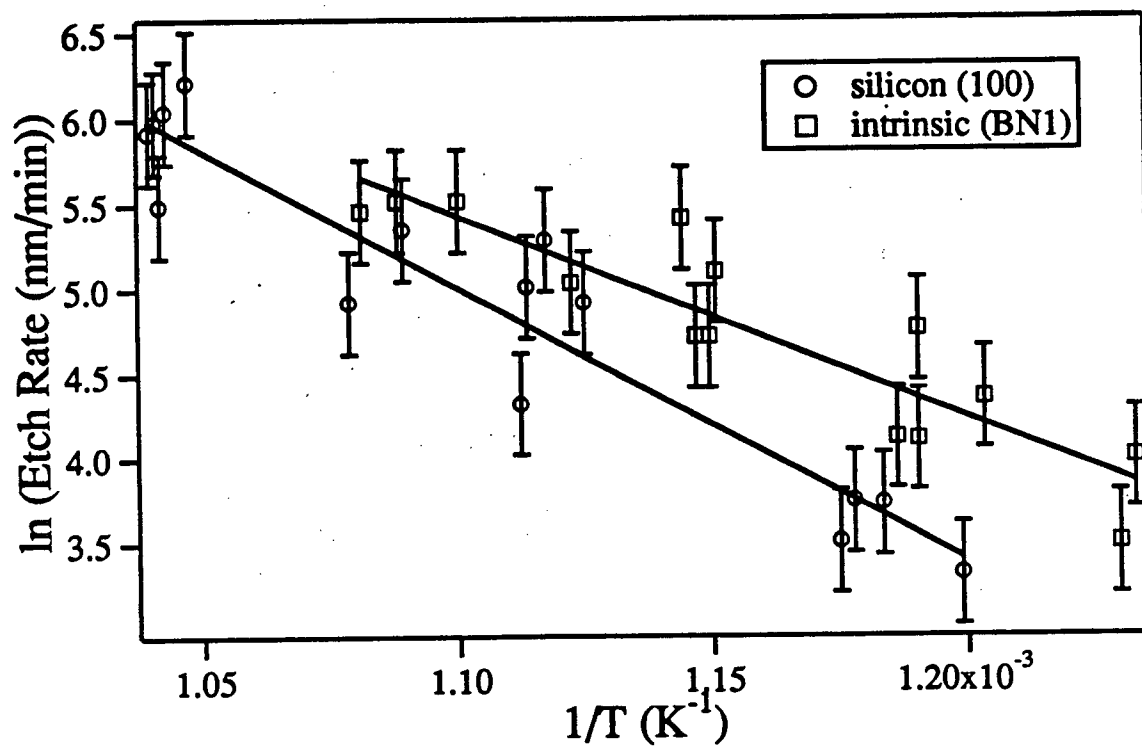
Figure 3.27 ln (etch rate) versus 1/T for etching of intrinsic silicon (100) and polycrystalline silicon (BN1 wafer) at 1 Torr Cl_2.
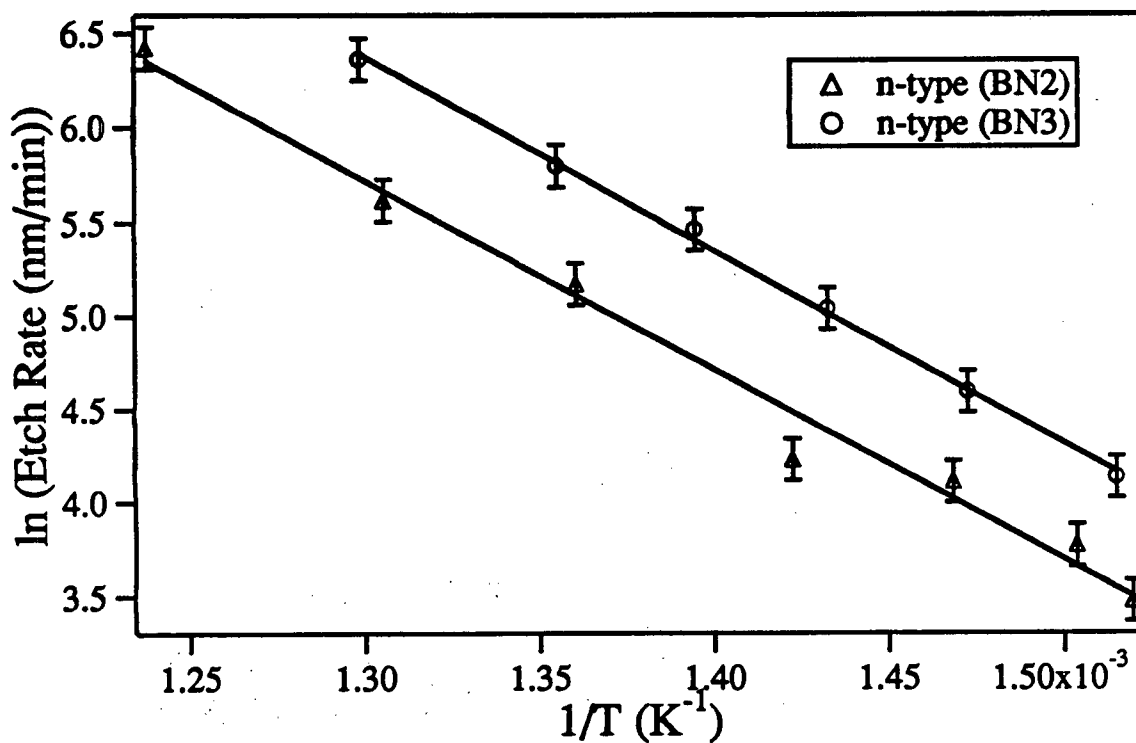
Figure 3.28 ln (etch rate) versus 1/T for etching of n-type polycrystalline silicon at 1 Torr Cl_2

Table 3.10 Activation enthalpies and preexponentials factors from weighted least squares fit of the ln (etch rate) versus 1/T data presented in Figures 3.27 and 3.28 for etching of polycrystalline silicon and silicon (100) by 1.0 Torr Cl_2.

Wafer	Activation Enthalpy kJ mol^{-1}	Preexponential Factor nm min^{-1}
BN1 (intrinsic)	99 ± 16	$10^{8.0 \pm 1.0}$
silicon (100)	134 ± 13	$10^{9.9 \pm 0.7}$
BN2 (n-type)	84 ± 4	$10^{8.2 \pm 0.3}$
BN3 (n-type)	86 ± 5	$10^{8.6 \pm 0.4}$

concentrations. As a result, the Cl partial pressure dependence was not examined. The temperature dependence was determined by measuring the etch rate at temperatures ranging from 150 to 290 °C and from 25 to 90 °C for intrinsic (BN1 wafer) and n-type (BN2 wafer) polycrystalline silicon respectively. A Cl atom partial pressure of 0.17 Torr was employed in etching both wafers. Assuming the rate expression is of the form given in equation (3.4), rate constants have been calculated from the etch rates and are presented in an Arrhenius plot as ln (k) versus 1/T (Figure 3.29). Once again weighted linear least squares regression was performed on the two data sets resulting in two linear plots. Weighting factors were based on an estimated error of ±10% in the etch rates. The Arrhenius preexponential factors and the activation enthalpies obtained from the fit can be used to write rate constant expressions

$$k \text{ (intrinsic)} = 10^{5.9 \pm 0.2} \text{ nm min}^{-1} \text{ Torr}^{-1} \exp^{(-28.2 \pm 1.2 \text{ kJ/mol})/RT} \tag{3.8}$$

$$k \text{ (n-type)} = 10^{7.9 \pm 0.2} \text{ nm min}^{-1} \text{ Torr}^{-1} \exp^{(-27.8 \pm 1.5 \text{ kJ/mol})/RT} \tag{3.9}$$

for the etching of intrinsic and n-type polycrystalline silicon respectively.

3.6 Unsuccessful Experiments

On the following pages, a brief discussion will be given of experiments that were attempted, but had to be abandoned. These experiments, although not essential to the overall success of the study, would have provided additional information useful in obtaining an overall understanding of the etching process. The reasons why these experiments were attempted and why they eventually failed will be addressed.

3.6.1 Mass Spectrometry Study

When studying any chemical reaction, it is important to identify the reaction products. This is also true in the etching reactions of chlorine and bromine with silicon. It is possible to speculate on reaction products from thermodynamic data, but they may not represent the products produced under the experimental conditions employed in the etching studies. Product identification can be
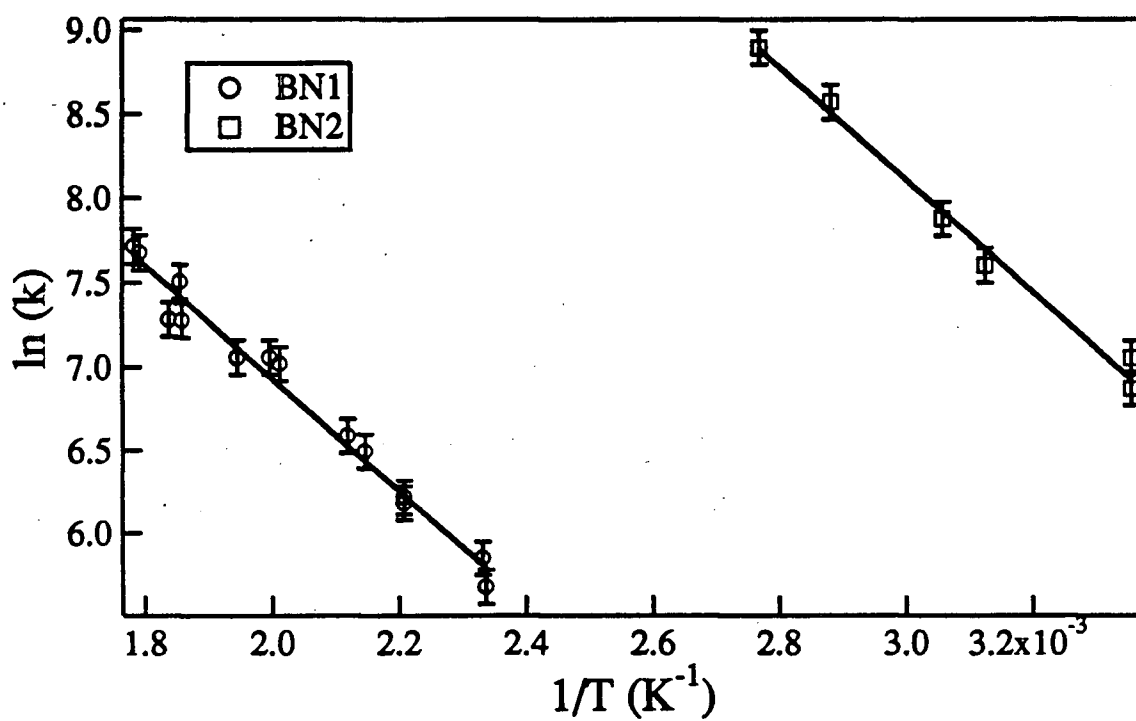
107

Figure 3.29 ln (k) versus 1/T for etching of intrinsic (BN1 wafer) and n-type (BN2 wafer) polycrystalline silicon at a Cl atom partial pressure of 0.17 Torr.

achieved through a mass spectrometry study of the reaction, but if the results from such a study are to be valid, care must be taken in designing the experiment to insure that the products detected are indeed those leaving the reacting surface and not those formed from secondary reactions in the gas phase.

With this in mind, a specially designed Pyrex reactor was mounted to a quadrupole mass spectrometer such that the sampling pinhole of the spectrometer was within a centimeter of the holder on which the sample was placed. Unfortunately difficulties were encountered in encouraging the failing electronics of the 25 year old instrument to work and after a period of about a year, the project was abandoned. Although this failure was disappointing, a thermal desorption study by Jackman et al. in 1989 on the reaction of Br_2 with silicon[44] along with a similar study with Cl_2 and silicon[39] in 1986, provided information on the types of reaction products expected in our etching studies.

3.6.2 F_2 Etching

The half order pressure dependence of Cl_2 and Br_2 etching of silicon discussed above proved to be very interesting and somewhat surprising in light of two previous pressure dependence studies on these etching systems by Sveshnikova et al.[47] and Ogryzlo et al.[41] In both of these studies, the non-linear increase in reaction rate with increasing pressure was interpreted in terms of a saturation of available adsorption sites. The question was raised as to whether this behavior is unique for Cl_2 and Br_2, or if F_2 also displays the same half order dependence.

To investigate the F_2 pressure dependence of the reaction with silicon, etching experiments were performed using a 10% F_2 mixture in He. Etch rates of intrinsic polycrystalline silicon were measured at F_2 partial pressures ranging from 0.1 to 10 Torr and at temperatures of 185 and 215 °C. Unfortunately the results were extremely inconsistent, so much so that the pressure dependence could not be ascertained. The source of the scatter was assumed to be impurities in the F_2/He mixture, although this could not be proven. Without a proper pump to handle F_2, and the difficulties experienced in obtaining reproducible results, the study was discontinued.

3.6.3 X-ray Photoelectron Spectroscopy Studies

With the arrival of a new x-ray photoelectron spectrometer in the department in 1988-89, it was felt this new facility would provide useful information in understanding chlorine and bromine etching of silicon. X-ray photoelectron spectroscopy is an effective surface analysis technique, having a probing depth of only 1-2 nm. Monochromatic x-rays, typically Mg Kα (1254 eV) or Al Kα (1487 eV) radiation, are directed at a surface under high vacuum where they interact with a surface atom, causing the emission of a core electron. The kinetic energy of the emitted electrons is not only unique for a particular atom, but also for the chemical environment of that atom. In this way it is possible to determine the chemical species present on a surface. Although this technique requires high vacuum conditions and as a result cannot be used *in situ* in etching experiments, it does provide a method of determining chemisorbed species present on the silicon surface after etching.

The main drawback with the present x-ray photoelectron spectrometer is that a loadlock transfer system is as yet not in place. This means samples removed from the etching reactor must be brought out to atmosphere and taken to the spectrometer for analysis. Surface species such as silicon bromides may not be stable in the presence of O_2 or H_2O and hence will not be detected. This is supported by the x-ray photoelectron spectroscopy results obtained on a number of etched samples which indicated the presence of only Si and SiO_2. Since it was felt the surface analyzed was not indicative of the surface after etching and provided no additional information, the x-ray photoelectron spectroscopy results have not been included.

Chapter 4. Discussion

4.1 Overview

The discussion of the experimental results will begin with an analysis of the Cl and Br atom etching experiments followed by an analysis of the molecular etching results. This order is chosen as the results obtained from the analysis of the atom etching experiments will have implications in the discussion of the molecular etching results. Mechanisms will be proposed to account for the observed kinetics of the reaction of Br_2 and Cl_2 with silicon. Arguments will be presented which favour only one of those reaction mechanisms, namely a reversible dissociative adsorption mechanism. The rate constants for the reactions, along with their activation enthalpies, will be discussed in terms of the proposed reaction steps.

The enhancement in etch rates resulting from the presence of n-type dopants will be addressed by first reviewing the findings of previous studies that have investigated the dopant effect in fluorine etching of silicon. The results from the present study will be discussed in terms of these earlier proposals and in view of the differences observed in the rate constants for the etching of intrinsic and n-type silicon.

4.2 Atomic Halogen Etching of Silicon

4.2.1 Br Atom Etching of Intrinsic (BN1 wafer) and n-type (BN2 wafer) Silicon

The reaction of Br atoms with silicon was determined in section 3.3 to be first order with respect to Br partial pressure. The reaction can be written as

$$Br + Si \xrightarrow{k_1} SiBr_x \qquad (4.1)$$

where Si is a silicon or partially brominated silicon surface atom which reacts to produce either gaseous product (where x=1,2,3 or 4 depending upon temperature) or some precursor which forms that product in a subsequent non rate-determining step. The order of the reaction with respect to Br atom concentration has not been previously reported and hence there are no studies with which to compare this result. However the first order dependence is consistent with findings

111

from similar studies on F atom etching of silicon[20], as well as from Br atom etching of aluminium[71] and gallium arsenide[72].

Once the pressure dependency of the reaction was established, values of k_1 were calculated by dividing the etch rates by the Br atom partial pressure. An Arrhenius temperature dependency was assumed for k_1 and values of ln (k_1) were plotted versus $1/T$ in Figure 3.21. A weighted linear least squares fit of this data yield the following expressions for the first order rate constant k_1 for intrinsic and n-type silicon;

$$k_1(\text{intrinsic}) = 10^{7.5\pm0.2} \text{ nm min}^{-1} \text{ Torr}^{-1} \exp^{(-63\pm1 \text{ kJ/mol})/RT} \qquad (4.2)$$

$$k_1(\text{n-type}) = 10^{9.3\pm0.3} \text{ nm min}^{-1} \text{ Torr}^{-1} \exp^{(-55\pm2 \text{ kJ/mol})/RT} \qquad . \qquad (4.3)$$

The rate constant k_1 for n-type silicon is considerably larger than that for intrinsic silicon. This is apparent in the above rate constant expressions, as well as in the Arrhenius plot presented in Figure 3.21. The larger k_1 value, and hence larger etch rates, is also reflected in the lower temperatures employed in etching n-type silicon. A temperature range of 140 to 270 °C was sufficient to produce the same reaction rates observed in the range 310 to 470 °C for intrinsic silicon. The enhancement in the reaction rate of n-type silicon can be determined by evaluating the ratio of k_1(n-type) to k_1(intrinsic) for a given temperature. Due to the small difference in the activation enthalpies of the two rate constants, the ratio will show a small temperature dependence. At an intermediate temperature of 300 °C, the rate constant k_1 has values of 57 and 19000 nm min^{-1} Torr^{-1} for intrinsic and n-type silicon respectively, yielding an enhancement factor of 340. Enhanced etch rates were also observed for the etching of n-type silicon by Br_2, Cl_2 and Cl atoms. Consequently, the effect of doping on reaction rates will be discussed for all etchants in detail in section 4.5.

In spite of the large enhancements in etch rates for n-type silicon, the activation enthalpies of 63 and 55 kJ mol^{-1} for the two respective rate constants are very similar. The differences in etch rates between the two silicon wafers is principly attributed to differences in the preexponential factors. These factors differ by almost two orders of magnitude. It is also instructive to consider the magnitudes of the two preexponential factors. Using a value of 2.33 g cm^{-3} for the density of

silicon, the preexponential factors can be converted from units of nm min^{-1} Torr^{-1} to units of molec^{-1} cm^{-2} s^{-1} Torr^{-1}, which represents the flux of silicon product molecules leaving the reacting surface per unit time and per unit etchant pressure. Converting the preexponential factors in equations (4.2) and (4.3) yields

$$A_1 \text{ (intrinsic)} = 2.6 \times 10^{21} \text{ molec cm}^{-2} \text{ s}^{-1} \text{ Torr}^{-1} \tag{4.4}$$

$$A_1 \text{ (n-type)} = 1.7 \times 10^{23} \text{ molec cm}^{-2} \text{ s}^{-1} \text{ Torr}^{-1} \quad . \tag{4.5}$$

If k_1 is the rate constant for an elementary rate controlling step, then according to kinetic theory A_1 is a frequency factor and should be less than or equal to the collision frequency of reactant at the surface. The frequency of Br atom collisions on the reacting surface is given by

$$z = \left(\frac{P^2}{2\pi m k T} \right)^{1/2} . \tag{4.6}$$

For Br atoms with a mass of 1.33×10^{-25} kg and a temperature of 300 °C, the collision frequency is equal to 1.6×10^{20} atoms cm^{-2} s^{-1} Torr^{-1}, significantly less than preexponential factors given in equations (4.4) and (4.5). Preexponentials larger than collision frequency have also been observed in the Cl atom etching of silicon[42] and the chemical vapor deposition of silicon[73]. This does not mean the experimentally determined values of k_1 are incorrect, but rather the rate constant k_1 does not represent an elementary reaction step. It is therefore quite probable that the reaction between a Br atom and a halogenated silicon species is preceded by the adsorption of Br atoms. Such a reaction could be represented by the elementary steps

$$\text{Br} \; \underset{k_{-2}}{\overset{k_2}{\rightleftharpoons}} \; \text{Br}_{ads} \tag{4.7, 4.-7}$$

$$\text{Br}_{ads} \; \overset{k_3}{\longrightarrow} \; \text{SiBr}_x \tag{4.8}$$

where Br_{ads} is an adsorbed Br atom on what is most likely a partially brominated silicon surface. Assuming a steady state concentration for Br_{ads}, i.e.

$$\frac{d[Br_{ads}]}{dt} = k_2 P_{Br} - k_{-2}[Br_{ads}] - k_3[Br_{ads}] \approx 0 \quad , \tag{4.9}$$

then an expression for the overall reaction can be given as

$$Etch\ Rate = k_3\left(\frac{k_2}{k_{-2} + k_3}\right) P_{Br} \quad . \tag{4.10}$$

where P_{Br} is the partial pressure of Br atoms. When the equilibrium given by reactions (4.7) and (4.-7) is maintained and $k_{-2} \gg k_3$, then the etch rate expression reduces to

$$Etch\ Rate = k_3\left(\frac{k_2}{k_{-2}}\right) P_{Br} \quad . \tag{4.11}$$

The experimentally measured preexponential factor, A_{exp}, would then be given by

$$A_{exp} = \frac{A_2 A_3}{A_{-2}} \quad . \tag{4.12}$$

If A_2 is taken as the collision frequency of Br atoms on the surface (approximately 10^{20} atoms $cm^{-2}\ s^{-1}\ Torr^{-1}$) and A_{exp} is the extrapolated preexponential factor determined from experimentally measured rate constants, then the ratio A_3/A_{-2} would have values of 10^{-1} and 10^{-3} for the intrinsic and n-type silicon wafers respectively. Since the two reactions (4.-7) and (4.8) involve surface adsorbed species, the frequency factors A_{-2} and A_3 can be thought of as vibrational frequencies of an adsorbed species. With this in mind, the values of A_3/A_{-2} required to maintain the equality in equation (4.12) do not appear unreasonable.

114

4.2.2 Cl Atom Etching of Intrinsic (BN1 Wafer) and n-type (BN2 Wafer) Silicon

The pressure dependence of Cl atom etching was not determined experimentally in the present study and to the author's best knowledge has not been reported in the literature. In light of the pressure dependence of the Br atom etching reaction discussed in section 3.3, a first order dependence for Cl atom etching is assumed. This is consistent with the pressure dependence found in the first order Cl atom etching of tungsten and tungsten silicide films[74] and molybdenum films[75]. The reaction with silicon can then be written as

$$Cl + Si \xrightarrow{\quad k_1 \quad} SiCl_x \qquad\qquad (4.13)$$

where Si is a silicon or partially chlorinated silicon surface species and $SiCl_x$ (where x=1,2,3 or 4 depending upon temperature) is a gaseous product, or some precursor which forms that product in a subsequent non rate-determining step. Values for k_1 were determined from the experimentally measured etch rates and the Cl atom partial pressure using equation (3.4). Assuming k_1 to have an Arrhenius temperature dependency, a linear least squares fit of the ln (k_1) values plotted versus 1/T in Figure 3.29 yielded the following two equations

$$k_1 \text{ (intrinsic)} = 10^{5.9\pm0.2} \text{ nm min}^{-1} \text{ Torr}^{-1} \exp^{(-28.2\pm1.2 \text{ kJ/mol})/RT} \qquad\qquad (4.14)$$

$$k_1 \text{ (n-type)} = 10^{7.9\pm0.2} \text{ nm min}^{-1} \text{ Torr}^{-1} \exp^{(-27.8\pm1.5 \text{ kJ/mol})/RT} \qquad\qquad (4.15)$$

The Cl atoms reacted at an enhanced rate with n-type compared to intrinsic silicon, as they did for Br atom etching. The larger magnitude of k_1 for n-type silicon is obvious from the these two expressions and from the data plotted in Figure 3.29. This is also reflected in the differences in the two temperature ranges of 25 to 90 °C and 150 to 290 °C required to obtain comparable etch rates for n-type and intrinsic silicon respectively. The degree of enhancement in etch rates can be determined by evaluating the two expressions (4.14) and (4.15) at an intermediate temperature of 125 °C. Calculating the ratio of k_1(n-type) to k_1(intrinsic) yields an enhancement factor 89. The activation enthalpies associated with k_1 for the etching of the intrinsic and n-type silicon are both

approximately 28 kJ mol^{-1}. The difference between the two rate constants is contained only in the preexponential factors, which differ by two orders of magnitude.

The preexponential factors in the two rate constants given in equations (4.16) and (4.17), when converted to units of molec cm^{-2} s^{-1} Torr^{-1}, have values of

$$A_1(\text{intrinsic}) = 6.6 \times 10^{19} \text{ molec cm}^{-2} \text{ s}^{-1} \text{ Torr}^{-1} \tag{4.16}$$

$$A_1(\text{n-type}) = 6.6 \times 10^{21} \text{ molec cm}^{-2} \text{ s}^{-1} \text{ Torr}^{-1} \tag{4.17}$$

These values can be compared to the Cl collision frequency of 2.9×10^{20} atoms cm^{-2} s^{-1} Torr^{-1}, calculated from equation (4.6) at a temperature of 125 °C. If the product leaving the surface is SiCl$_2$, then the values of the preexponential should be less than one half the Cl collision frequency, i.e. 1.5×10^{20} atoms cm^{-2} s^{-1} Torr^{-1}, or if the product is SiCl$_4$, then these values should be less than one quarter of the Cl collision frequency, i.e. 7.3×10^{19} atoms cm^{-2} s^{-1} Torr^{-1}. Although these preexponential factors are not as large as those observed in Br atom etching, the value for A_1(n-type) is still one to two order of magnitude larger than that expected based on the collision frequency of Cl atoms. This difference can be explained, as it was for the Br atom etching of silicon, by proposing a mechanism whereby reversible adsorption of Cl atoms precedes the reaction of Cl with silicon, i.e.

$$\text{Cl} \underset{k_{-2}}{\overset{k_2}{\rightleftarrows}} \text{Cl}_{\text{ads}} \tag{4.18, 4.-18}$$

$$\text{Cl}_{\text{ads}} \xrightarrow{k_3} \text{SiCl}_x \tag{4.19}$$
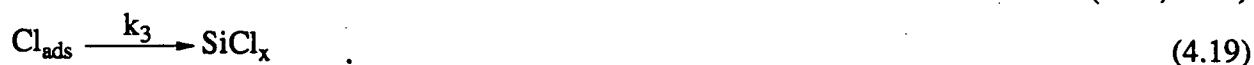
The reaction given by (4.19) is between an adsorbed Cl atom, Cl$_{\text{ads}}$, and a chlorinated surface species forming the product SiCl$_x$. When an equilibrium concentration of Cl$_{\text{ads}}$ is maintained by reactions (4.18) and (4.-18), the rate expression can be written as

$$\text{Etch Rate} = k_3 \left(\frac{k_2}{k_{-2}} \right) P_{\text{Cl}} \tag{4.20}$$

116

and the preexponential factor for the rate constants $k_3 k_2/k_{-2}$ is given by equation (4.12). The value of A_3/A_{-2} required to maintain the equality in equation (4.12) need be only 10^{-2} for the n-type silicon wafer and close to unity for the intrinsic silicon wafer, which do not appear unreasonable.

4.3 Molecular Halogen Etching of Silicon
4.3.1 Br_2 Etching of Intrinsic and n-type Silicon

The etch rates of both intrinsic and n-type silicon were found to increase non-linearly with increasing Br_2 pressure and plots of ln (etch rate) versus ln (Br_2 pressure) indicated a reaction order of one half with respect to Br_2 pressure for all data sets. The etch rates, when plotted versus (Br_2 pressure)$^{1/2}$ (Figures 3.6, 3.8, 3.11, 3.13, 3.16 and 3.17), were found to follow the empirical rate equation

$$\text{Etch Rate} = C_1 (Br_2 \text{ Pressure})^{1/2} - C_2 \qquad (4.21)$$

where C_1 and C_2 are temperature dependent constants. By determining the temperature dependencies of the constants C_1 and C_2, empirical expressions can be written to characterize the etch rates of the various wafers at the temperatures and Br_2 pressures employed in this study. An Arrhenius form for that temperature dependency has been assumed, i.e.

$$k = A\, e^{-E_a/RT} \qquad (4.22)$$

where k is the rate constant (in this case C_1 or C_2), R is the gas constant, T is the temperature, A is a temperature independent preexponential factor and E_a is the activation enthalpy. Plotting ln (C_1) or ln (C_2) versus $1/T$ and performing a weighted linear least squares fit of the data, the following expressions can be determined.

$$\text{Etch Rate (AT1)} = 10^{9.3 \pm 0.4} \text{ nm min}^{-1} \text{ Torr}^{-1/2} \exp^{-(118 \pm 15 \text{ kJ/mol})/RT} (Br_2 \text{ Pressure})^{1/2} \qquad (4.23)$$

$$\text{Etch Rate (AT2)} = 10^{9.8 \pm 1.0} \text{ nm min}^{-1} \text{ Torr}^{-1/2} \exp^{-(100 \pm 13 \text{ kJ/mol})/RT} (Br_2 \text{ Pressure})^{1/2} \qquad (4.24)$$

Etch Rate (Silicon (100)) = $10^{9.1\pm0.4}$ nm min^{-1} Torr$^{-1/2}$

$$\exp{}^{-(121\pm7\text{ kJ/mol})/RT}\text{ (Br}_2\text{ Pressure)}^{1/2} \qquad (4.25)$$

Etch Rate (BN1) = $10^{10.1\pm0.5}$ nm min^{-1} Torr$^{-1/2}$ $\exp{}^{-(131\pm8\text{ kJ/mol})/RT}$ (Br$_2$ Pressure)$^{1/2}$

$$- 10^{10.1\pm0.5}\text{ nm min}^{-1}\exp{}^{-(144\pm8\text{ kJ/mol})/RT} \qquad (4.26)$$

Etch Rate (BN2) = $10^{8.7\pm0.3}$ nm min^{-1} Torr$^{-1/2}$ $\exp{}^{-(86\pm4\text{ kJ/mol})/RT}$ (Br$_2$ Pressure)$^{1/2}$

$$- 10^{8.2\pm1.4}\text{ nm min}^{-1}\exp{}^{-(91\pm21\text{ kJ/mol})/RT} \qquad (4.27)$$

Etch Rate (BN3) = $10^{9.4\pm0.7}$ nm min^{-1} Torr$^{-1/2}$ $\exp{}^{-(95\pm8\text{ kJ/mol})/RT}$ (Br$_2$ Pressure)$^{1/2}$

$$- 10^{10.6\pm0.8}\text{ nm min}^{-1}\exp{}^{-(121\pm16\text{ kJ/mol})/RT} \qquad . \qquad (4.28)$$

Since the etch rates for n-type silicon are observed to vary with doping level, the expressions for n-type silicon (AT2, BN2 and BN3) can only be used to predict the etch rates of wafers with similar doping levels. It should be noted that due to the considerable scatter in the etch rate data for the wafers AT1, AT2 and silicon (100), the etch rate expressions given above for these wafers contain only the C_1 term. Determining accurate values for the relatively small intercepts from these data sets was not possible. However the contribution of C_2 to the overall etch rate is small, especially at larger Br$_2$ pressures. For example, the etch rates calculated for BN1 at 570 °C and a Br$_2$ pressure of 10 Torr, differ by only 5% when contributions from C_2 are neglected. Therefore the above expressions containing only the C_1 term do provide a good indication of the observed etch rates.

The etch rates calculated from the two expressions for intrinsic polycrystalline wafers AT1 and BN1 yield comparable values. For example, the etch rates calculated from equations (4.23) and (4.26) at a temperature of 520 °C and a Br$_2$ pressure of 10 Torr are 106 and 90 nm min^{-1} for the two wafers respectively. These rates are considerably faster than the 13 nm min^{-1} etch rate calculated using equation (4.25) for silicon (100) under the same pressure and temperature conditions. This result is not surprising as polycrystalline silicon contains many unsaturated bonds and crystal defects, especially in the grain boundary regions. Their presence helps to facilitate the reaction with the etchants, resulting in faster etch rates.

The etch rates for n-type wafers AT2, BN2 and BN3 were also similar. Using equations (4.24), (4.27) and (4.28) given above and a temperature of 400 °C and a Br$_2$ pressure of 10 Torr,

etch rates of 345, 290 and 285 nm min^{-1} are calculated for the three wafers respectively. The similarity in etch rates in not surprising considering the small range in doping levels of the three wafers. All three doped wafers etched at much faster rates than the intrinsic wafer, as indicated by the lower temperatures required to obtain comparable etch rates. The effect of n-type dopants on the etch rates will be discussed in detail in section 4.5.

The half order dependency of the etch rate on Br_2 pressure is contrary to the results from the only previous study of Br_2 etching of silicon. In this study by Sveshnikova et al.[47], silicon (100) and (111) etch rates were found to increase with increasing Br_2 pressure up to a saturation limit. The point at which the etch rates saturated varied from 4 to 15 Torr for etching temperatures ranging from 490 to 550 °C. A representative set of etch rate data measured as a function of Br_2 pressure at a temperature of 550 °C for the (100) face of silicon has been reproduced from the paper of Sveshnikova et al. and presented in Figure 4.1. The original etch rates, which were determined by sample weight loss and reported in units of moles cm^{-2} s^{-1}, have been converted to units of nm min^{-1} in Figure 4.1. The authors chose to represent the Br_2 pressure dependency of the reaction by the expression

$$W = W_{lim}\left(\frac{aP}{1 + aP}\right)$$

(4.29)

where W_{lim} is the reaction rate in the zero order region (plateau region), a is a temperature dependent constant, and P is the partial pressure of Br_2. Thus at low pressures when $aP \ll 1$, the reaction should become first order with respect to Br_2 pressure, while at high pressures when $aP \gg 1$, a transition to zero order kinetics should be observed. However when this data is plotted as ln (etch rate) versus ln (Br_2 pressure) (Figure 4.2), the results are contrary to those predicted by equation (4.29). The data can be represented by two straight lines, one with a slope of zero encompassing the three highest pressure points, and the second line passing through the remaining points with a slope of 0.56. There appear to be no data points corresponding to a first order regime
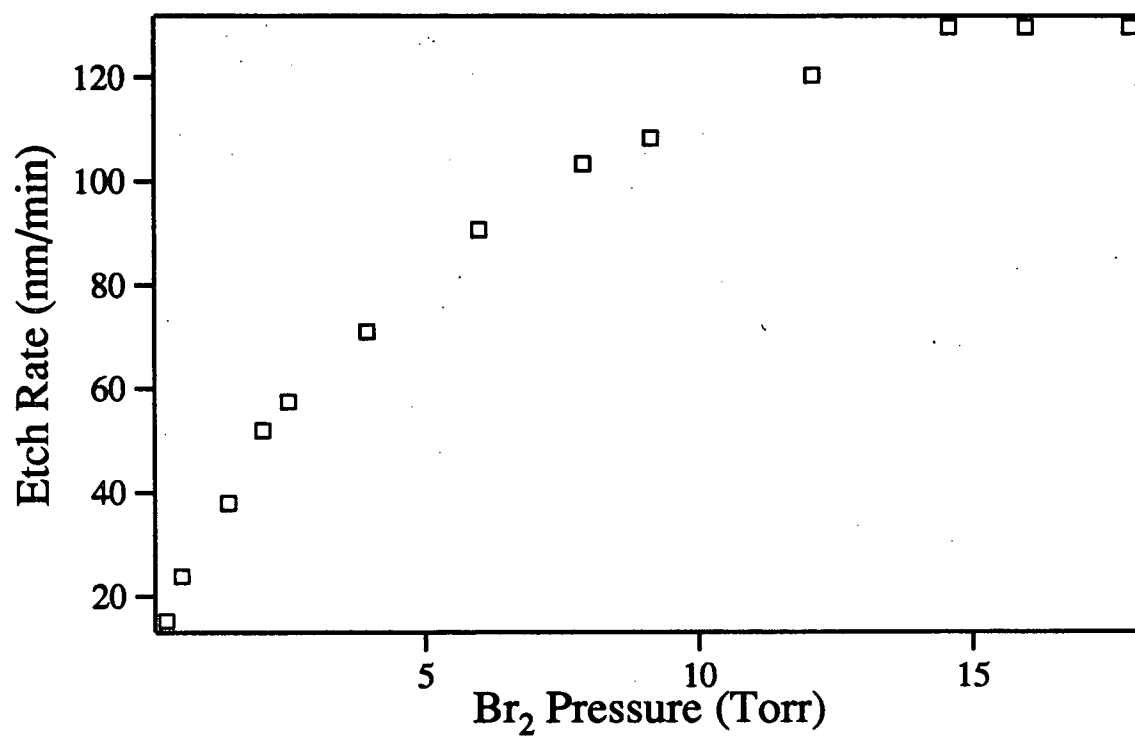
Figure 4.1 Etch rate versus Br$_2$ pressure for the etching of silicon (100) for data extracted from Sveshnikova et al.[47]
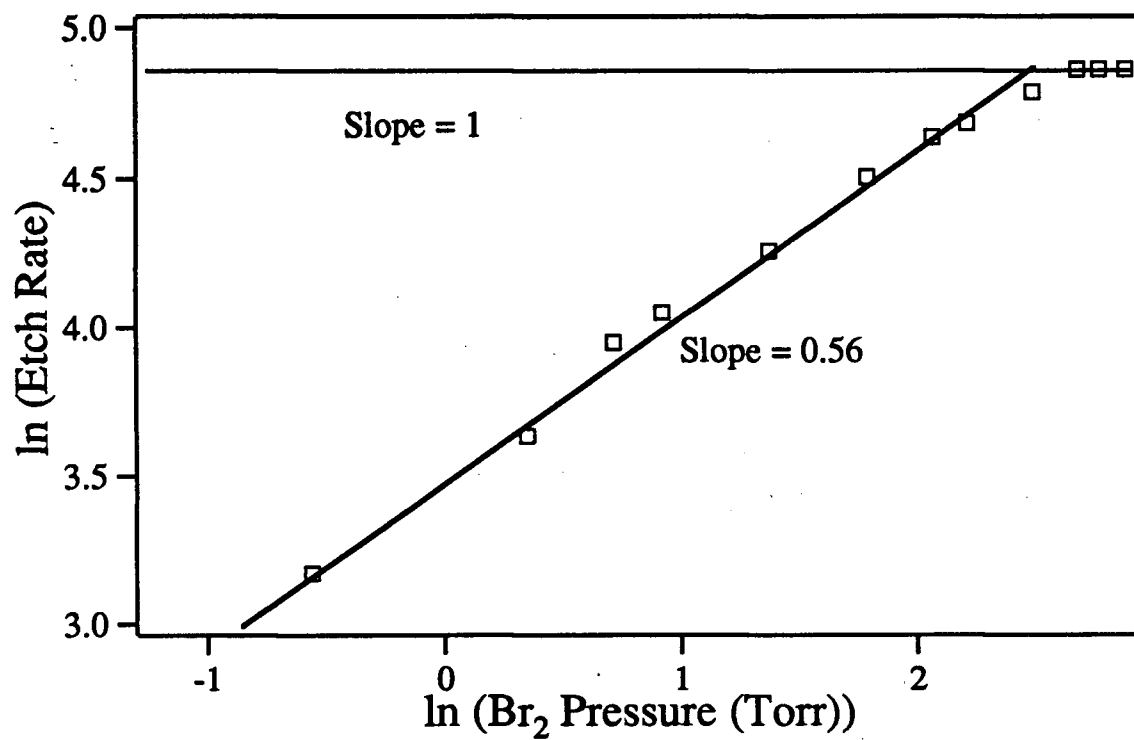
Figure 4.2 ln (etch rate) versus ln (Br_2 Pressure) for etching of silicon (100) taken from Sveshnikova et al.[47]

as predicted by equation (4.29) at low pressures. Also the abrupt change in reaction order from half order to zero order at a Br_2 partial pressure of 15 Torr is difficult to explain. It is possible that because the etching experiments were carried out in an atmosphere of Ar, the reaction becomes limited by the diffusion of reactant to the surface. This can only be considered speculation in view of the limited experimental details provided. It is interesting to note that in a previous study, Sveshnikova et al.[76] reported an increase of 63% in the etch rate for silicon (100) upon going from a Br_2 pressure of 34 to 180 Torr at a temperature of 450 °C. This suggests the saturation limit reported in their second paper may be due to their experimental technique as opposed to a fundamental characteristic of the reaction.

The half order Br_2 pressure dependency of the etching reaction is indicative of a mechanism involving at least two elementary steps, the first step being the reversible dissociation of Br_2 producing Br atoms and the second step being the subsequent reaction of those atoms with the silicon surface in a first order rate controlling process. The dissociation of Br_2 must be reversible in order for the half order dependence to be observed and may be occurring on the silicon surface or in the gas phase. Each of these two possibilities will be addressed separately beginning with dissociation on the silicon surface.

4.3.1.1 The Reversible Dissociative Adsorption Mechanism

This mechanism can then be written

$$Br_2 \underset{k_{-4}}{\overset{k_4}{\rightleftharpoons}} 2\,Br_{ads} \qquad\qquad (4.30, 4.-30)$$

$$Br_{ads} \xrightarrow{\ k_5\ } SiBr_x \qquad\qquad (4.31)$$

where Br_2 is the gas phase bromine molecule and Br_{ads} is a Br atom adsorbed on what is probably a partially brominated surface. The first step is the reversible dissociative adsorption of Br_2 on such a silicon surface with the equilibrium given by the rate constants k_4/k_{-4}. The second step is the reaction of an adsorbed bromine atom (Br_{ads}) to produce a species which is either gaseous

product (where x=1,2,3 or 4 depending upon the temperature) or some precursor which forms that product in a subsequent non rate-determining step. It follows that the etch rate in units of nm min^{-1} (i.e. units which are independent of surface area) is determined by the rate of reaction (4.31), i.e.

$$\text{Etch Rate} = k_5 [Br_{ads}]. \tag{4.32}$$

Once a constant etch rate is established, the rate of formation of Br_{ads} is equal to its rate of removal, i.e.

$$2k_4 P_{Br_2} = 2k_{-4}[Br_{ads}]^2 + k_5[Br_{ads}] \qquad . \tag{4.33}$$

Solving this quadratic equation for Br_{ads} yields

$$[Br_{ads}] = \frac{k_5}{4k_{-4}} \left(1 + \frac{16k_4 k_{-4}}{k_5^2} P_{Br_2}\right)^{1/2} - \frac{k_5}{4k_{-4}} \qquad . \tag{4.34}$$

Substituting this expression into equation (4.32) and rearranging yields

$$\text{Etch Rate} = \frac{k_5^2}{4k_{-4}} \left(1 + \frac{16k_4 k_{-4}}{k_5^2} P_{Br_2}\right)^{1/2} - \frac{k_5^2}{4k_{-4}} \qquad . \tag{4.35}$$

At low bromine pressures where the term within the square root approaches 1,

$$\left(1 + \frac{16k_4 k_{-4}}{k_5^2} P_{Br_2}\right)^{1/2} \approx \left(1 + \frac{16k_4 k_{-4}}{2k_5^2} P_{Br_2}\right) \tag{4.36}$$

and equation (4.35) reduces to

$$\text{Etch Rate} = 2k_4 P_{Br_2} \tag{4.37}$$

i.e. the reaction becomes first order with respect to bromine pressure as the dissociative adsorption equilibrium breaks down.

At high bromine pressures, $16(k_4 k_{-4}/k_5^2)P_{Br_2} \gg 1$, and equation (4.35) reduces to

$$\text{Etch Rate} = k_5 \left(\frac{k_4}{k_{-4}}\right)^{1/2} P_{Br_2}^{1/2} - \frac{k_5^2}{4k_{-4}}$$

(4.38)

This rate law is consistent with the empirical rate law obtained at high pressures given by equation (3.2). By using the slopes and intercepts calculated from plots of etch rate versus $(Br_2 \text{ pressure})^{1/2}$ and given in Tables 3.1 through 3.6, values for the first order rate constants which control the etch rate at low pressures, k_4, and the half order constants which control the etch rate at high pressures, $(k_4/k_{-4})^{1/2}k_5$, have been calculated and are listed as a function of temperature in Table 4.1. Also included in this table are the errors associated with each rate constant value. These errors are based on the uncertainties in determining the slopes and intercepts in plots of etch rate versus $(Br_2 \text{ pressure})^{1/2}$. Due to the scatter in the experimental data collected for the first three wafers, namely AT1, AT2 and silicon (100), accurate values for the intercepts could not be determined. This prevented the determination of the first order rate constant k_4 for these wafers.

The temperature dependencies of the low-pressure first-order rate constant k_4 and the "composite" half order rate constant $(k_4/k_{-4})^{1/2}k_5$, which are listed in Table 4.1, can be used to obtain the activation enthalpies for the processes which they control. An Arrhenius form for that temperature dependency has been assumed. Arrhenius plots of $\ln(k_4)$ and $\ln(k_4/k_{-4})^{1/2}k_5)$ versus $1/T$ can be constructed for the wafers AT1, AT2, silicon (100), BN1, BN2, and BN3 (Figures 4.3, 4.4, 4.5, 4.6, 4.7, and 4.8 respectively). Activation enthalpies and preexponential factors, along with their uncertainties, are calculated from a weighted linear least squares fit of these plots and given in Table 4.2. Although values for all six wafers are presented in the Table 4.2, those obtained for the last three wafers, namely BN1, BN2 and BN3, are considered the most accurate. The etch rates for these wafers were obtained using the high purity (99.99+%) Br_2 and only once the system and etching procedure were optimized. Rather than discarding the earlier results, they

124

Table 4.1 Rate constants k_4 and $(k_4/k_{-4})^{1/2}k_5$ for Br_2 etching of intrinsic and n-type silicon.

Wafer	Temperature (°C)	k_4 (nm min^{-1} Torr^{-1})	$(k_4/k_{-4})^{1/2}k_5$ (nm min^{-1} Torr$^{-1/2}$)
intrinsic (AT1)	476	N/A	11.1 ± 0.5
	500	N/A	22.4 ± 0.6
	520	N/A	33.2 ± 0.9
n-type (AT2)	350	N/A	25.4 ± 0.9
	375	N/A	47.4 ± 1.8
	400	N/A	112 ± 7
silicon (100)	520	N/A	14.2 ± 0.5
	530	N/A	16.3 ± 0.7
	540	N/A	20.5 ± 0.9
	550	N/A	28.4 ± 1.3
	565	N/A	35.9 ± 2.1
	580	N/A	49.6 ± 2.9
intrinsic (BN1)	540	97 ± 12	44.0 ± 0.7
	570	136 ± 13	94.2 ± 1.8
	600	278 ± 21	167 ± 3
n-type (BN2)	360	95 ± 26	41.3 ± 1.1
	385	170 ± 36	81.0 ± 1.4
	410	300 ± 69	139 ± 3
n-type (BN3)	360	62 ± 17	38.0 ± 1.0
	385	136 ± 18	67.3 ± 1.2
	410	196 ± 29	138 ± 3
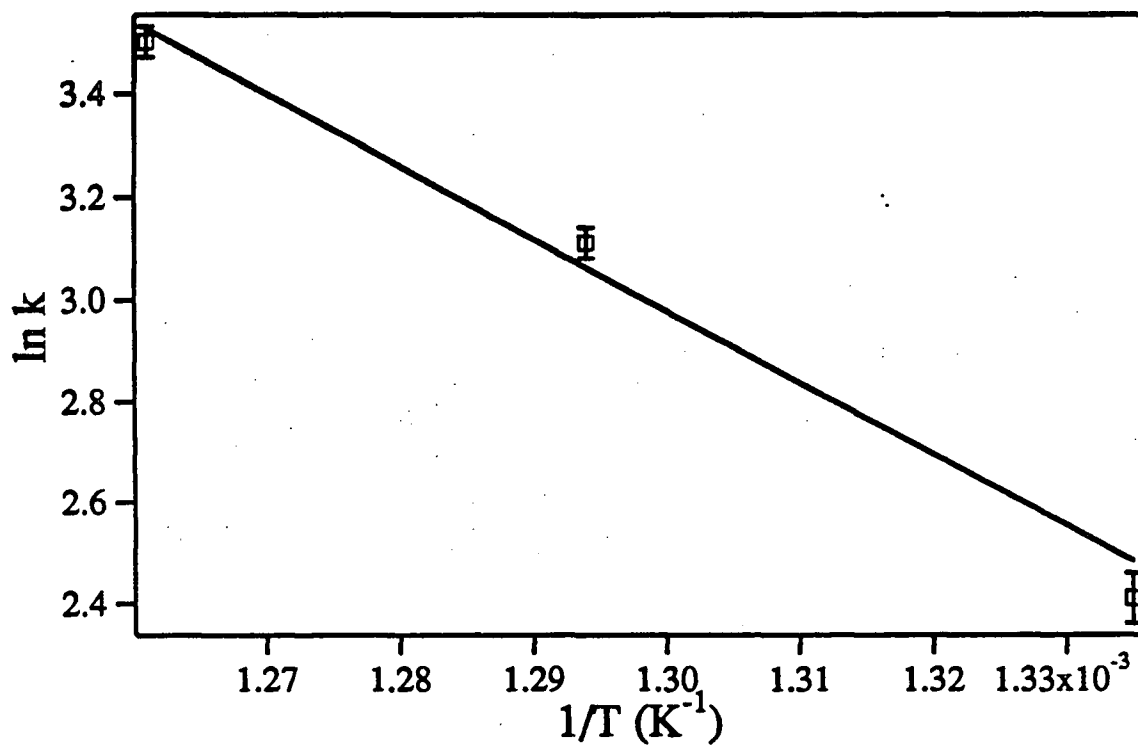
Figure 4.3 ln $(k_5(k_4/k_{-4})^{1/2})$ versus 1/T for Br_2 etching of intrinsic polycrystalline silicon (AT1 wafer).
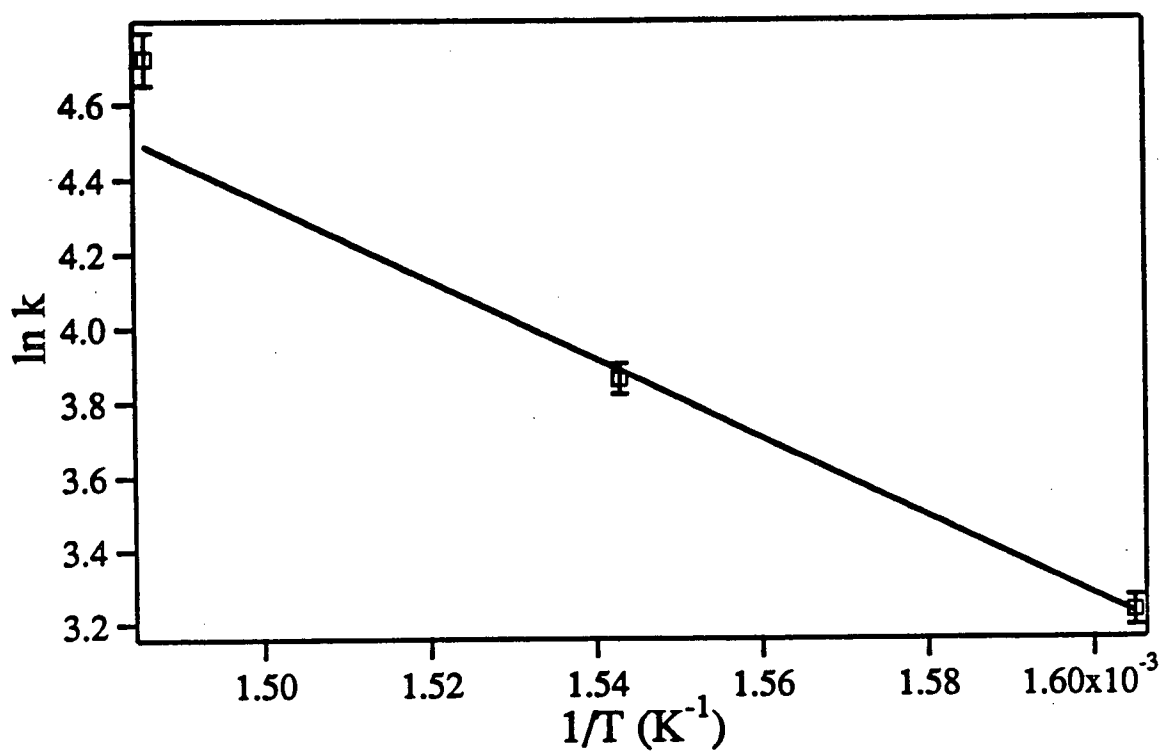
Figure 4.4 ln $(k_5(k_4/k_{-4})^{1/2})$ versus $1/T$ for Br_2 etching of n-type polycrystalline silicon (AT2 wafer).
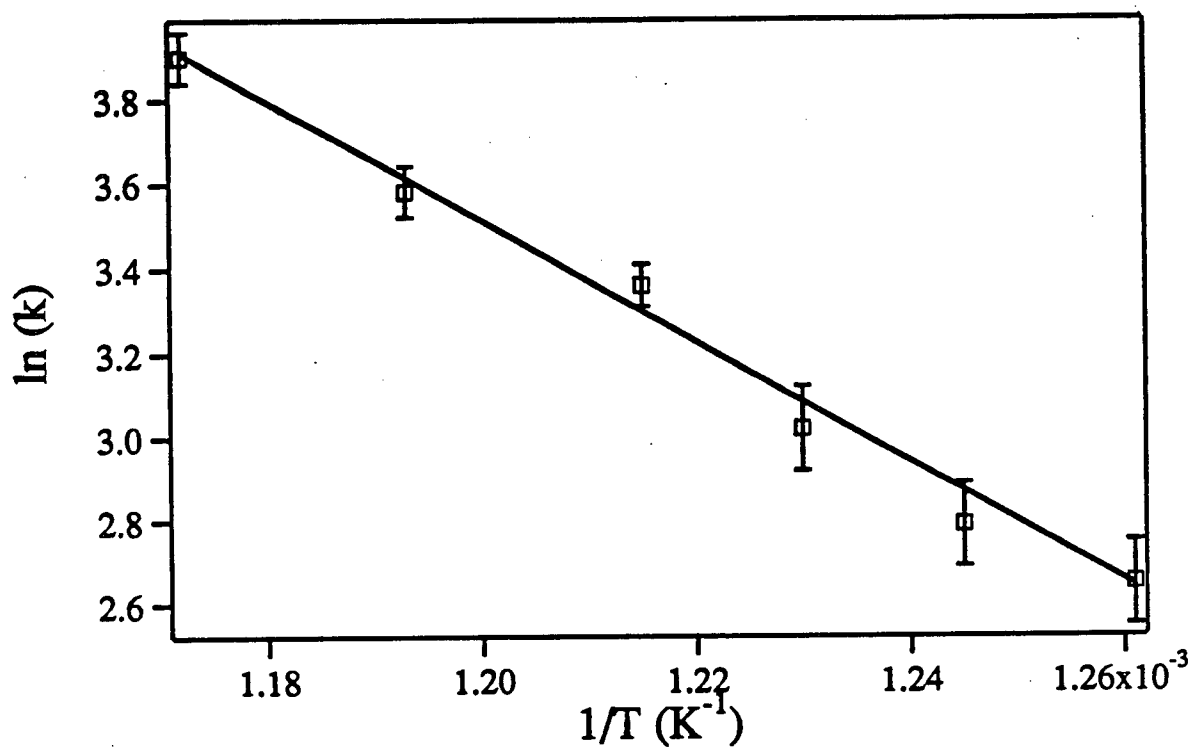
Figure 4.5 ln $(k_5(k_4/k_{-4})^{1/2})$ versus 1/T for Br_2 etching of silicon(100).
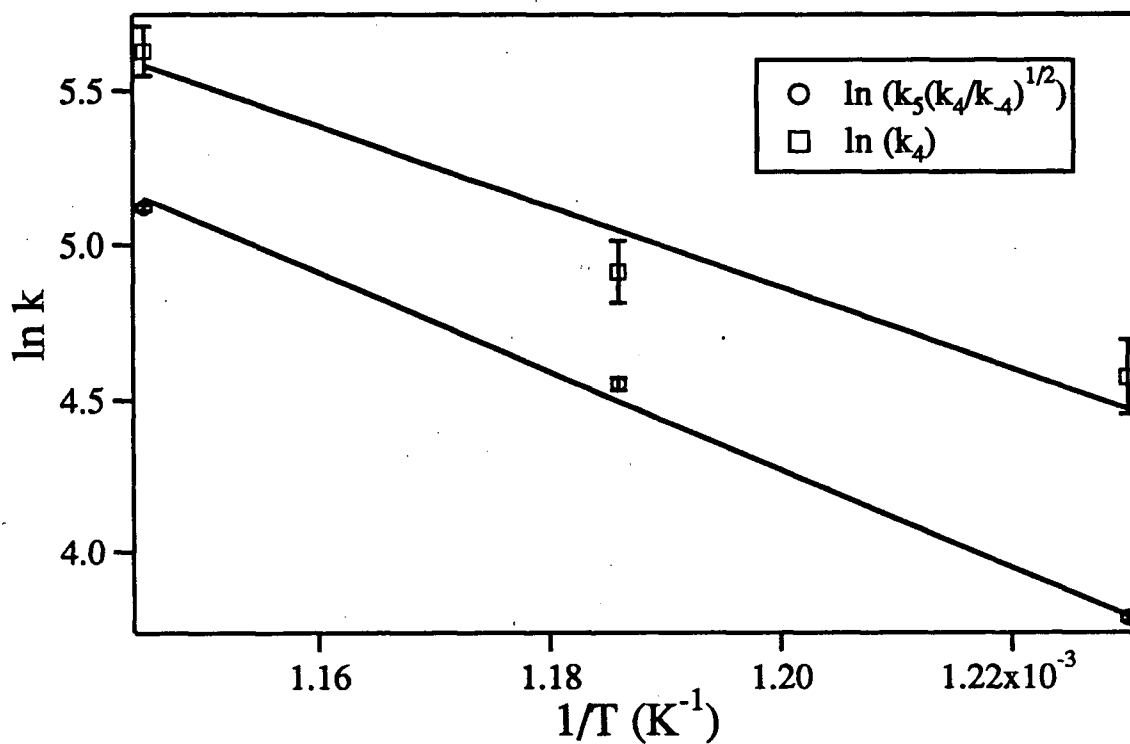
Figure 4.6 ln $(k_5(k_4/k_{-4})^{1/2})$ and ln (k_5) versus 1/T for Br_2 etching of intrinsic polycrystalline silicon (BN1 wafer).
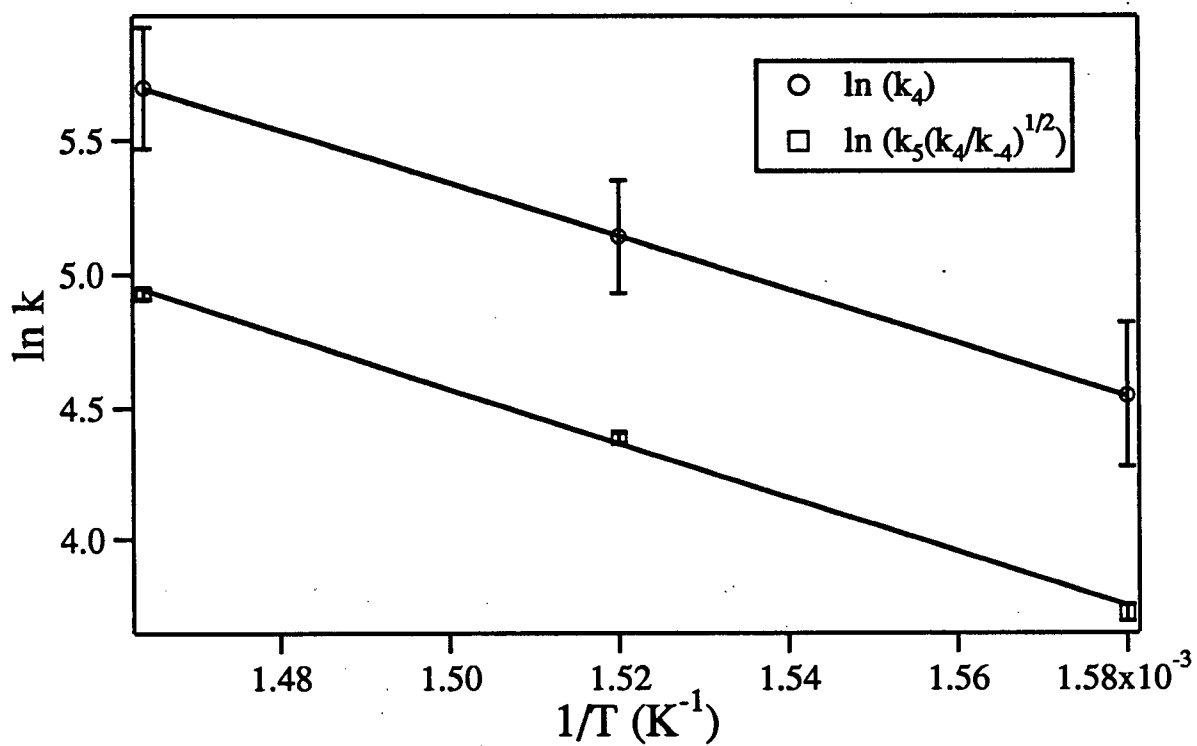
Figure 4.7 ln $(k_5(k_4/k_{-4})^{1/2})$ and ln (k_5) versus 1/T for Br_2 etching of n-type polycrystalline silicon (BN2 wafer).
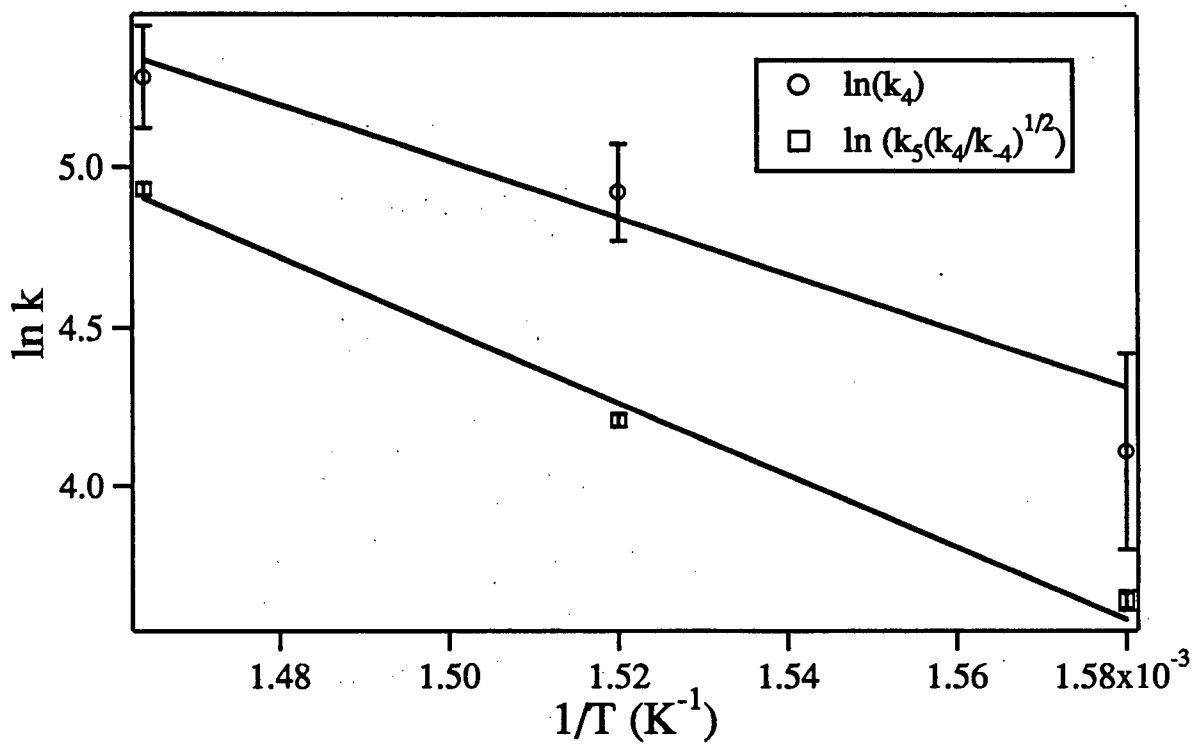
Figure 4.8 ln $(k_5(k_4/k_{-4})^{1/2})$ and ln (k_5) versus 1/T for Br_2 etching of n-type polycrystalline silicon (BN3 wafer).

Table 4.2 Activation enthalpies and preexponential factors for the rate constants $(k_4/k_{-4})^{1/2}k_5$ and k_4 determined from Br_2 etching of silicon.

Rate Constant	$(k_4/k_{-4})^{1/2}k_5$		k_4	
Wafer	A	E_a	A	E_a
	(nm min^{-1} Torr$^{-1/2}$)	kJ mol^{-1}	(nm min^{-1} Torr^{-1})	kJ mol^{-1}
intrinsic (AT1)	$10^{9.3 \pm 1.0}$	118 ± 15	N/A	N/A
n-type (AT2)	$10^{9.8 \pm 1.0}$	100 ± 13	N/A	N/A
silicon (100)	$10^{9.1 \pm 0.4}$	121 ± 7	N/A	N/A
intrinsic (BN1)	$10^{10.1 \pm 0.5}$	131 ± 8	$10^{8.9 \pm 1.5}$	109 ± 23
n-type (BN2)	$10^{8.7 \pm 0.3}$	86 ± 4	$10^{8.8 \pm 2.1}$	83 ± 27
n-type (BN3)	$10^{9.4 \pm 0.7}$	95 ± 8	$10^{8.1 \pm 1.6}$	75 ± 21

are included in the table but meant only to reinforce the more accurate results from the intrinsic wafer BN1 and the two n-type wafers BN2 and BN3.

There are a number of interesting points to be made from the data in Table 4.2. The activation enthalpies for the composite rate constant $(k_4/k_{-4})^{1/2}k_5$ determined from etch rates of the six wafers can be divided into two groups. The intrinsic wafers have values ranging from 118 to 131 kJ mol^{-1}, while those for the n-type wafers have lower values ranging from 86 to 100 kJ mol^{-1}. The activation enthalpies for the first order rate constant k_4 were determined for the last three wafers only and ranged from 75 kJ mol^{-1} for one of the n-type wafer to 109 kJ mol^{-1} for the intrinsic wafer. Since k_4 is the rate constant for the dissociation of Br_2 on the silicon surface, the experimentally determined activation enthalpies are not unreasonable in view of the 198 kJ mol^{-1} bond enthalpy of Br_2. The preexponential factors for these first order rate constants have values that range from 10^8 to 10^9 nm min^{-1} Torr^{-1}, or in units of product flux from the surface, approximately 10^{22} to 10^{23} molec cm^{-2} s^{-1} Torr^{-1}. These values are considerably larger than the collision frequency of Br_2 at the surface which is approximately 10^{20} molec cm^{-2} s^{-1} Torr^{-1}. A preexponential factor larger than collision frequency has also been observed in the atom etching results discussed in section 4.2. In view of the common occurrence of such large preexponential factors, even in the reactions of atoms, it would appear that they are not necessarily an indication of an incorrect mechanism, but simply an indication that the reaction is not an "elementary step" , i.e. it is really a composite of at least two elementary steps. In the present reaction the steps could be the reversible physisorption of a Br_2 molecule on the halogenated silicon surface followed by its dissociation on that surface.

Although the reversible dissociative adsorption mechanism discussed above provides a rationalization for the half order Br_2 pressure dependency of the etching reaction, it is not unique in that regard. Half order kinetics will also prevail if the first step in the reaction, namely reversible dissociation of Br_2 molecules, occurs in the gas phase as opposed to formation on the silicon surface.

4.3.1.2 The Gas Phase Dissociation Mechanism

At the gas pressures employed in this study, the gas phase dissociation of Br_2 is a bimolecular process and can be represented by the reactions

$$Br_2 + Br_2 \underset{k'_{-4}}{\overset{k'_4}{\rightleftharpoons}} Br + Br + Br_2 \qquad\qquad (4.39, 4.-39)$$
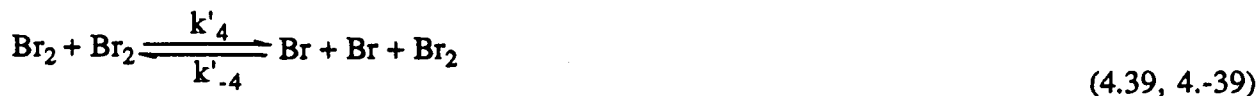
where the recombination of Br atoms is a termolecular process. The Br atoms produced in the gas phase subsequently react with the silicon surface in a first order reaction

$$Br + Si \xrightarrow{\ k_1\ } SiBr_x \qquad . \qquad\qquad (4.40)$$

Reaction (4.40) given above is the same as reaction (4.1), namely that between a gas phase Br atom and the silicon surface, and is therefore controlled by the same rate constant k_1. The overall reaction will display half order dependency on Br_2 pressure as long as reactions (4.39) and (4.-39) maintain an equilibrium concentration of Br atoms, Br_{eq}, over the the silicon surface.

There is the question of whether or not the Br_2 molecules spend sufficient time in the heated region before reaching the silicon sample in order to build up an equilibrium concentration of Br atoms. The time required to reach an equilibrium concentration may be quite long in view of the termolecular collision required in reaction (4.-39). In fact it is easy to calculate the time required to reach $1/e$ of Br_{eq} through gas phase dissociation of Br_2. For the reactions (4.39) and (4.-39), an expression for the change in Br concentration can be written as

$$\frac{dBr}{dt} = 2k_4 \left[Br_2\right]^2 - 2k_{-4}\left[Br\right]^2 Br_2 \qquad . \qquad\qquad (4.41)$$

If we assume the degree of dissociation is small and the concentration of Br_2 remains constant, then rearranging equation (4.41) leads to the expression

134

$$\int \frac{dBr}{\left(\frac{k_4}{k_{-4}}Br_2 - (Br)^2\right)} = \int 2k_{-4}Br_2 dt \qquad \text{.}$$

$$(4.42)$$

Integrating both sides and substituting $Br_{eq} = (k_4 Br_2/k_{-4})^{1/2}$ yields

$$t = \frac{1}{4Br_{eq}k_{-4}Br_2} \ln\left(\frac{Br_{eq} + Br_t}{Br_{eq} - Br_t}\right)$$

$$(4.43)$$

where Br_t is the Br atom concentration at time t. The rate constant k_{-4} has been determined by Ip and Burns[77] and was found to have a value of

$$\log_{10}(k_{-4}) = 10.89 - 3.01 \log_{10}(T/300) \qquad (4.44)$$

with k_{-4} in units of l^2 mol^{-2} s^{-1}. Evaluating this expression for a temperature of 600 °C and converting to more convenient units, k_{-4} is equal to 1.01 Torr^{-2} s^{-1}. Using this value for k_{-4} and a Br$_2$ pressure of 1 Torr, a time of 7 seconds is required in order for the Br atom concentration to reach 1/e of its equilibrium value. For the molecular etching reactor described in section 2.2.1 and under this temperature and Br$_2$ pressure, the Br$_2$ flow velocity is 90 cm s^{-1}. This results in a resident time of less than 80 milliseconds for Br$_2$ molecules in the heated region of the flow reactor before they arrive at the silicon surface. Since half order kinetics are observed only if the Br atom concentration is near the equilibrium value, it is clear that Br$_2$ gas phase dissociation occurs too slowly to account for the experimental results. However there is an alternative route for the formation of Br atoms prior to adsorption and subsequent reaction on the silicon surface, namely the dissociation of Br$_2$ on the reactor walls in the heated region upstream from the sample.

4.3.1.3 The Wall Catalyzed Dissociation Mechanism

This mechanism can be represented by the reactions

$$\text{Br}_2 + \text{wall} \underset{k''_{-4}}{\overset{k''_4}{\rightleftharpoons}} \text{Br} + \text{Br} + \text{wall}$$

$$\text{Br} + \text{Si} \xrightarrow{k_1} \text{SiBr}_x \qquad . $$

(4.45, 4.-45)

(4.46)
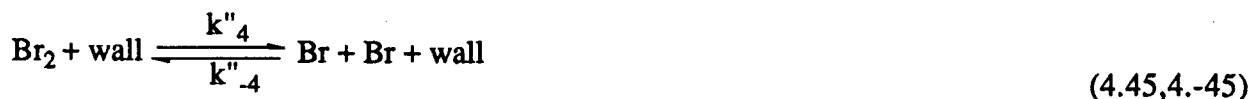
The wall catalyzed recombination of Br atoms in reaction (4.-45) is relatively fast at low pressures compared to the gas phase three body reaction given in (4.-39) and can provide a significant pathway for Br atom recombination under the experimental conditions employed in this study. The rate constant k_4'' has not been published, although values for the recombination coefficient, γ, ranging from 6×10^{-5} and 4×10^{-4} for oxy-acid coated Pyrex surfaces[66,78] to less than 10^{-3} for clean Pyrex surfaces[79] have been reported. Provided we write $k_4''\text{wall}=k_4$, $k_{-4}''\text{wall}=k_{-4}$, $k_1\text{Si}=k_5$ and $\text{Br}=\text{Br}_{ads}$, then the set of equations (4.32 to 4.38) developed for the reversible dissociative adsorption mechanism may be applied to the present one. The rate constants now take on a slightly different meaning. (1) The rate constant k''_4 governs the dissociation of Br_2 into gas phase atoms and must have an activation enthalpy equivalent to the bond enthalpy of Br_2 (i.e. 198 kJ mol^{-1}). (2) The preexponential factor for k''_4 contains a measure of the surface area available for the dissociation of Br_2. This area corresponds to the inner walls of the heated portion of the reactor tube located upstream from the silicon sample. This area is orders of magnitude larger than the surface area of the sample being etched and could account for the larger than collision frequency preexponential factor determined experimentally for k''_4.

Assuming wall-catalyzed dissociation is capable of producing an equilibrium concentration of Br atoms over the silicon surface, is the concentration sufficient to account for the observed etch rates? An expression for k_1 was experimentally determined by measuring the etch rate of intrinsic (BN1) and n-type (BN2) silicon in the presence of Br atoms produced upstream in a microwave discharge (section 4.2.1). By calculating the Br_{eq} concentrations from thermodynamic data[80] (which can be as high as 3% of the Br_2 concentration at 600 °C) and by making use of the rate constant expressions for k_1 provided in equation (4.2) and (4.3) for intrinsic and n-type silicon respectively, it is possible to calculate the etch rates expected from Br_{eq}. The etch rates calculated for the three experimental temperatures employed in etching each wafer are plotted versus Br_2 pressure (solid lines) in Figures 4.9 and 4.10 for intrinsic and n-type silicon respectively. Also
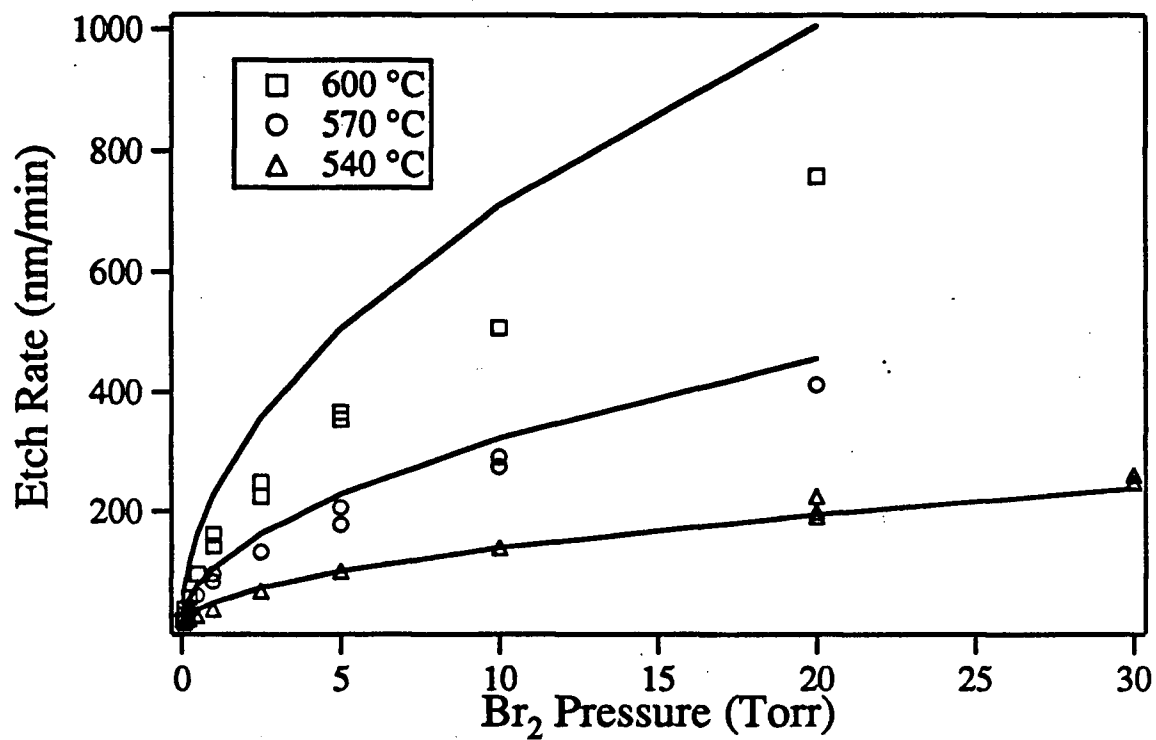
Figure 4.9 Etch rate of intrinsic polycrystalline silicon (BN1 wafer) versus Br_2 pressure. Solid lines represent predicted etch rates based on Br_{eq} concentrations.
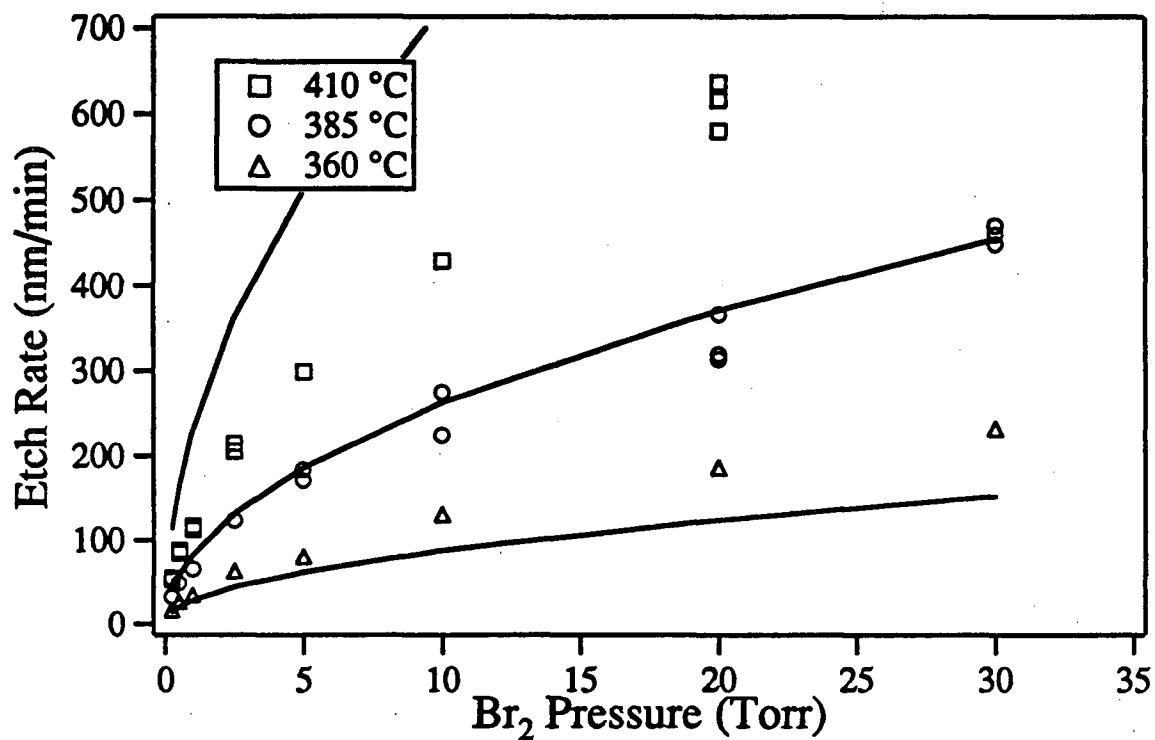
Figure 4.10 Etch rates of n-type polycrystalline silicon (BN2 wafer) versus Br_2 pressure. Solid lines represent predicted etch rates based on Br_{eq} concentrations.

included in these plots are the experimentally measured Br_2 etch rates for the same two wafers originally presented in Figures 3.10 and 3.12.

The preexponential factor in k_1, determined from the etching of intrinsic silicon, was adjusted within the experimental error limits to pin the calculated etch rates to those measured at the lowest of the three temperatures. The etch rates for the two higher temperatures were then calculated using the adjusted preexponential factor (Figure 4.9). From the data presented, it is obvious that Br_{eq} atom concentrations could account for the observed Br_2 etch rates of intrinsic polycrystalline silicon. However, it is curious that the predicted etch rates at the two higher temperatures lie above those measured experimentally. In fact it is not difficult to show that in order to fit the data at all three temperatures, the activation enthalpy for the Br atom etching of silicon would have to be approximately 35 kJ mol^{-1} in the temperature range of 540 to 600 °C and not the 63 kJ mol^{-1} determined experimentally in the lower temperature range of 310 to 470 °C. It should be pointed out that this discrepancy in activation enthalpies is not strong evidence against this mechanism for the following reason. The preexponential factor in k_1 was found to be larger than that expected based on collision frequency and suggested the presence of at least two elementary reaction steps. It is possible that at the higher temperatures employed in the Br_2 etching experiments, the atom etching reaction may proceed by a different rate controlling step with a smaller activation energy.

For the etching of n-type silicon, choosing the maximum error limits of the preexponential factor and activation enthalpy of k_1, the etching from Br_{eq} is still insufficient to account for the observed etch rates at the lowest temperature of 360 as shown in Figure 4.10. The etch rates based on Br_{eq} could account for the observed etch rates at the two higher temperatures of 385 and 410 °C. However, k_1 requires a *negative* activation enthalpy of approximately -15 kJ mol^{-1} in order for the predicted etch rates based on Br_{eq} to fit the experimentally measured rates. This negative activation enthalpy for k_1 is in contrast to the 55 kJ mol^{-1} measured from Br atom etching experiments, albeit in the lower temperature range of 140 to 270 °C.

There is a further difficulty with the wall-catalyzed dissociation mechanism in view of the experimentally measured rate constants. Since k''_4 is the rate constant for the dissociation of Br_2

(with the wall behaving as a third body), it should have an activation enthalpy of 198 kJ mol^{-1}. Experimentally a much lower value of 109 kJ mol^{-1} was determined for the etching of intrinsic silicon. The values obtained for the etching of n-type silicon were even lower at 83 and 75 kJ mol^{-1} for the wafers BN2 and BN3 respectively.

In view of the inability of the gas phase dissociation and wall-catalyzed dissociation mechanisms to account for the observed reaction rates and activation enthalpies, the reversible dissociative adsorption mechanism is considered the most reasonable in describing the reaction of Br$_2$ with silicon.

4.3.1.4 Conclusions From the Br$_2$ Etching Experiments

In view of the discrepancies between these last two mechanisms and the observed reaction kinetics, only the reversible dissociative adsorption mechanism appears to be consistent with the experimental results. There are two additional pieces of evidence which lend further support to the reversible dissociative adsorption mechanism. The etching reaction was faster for n-type than intrinsic silicon and the enhancement in the resulting etch rates were larger for Br atoms than for Br$_2$, as discussed in detail in section 4.5. If silicon etching by Br$_2$ proceeded through gas phase dissociation producing the species Br, then the enhancements in etch rates for both molecular and atomic etchants should be similar. The fact that this is not observed lends supports to a mechanism whereby Br$_2$ first adsorbs onto the silicon surface and then undergoes dissociation. The second piece of evidence comes from the thermal desorption spectroscopy study by Jackman et al.[44] originally discussed in section 1.3.2.2.3. The results from this study clearly demonstrate the ability of Br$_2$ to dissociate on and react with an intrinsic silicon surface producing various silicon bromide species, Br and Br$_2$ at the temperatures employed in this study.

The reaction of Br$_2$ with silicon is characterized by two rate constants. The first order rate constant k_4 dominates at low pressures and a half order composite rate constant $(k_4/k_{-4})^{1/2}k_5$ dominates at high pressures. Activation enthalpies and preexponential factors determined for these two constants are summarized in Table 4.2.

140

4.3.1.5 Potential Energy Curves for Etching of Silicon by Br_2

A potential energy level diagram for Br_2 etching of intrinsic (BN1) and n-type (BN2 and BN3) silicon can be constructed from the activation enthalpies summarized in Table 4.2. These curves are presented in Figures 4.11, 4.12 and 4.13 for the three wafers respectively. Since it was not possible to determine k_4 activation enthalpies for Br_2 etching of wafers AT1, AT2 and silicon (100), results from these wafers are not presented in potential energy curve diagrams. The position of $Br_{2(g)}$ is assigned a value of 0 kJ mol^{-1} on the potential energy scale. The potential energy curve for Br_2 etching contains two maxima. The first maximum corresponds to the dissociation of Br_2 on the silicon surface leading to the formation of $2Br_{ads}$. This reaction step is governed by the rate constant k_4 and found to have activation enthalpies of 109 kJ mol^{-1} for intrinsic silicon and 83 and 75 kJ mol^{-1} for the two n-type wafers. The second maximum corresponds to the reaction of Br_{ads} leading to formation of product. The position of this barrier is only known with respect to $Br_{2(g)}$ by the activation enthalpy for the composite rate constant $(k_4/k_{-4})^{1/2}k_5$. This places the second maxima at 131 kJ mol^{-1} for intrinsic silicon and at 86 and 95 kJ mol^{-1} for the two n-type wafers. The energy difference between Br_{ads} and the second maximum corresponds to the activation enthalpy associated with k_5, which is unknown. The positions of $2Br_{ads}$ and Br_{ads} between the two maxima are therefore also undetermined except that Br_{ads} must lie at one half the energy of $2Br_{ads}$ relative to $Br_{2(g)}$. The formation of product is highly favoured thermodynamically. The position of product in the diagrams is therefore very negative and is not included.

4.3.1.6 On the Transition State for the Br and Br_2 Etching Reactions

An obvious question is whether the Br atom etching reaction proceeds through the same intermediate (Br_{ads}) observed in Br_2 etching. The experimentally determined activation enthalpies suggest that it does not. For Br_2 etching of intrinsic silicon the position of the second maxima is only 32 kJ mol^{-1} higher in energy than $Br_{(g)}$ (i.e. 1/2 of 198 kJ mol^{-1}), whereas the activation enthalpy for the corresponding atom reaction is 63 kJ mol^{-1}. For n-type silicon the position of the second maxima is negative with respect to $Br_{(g)}$ whereas the activation enthalpy for the corresponding atom reaction is 55 kJ mol^{-1}. This anomaly can be explained if the reaction of gas

141
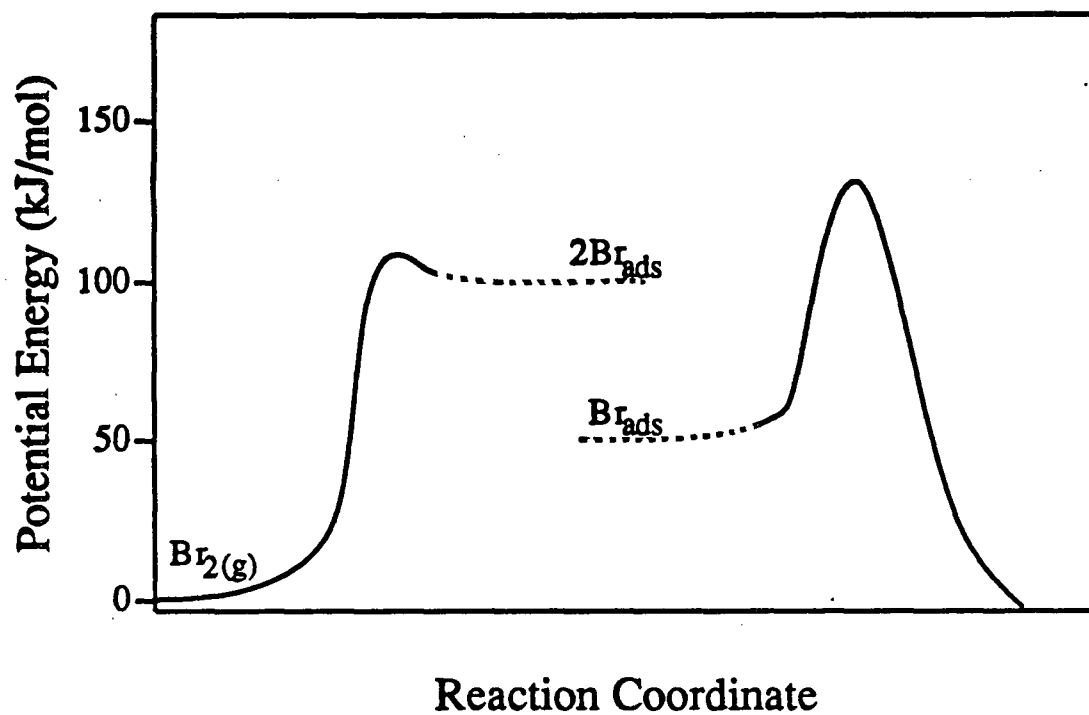
Figure 4.11 Potential Energy Curve Diagram for Br_2 etching of intrinsic polycrystalline silicon (BN1 wafer).
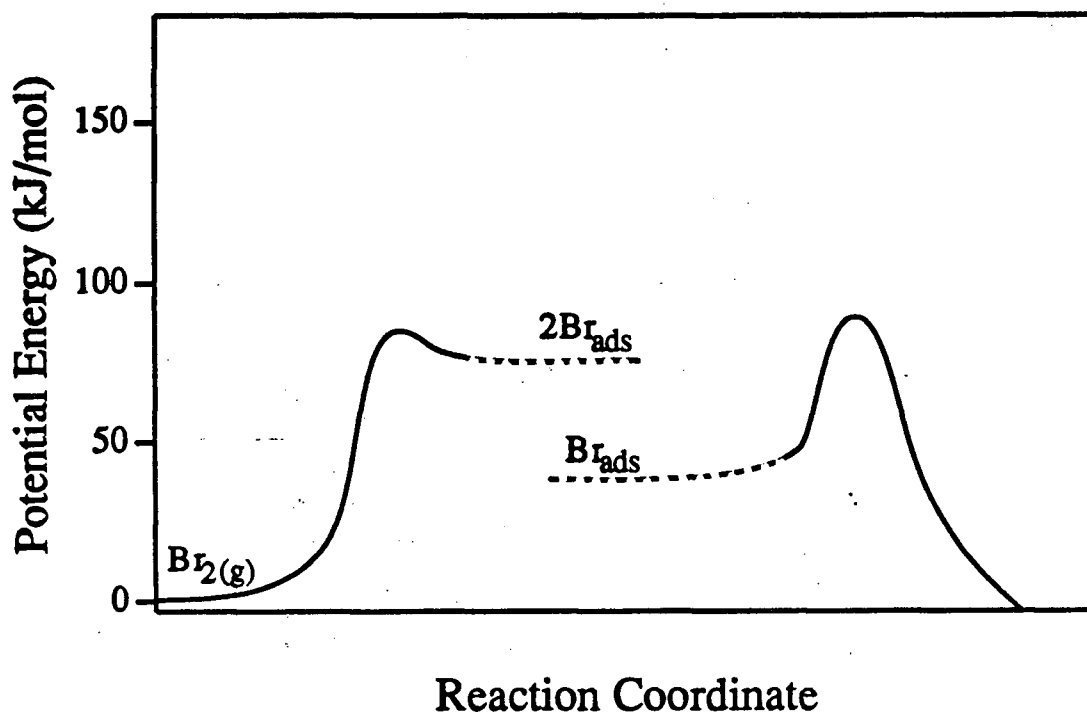
Figure 4.12 Potential Energy Curve Diagram for Br_2 etching of n-type polycrystalline silicon (BN2 wafer).
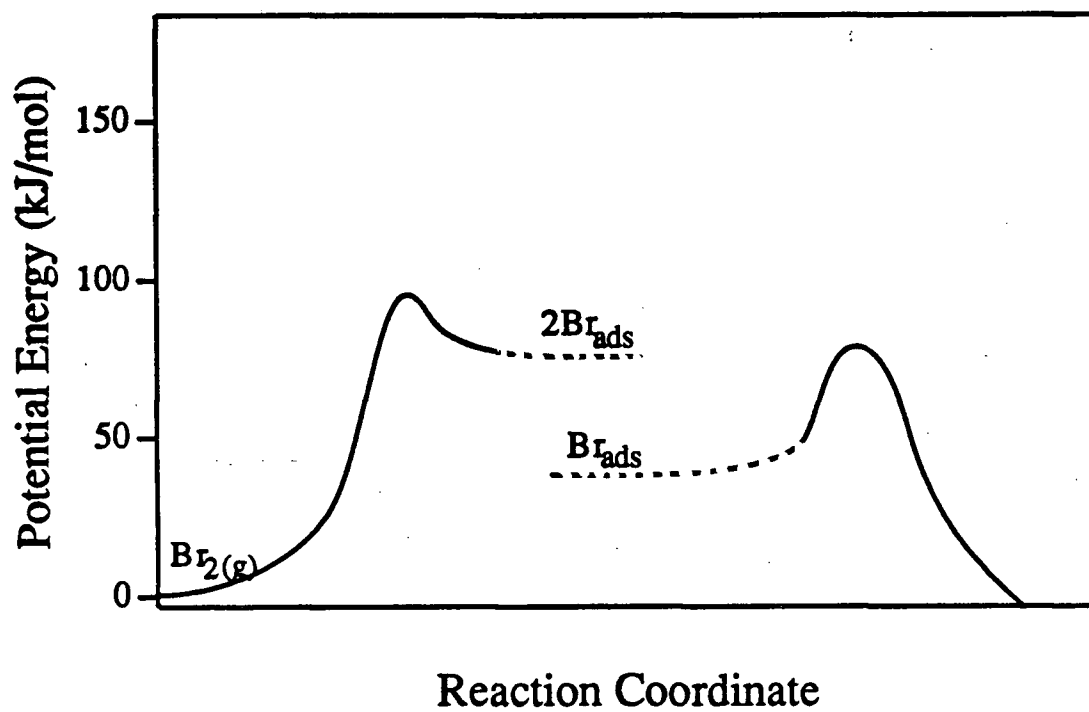
Figure 4.13 Potential Energy Curve Diagram for Br_2 etching of n-type polycrystalline silicon (BN3 wafer).

phase Br atoms passes through a different rate controlling step. Such a situation is not unreasonable. The formation of product in the reaction of Br_2 with silicon most likely arises from a disproportionation of silicon bromides on the surface, diagrammatically represented in Figure 4.14a. In the reaction of Br atoms with silicon, there is the possibility of a "free" physisorbed Br atom reacting directly with a silicon bromide species on the surface as illustrated in Figure 4.14b, which could be the dominant process forming product molecules. Differences in reaction pathways for F_2 and F etching of silicon have been reported by Stinespring and Freedman[21]. In their x-ray photoelectron spectroscopy study, the authors found that F_2 was dissociatively chemisorbed on silicon forming SiF_2-like surface species. These species were restricted to a monolayer coverage. In contrast, F atom uptake extended well beyond monolayer coverage, suggesting that the atoms were able to penetrate into several atomic layers of the silicon lattice, thus providing an alternative route for product formation.

4.3.2 Cl_2 Etching of Intrinsic and n-type Silicon

From the results presented in section 3.3.1 for Cl_2 etching of intrinsic (BN1) and n-type (BN2) polycrystalline silicon, the reaction rate was found to have a half order dependency on the Cl_2 pressure. The etch rates for the two wafers obeyed the empirical rate expression given in equation (3.2), namely

$$Etch \; rate = C_1(Cl_2 \; pressure)^{1/2} - C_2 \qquad .$$

Assuming an Arrhenius temperature dependency for the constants C_1 and C_2, and using the values of these constants determined at the three temperatures given in Tables 3.8 and 3.9, the following expressions can be used to characterize the etch rates of the two silicon wafers within the temperature and Cl_2 pressure ranges employed.

$$Etch \; Rate \; (intrinsic) = 10^{9.6\pm0.5} \; nm \; min^{-1} \; Torr^{-1/2} \; exp^{(-116\pm7 \; kJ/mol)/RT} \; (Cl_2 \; Pressure)^{1/2} \quad (4.47)$$
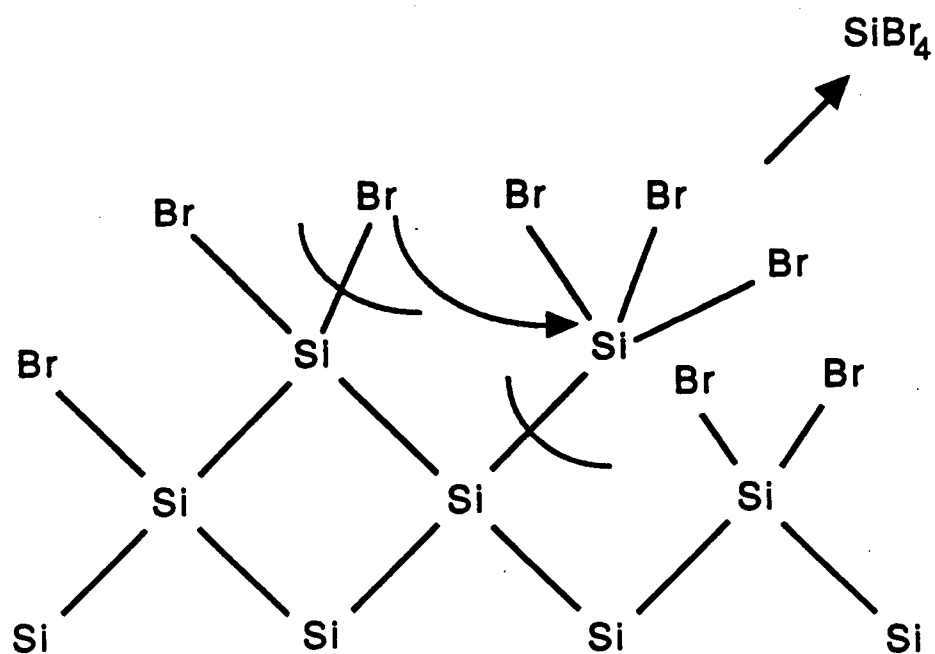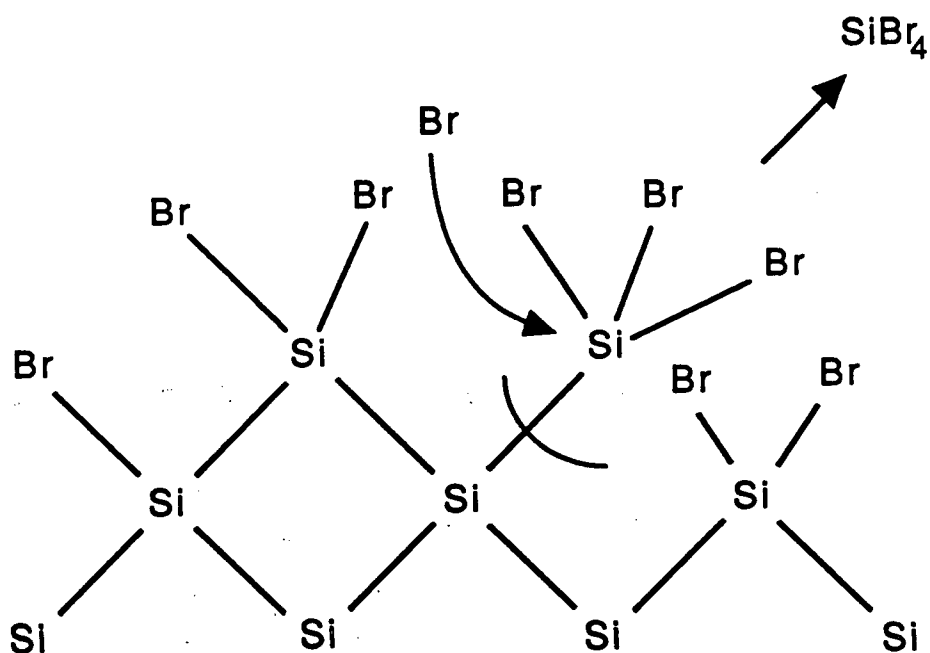
Figure 4.14 Possible reaction pathways for etching of silicon by (a) Br_2 molecules and (b) Br atoms.

Etch Rate (n-type) = $10^{8.2\pm0.2}$ nm min^{-1} Torr$^{-1/2}$ exp $^{(-82\pm3\,\text{kJ/mol})/RT}$ (Cl$_2$ Pressure)$^{1/2}$

$$- 10^{7.1\pm0.9} \text{ nm min}^{-1} \text{ exp }^{(-77\pm12\,\text{kJ/mol})/RT} \qquad (4.48)$$

Because of scatter in the etch rate data for intrinsic silicon, values for C_2 could not be determined and as a result the etch rate is given simply by C_1 multiplied by (Cl$_2$ pressure)$^{1/2}$. However, the values for C_2 are relatively small compared to C_1, and the contribution of C_2 to the overall etch rate is accordingly small. For example, at 400 °C and 10 Torr Cl$_2$, the etch rate for n-type silicon differs by only 6% when contributions from C_2 are neglected.

Although the half order dependency observed for the Cl$_2$ etching is consistent with the Br$_2$ etching results, it is not the interpretation proposed by Ogryzlo et al.[41] for the non-linear increase in the etch rate of n-type polycrystalline silicon with increasing Cl$_2$ pressure. The authors attributed the levelling off of the etch rate to a saturation of surface adsorption sites. Such a mechanism predicted a plateau in the etch rate resulting from the saturation of surface adsorption sites where zero order kinetics would be observed. However this plateau in etch rates was not observed at the maximum Cl$_2$ pressure of 10 Torr employed in their study, nor at the 30 Torr employed in the present study. Although their etch rate versus Cl$_2$ pressure data did produce a linear 1/(etch rate) versus 1/(Cl$_2$ pressure) plot as predicted by their mechanism, plotting the same etch rate data versus (Cl$_2$ pressure)$^{1/2}$ also provides an acceptable straight line (Figure 4.15). The four lower pressure points are well represented by a linear fit, with the highest pressure point falling below the line. For such a limited number of data points spanning a limited pressure range of 1 to 10 Torr, the half order kinetics appear equally acceptable in characterizing their results.

4.3.2.1 The Reversible Dissociative Adsorption Mechanism

The similarities between Cl$_2$ and Br$_2$ etching suggest that the reversible dissociative adsorption mechanism can also be used to describe the etching process for the Cl$_2$ system. The mechanism can be written as

$$\text{Cl}_2 \underset{k_{-4}}{\overset{k_4}{\rightleftharpoons}} 2\,\text{Cl}_{\text{ads}} \qquad\qquad (4.49, 4.-49)$$
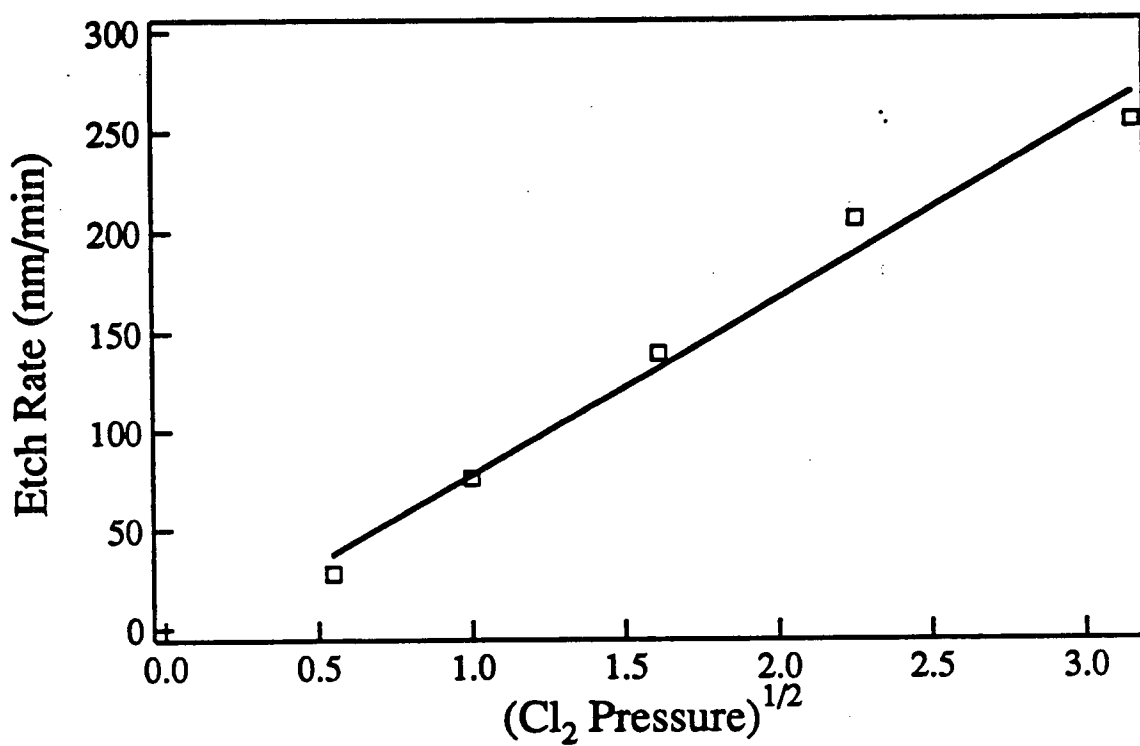
Figure 4.15 Etch rates versus $(Cl_2 \text{ Pressure})^{1/2}$ for etching of n-type polycrystalline silicon reproduced from Ogryzlo et al.[41]

$$Cl_{ads} \xrightarrow{\quad k_5 \quad} SiCl_x \qquad\qquad (4.50)$$

where the dissociation of Cl_2 occurs on a partially chlorinated silicon surface yielding two adsorbed species Cl_{ads}. This adsorbed species Cl_{ads} then reacts in a first order process forming either gaseous product $SiCl_x$, where x=1,2,3 or 4 depending upon temperature, or a precursor which forms that product in a subsequent non rate determining step. Using equations (4.30) to (4.36), analogous expressions can be derived to describe the etch rates at low Cl_2 pressures, i.e.

$$\text{Etch Rate} = 2k_4 P_{Cl_2} \qquad\qquad (4.51)$$

as well as at high Cl_2 pressures, i.e.

$$\text{Etch Rate} = k_5 \left(\frac{k_4}{k_{-4}}\right)^{1/2} P_{Cl_2}^{1/2} - \frac{k_5^2}{4k_{-4}} \qquad\qquad (4.52)$$

This rate law for high pressures is consistent with the empirical rate law given in equation (3.2). It is worth noting that although pressures employed in this study were not low enough to observe the first order kinetics predicted in equation (4.51), Madix and Schwarz[37] did observe a first order pressure dependence of Cl_2 etching of silicon (111) at pressures between 10^{-5} and 10^{-6} Torr and above 1050 K. Below this temperature a deviation from first order kinetics was reported, although the exact nature of that deviation was not specified.

Using the slopes and intercepts determined from plots of etch rate versus (Cl_2 pressure)$^{1/2}$ (Figures 3.24 and 3.26) and provided in Tables 3.7 and 3.8, values for the first order rate constant, k_4, which controls the etching reaction at low pressures, and the half order composite rate constant, $(k_4/k_{-4})^{1/2}k_5$, which controls the reaction at high pressures, have been calculated. Values for these rate constants are given in Table 4.3. Because of scatter in the etch rates for intrinsic silicon, accurate values for the intercepts, i.e. C_2, could not be determined. The magnitude of these intercepts is relatively small and very susceptible to uncertainties in the etch rate data.

Table 4.3. Rate constants k_4 and $(k_4/k_{-4})^{1/2}k_5$ for Cl_2 etching of silicon.

Wafer	Temperature (°C)	k_4 nm min^{-1} Torr^{-1}	$(k_4/k_{-4})^{1/2}k_5$ (nm min^{-1} Torr$^{-1/2}$)
intrinsic (BN1)	510	N/A	72 ± 4
	540	N/A	150 ± 9
	570	N/A	260 ± 13
n-type (BN2)	385	70 ± 10	50.2 ± 1.1
	410	124 ± 17	88.7 ± 1.9
	435	218 ± 40	146 ± 4

Without values for C_2, the rate constant k_4 could not be determined. If an Arrhenius form for the temperature dependence of the rate constants is assumed, then plotting the natural logarithm of the rate constant versus $1/T$ will yield an activation enthalpy and a preexponential factor. These plots for the intrinsic and n-type wafers are presented in Figures 4.16 and 4.17 respectively. The activation enthalpies and preexponential factors calculated from a weighted linear least squares fit of the data are given in Table 4.4. Since the rate constant k_4 controls the dissociation of Cl_2 on the silicon surface, the experimentally determined value of 87 kJ mol^{-1} for intrinsic silicon does not appear unreasonable in view of the 243 kJ mol^{-1} bond enthalpy of Cl_2. An activation enthalpies for $(k_4/k_{-4})^{1/2}k_5$ of 116 kJ mol^{-1} was determined for intrinsic and n-type silicon respectively. The preexponential factor in k_4 has a value of 4×10^{22} molec cm^{-2} s^{-1} $Torr^{-1}$, which is larger than the collision frequency of Cl_2 molecules on the surface. Larger than collision frequency preexponential factor was also observed for k_4 in Br_2 etching. This once again suggests that reversible dissociative adsorption does not occur in a single elementary step, but rather is composed of at least two steps. The first step could be the reversible physisorption of Cl_2 on the silicon surface followed by its dissociation on that surface.

4.3.2.2 The Wall Catalyzed Dissociation Mechanism

It can be argued that, as in the case of Br_2 etching, wall catalyzed dissociation of Cl_2 could produce an equilibrium concentration of Cl atoms, Cl_{eq}, which then react with the silicon surface. Using thermodynamic data[78] to calculate Cl_{eq} and the rate constants for the Cl atom etching of intrinsic and n-type silicon given in equations (4.15) and (4.16) respectively, the etch rates can be calculated based on Cl_{eq}. These etch rates are plotted versus Cl_2 pressure in Figure 4.18 and 4.19 for intrinsic and n-type silicon respectively (solid lines). Also included in the plots are the experimental etch rates measured for the two wafers. For intrinsic and n-type silicon, the predicted Cl_{eq} etch rates are considerably lower than those observed experimentally. It is clear that a gas phase dissociation mechanism cannot account for the observed Cl_2 etch rates, and that only the reversible dissociative adsorption mechanism discussed above is therefore consistent with the experimental results.

151
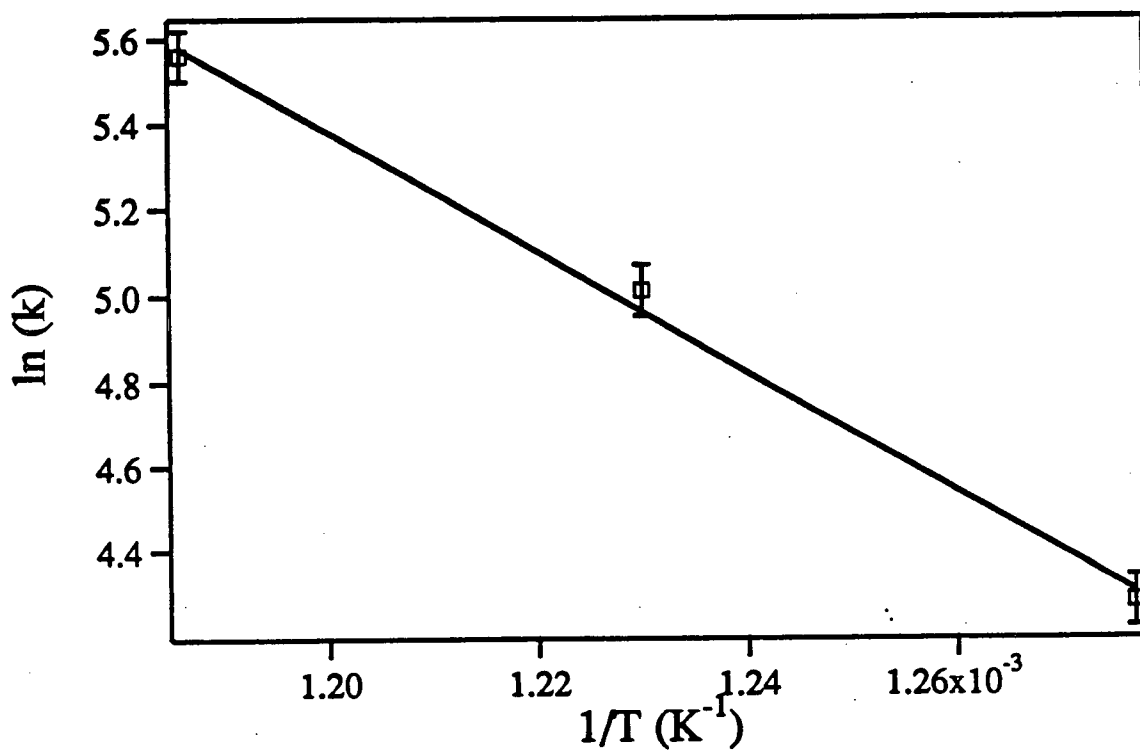
Figure 4.16 ln $(k_5(k_4/k_{-4})^{1/2})$ versus $1/T$ for Cl_2 etching of intrinsic polycrystalline silicon (BN1 wafer).
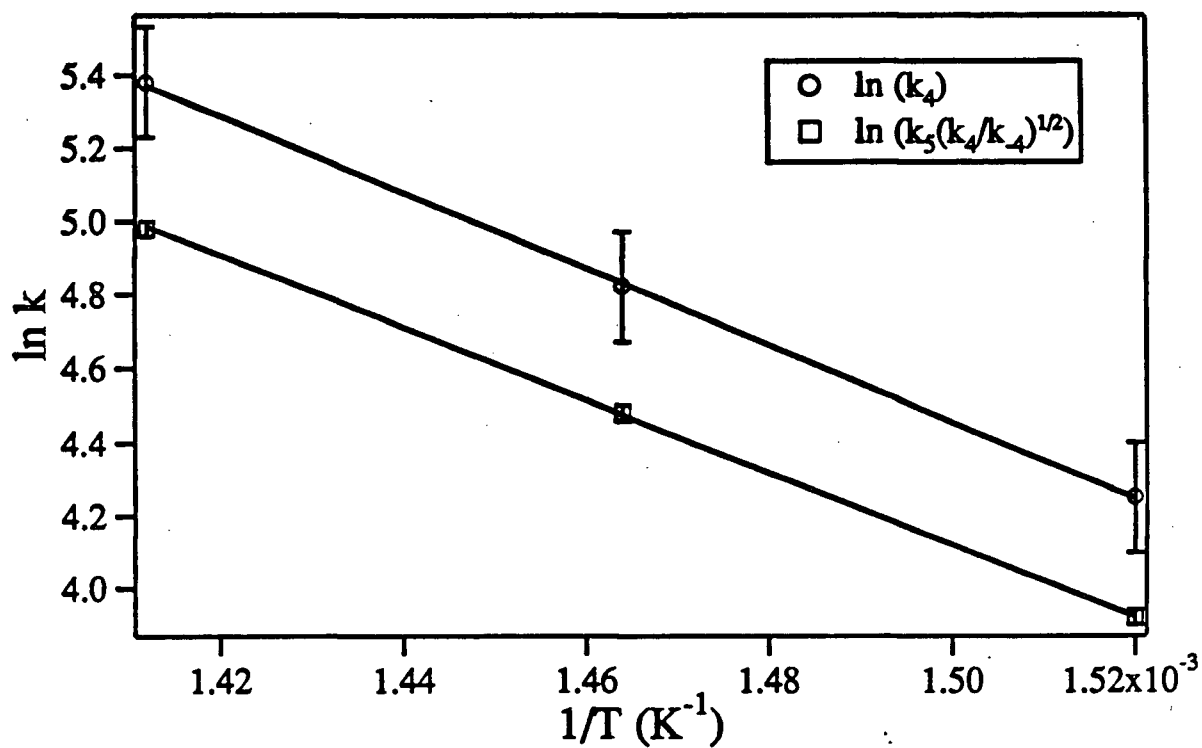
Figure 4.17 ln $(k_5(k_4/k_{-4})^{1/2})$ and ln (k_4) versus 1/T for Cl_2 etching of n- type polycrystalline silicon (BN2 wafer).

Table 4.4. Activation enthalpies and preexponential factors for the rate constants $(k_4/k_{-4})^{1/2}k_5$ and k_4 for Cl_2 etching of silicon.

Wafer	Rate Constant $(k_4/k_{-4})^{1/2}k_5$		Rate Constant k_4	
	A	Ea	A	Ea
	nm min^{-1} Torr$^{-1/2}$	kJ mol^{-1}	nm min^{-1} Torr^{-1}	kJ mol^{-1}
Intrinsic (BN1)	$10^{9.6\pm0.5}$	116 ± 7	N/A	N/A
n-type (BN2)	$10^{8.2\pm0.2}$	82 ± 3	$10^{8.7\pm1.4}$	87 ± 18
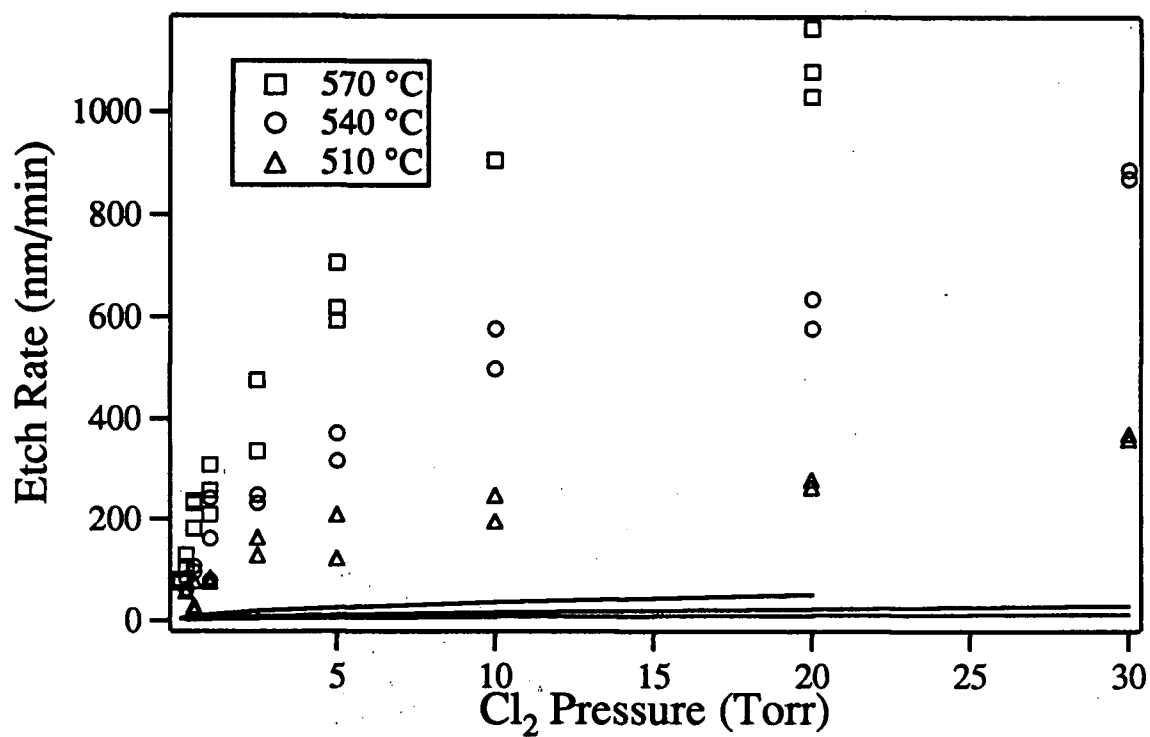
Figure 4.18 Etch rates of intrinsic polycrystalline silicon (BN1 wafer) versus Cl_2 pressure. Solid lines represent predicted etch rates based on Cl_{eq} concentrations.
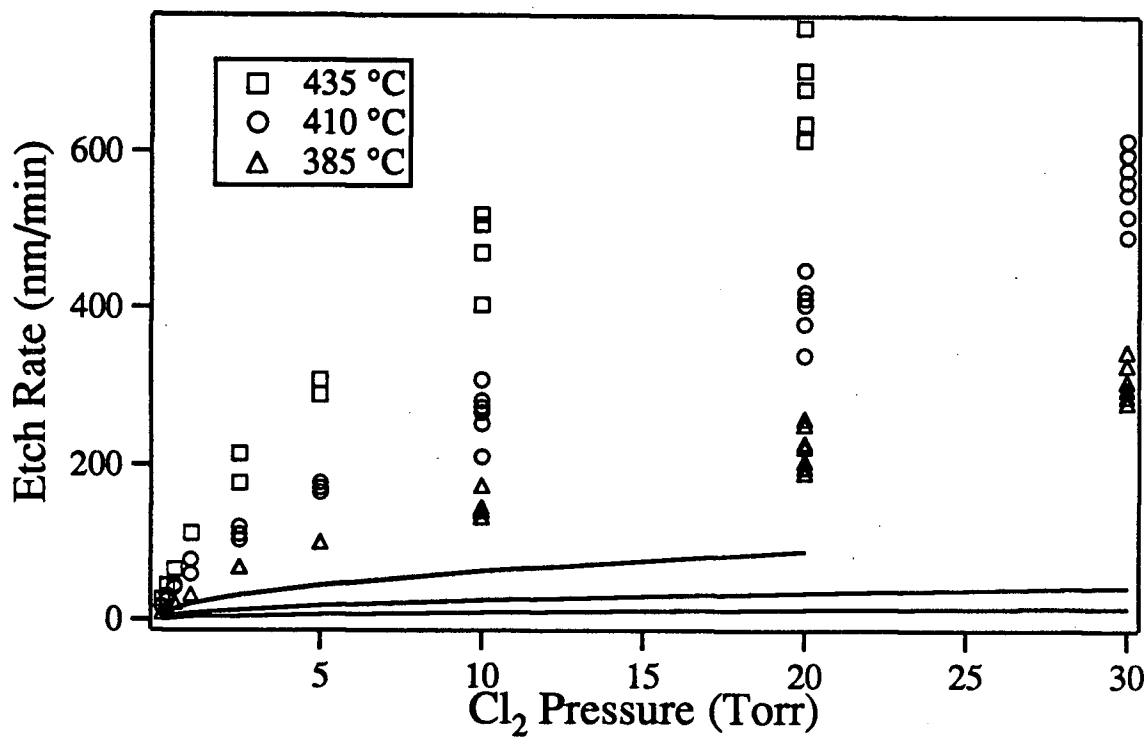
Figure 4.19 Etch rate of n-type polycrystalline silicon (BN2 wafer) versus Cl_2 pressure. Solid lines represent etch rates based on Cl_{eq} concentrations.

4.3.2.3 Conclusions From the Cl_2 Etching Experiments

The reaction of Cl_2 with silicon is characterized by a half order pressure dependency. Only a reversible dissociative adsorption mechanism is consistent with the experimental results. This is similar to the conclusions drawn from the Br_2 etching results discussed in section 4.3.1. It is also consistent with the thermal desorption spectroscopy study by Jackman et al.[39] on Cl_2 etching of silicon (100). The authors demonstrated the ability of Cl_2 to adsorb on a silicon surface, and to then dissociate and react with that surface to produce various silicon chloride products at temperatures comparable to those used in the present study.

The reaction of Cl_2 with silicon is characterized by two rate constants; a first order rate constant k_4, which dominates at low pressures, and the half order rate constant $(k_4/k_{-4})^{1/2}k_5$, which dominates at high pressures. Activation enthalpies and preexponential factors determined for these rate constants are summarized in Table 4.4.

4.3.2.4 Potential Energy Curve for Etching of Intrinsic Silicon by Cl_2

A potential energy level diagram can be constructed for Cl_2 etching of n-type (BN2) polycrystalline silicon using the activation energies provided in Table 4.4 and is presented in Figure 4.20. Since values for k_4 could not be determined in the etching of intrinsic silicon, a potential energy curve for only n-type silicon is provided. The $Cl_{2(g)}$ is assigned an energy of 0 kJ mol^{-1}. There are two maxima associated with the two rate controlling steps given by reactions (4.49) and (4.50) in Cl_2 etching of silicon. The first maximum lies at 87 kJ mol^{-1} and corresponds to the dissociative adsorption of Cl_2 on the silicon surface and is controlled by the first order rate constant k_4. The second maximum lies at 82 kJ mol^{-1} and is the energy barrier for the formation of product. Its position is known only with respect to $Cl_{2(g)}$ as given by the rate constant $(k_4/k_{-4})^{1/2}k_5$. The energy difference between Cl_{ads} and the second maximum corresponds to the activation enthalpy for k_5, which is undetermined. The positions of $2Cl_{ads}$ and Cl_{ads}, represented by the dashed lines, are also undetermined except that Cl_{ads} must lie at one half the energy of $2Cl_{ads}$.
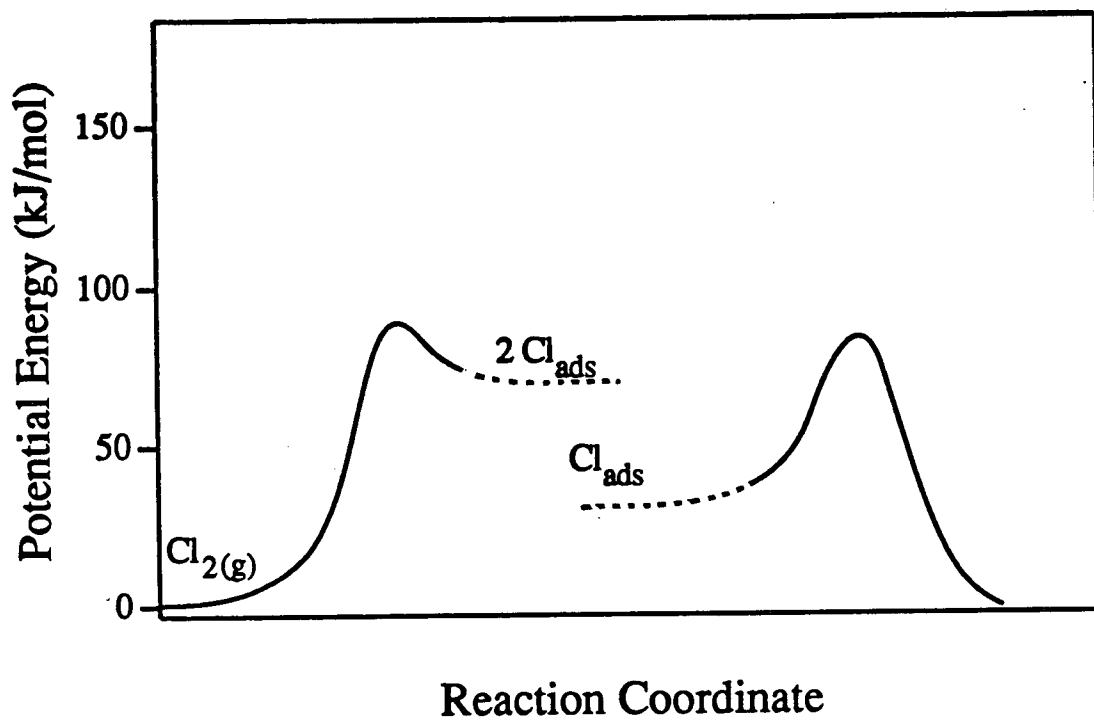
Figure 4.20 Potential energy curve for Cl_2 etching of n-type polycrystalline silicon (BN2 wafer).

4.3.2.5 On the Transition State for Cl and Cl$_2$ Etching Reactions

The activation enthalpy for the reaction of Cl atoms with silicon as given in the rate constant expressions (4.14) and (4.15) is 28 kJ mol^{-1}. Since the bond enthalpy for Cl$_2$ is 243 kJ mol^{-1}, the energy barrier for the rate controlling step in Cl atom etching lies at roughly 150 kJ mol^{-1} with respect to Cl$_{2(g)}$ (i.e. 1/2(243 kJ mol^{-1}) + 28 kJ mol^{-1}). The energy barrier for the formation of product in Cl$_2$ etching is given by the rate constant $(k_4/k_{-4})^{1/2}k_5$. For intrinsic silicon, the activation enthalpy is 116 kJ mol^{-1} and for n-type the value is only 82 kJ mol^{-1} (Table 4.4), both well below the 150 kJ mol^{-1} observed for Cl atom etching. This suggests the reaction between Cl atoms and silicon passes through a transition state different from that of the molecules. Product formation in the reaction with Cl$_2$ likely proceeds by disproportionation of chlorinated silicon species, as indicated in Figure 4.14a for the reaction of Br$_2$ with silicon. The transition state in atom etching may result from the reaction of a "free" physisorbed Cl atom with a chlorinated silicon species, thereby yielding product, as indicated in Figure 4.14b for Br atoms.

4.4 Comparison of Chlorine and Bromine Etching of Silicon

4.4.1 Cl and Br Atom Etching of Silicon

4.4.1.1 Reaction Rates of Cl and Br Atoms

A direct comparison of the Cl and Br atom etch rates is made in Figure 4.21 by plotting ln (k_1) versus 1/T. The first order rate constant k_1 for the reaction of Cl or Br atoms with silicon is equivalent to the etch rate per unit concentration of etchant in units of nm min^{-1} Torr^{-1}. The reaction with Cl occurs at considerably lower temperatures than with Br, as seen in Figure 4.21. For example a reaction rate equivalent to a ln (k_1) value of 7.0 is achieved for Cl etching of intrinsic silicon at a temperature of 240 °C while the same reaction rate for Br requires a temperature of 440 °C. This difference in reaction rates is also apparent for n-type silicon. A ln (k_1) value of 7.0 is observed at a temperature of 25 °C for Cl while a much higher temperature of 180 °C is needed to achieve the same reaction rate with Br atoms.
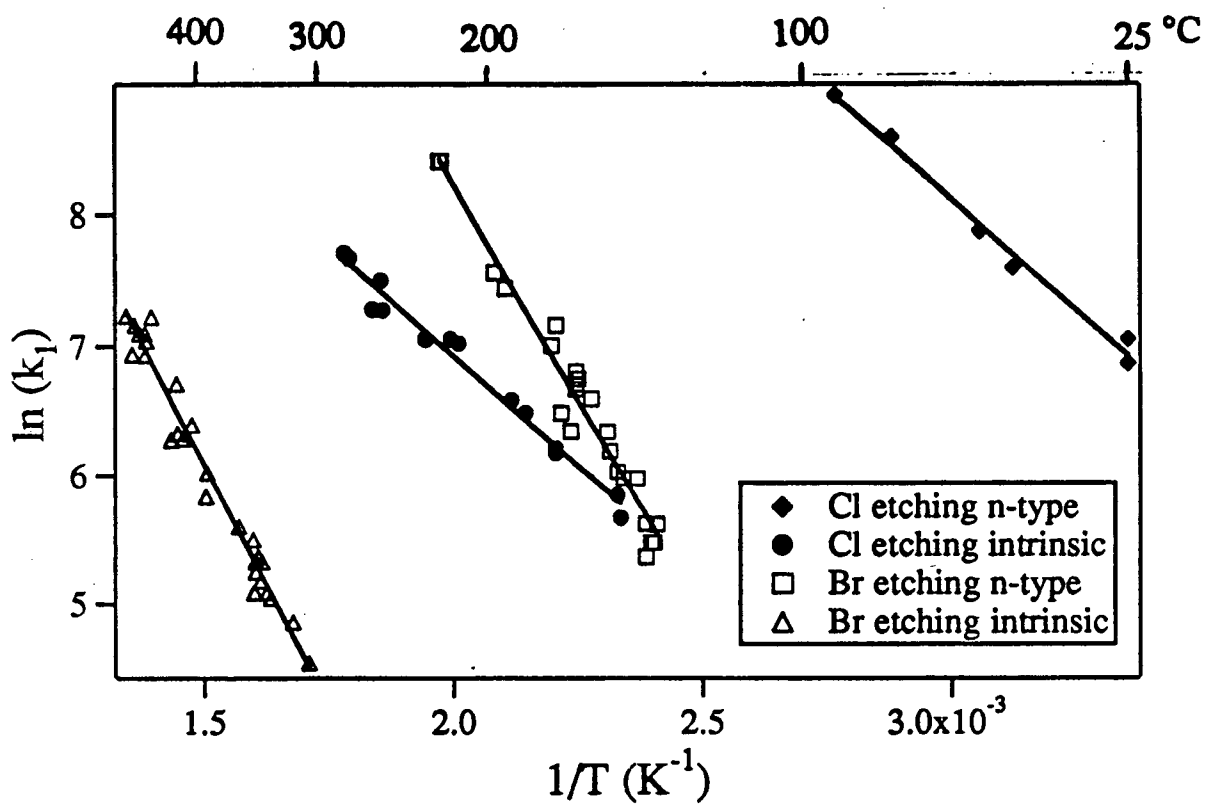
Figure 4.21 Comparison of the rate constant k_1 for Cl and Br atom etching of intrinsic (BN1 wafer) and n-type (BN2) wafer.

4.4.1.2 Activation Enthalpies for Cl and Br Atoms

The reaction with Cl is characterized by an activation enthalpy of 28 kJ mol^{-1}, as indicated by the rate constant expressions (4.14) and (4.15), for both intrinsic and n-type silicon. This similarity in activation enthalpies is readily apparent in Figure 4.21 where the plots of ln (k_1) versus 1/T for the two silicon types run parallel to each other. The 28 kJ mol^{-1} determined in this study is higher than 17.3 to 19.7 kJ mol^{-1} reported by Ogryzlo et al.[41] for the etching of various n-type silicon wafers. The differences in values may be related to the fitting of their data to an Arrhenius equation containing an extra term in the preexponential. This extra term accounted for the additional concentration of electrons in the conduction band of n-type material. Visual inspection of their data suggests the activation enthalpies may have been underestimated by this fitting procedure.

The slopes for the two Br data sets in Figure 4.21 also run roughly parallel to each other, but with considerably higher slopes, and hence higher activation enthalpies, than for Cl etching. Values of 63 and 55 kJ mol^{-1} for intrinsic and n-type silicon respectively are given in the rate constant expressions (4.2) and (4.3). The lower etch rates by Br atoms is therefore attributed to a larger activation enthalpy for k_1 rather than a smaller preexponential factor. Since accounting for the differences in activation enthalpies and reaction rates of Cl and Br atoms in terms of their chemical properties could benefit from a comparison of the kinetic data available for the F atom reaction with silicon, we make that comparison in the next section.

4.4.1.3 Significance of Activation Enthalpies for F, Cl and Br Atom Etching

Flamm et al.[20] have studied the etching of intrinsic silicon (100) by F atoms and found the process to be characterized by an activation enthalpy of 10.4 kJ mol^{-1}. The reaction was also observed to proceed rapidly, requiring much lower temperatures than those employed in the present study. For example, a temperature of -17 °C yielded the same reaction rate per unit concentration of etchant as that observed at 240 and 440 °C for Cl and Br etching respectively.

From the activation enthalpies and reaction rates for F, Cl and Br etching discussed above, the order of reactivity can be given as F>Cl>Br. The ordering is somewhat expected in view of the

general chemistries of the three halogens. In halogen atom reactions with methane, for example, F is observed to react explosively, while the reaction with Cl and Br is more controlled[81]. There are a number of factors that could be considered to contribute to those differences in reactivity. If we consider the exothermicities of the three reactions to form the most stable products,[82]

$$2F_2 + Si \longrightarrow SiF_4 \qquad \Delta H = -1615 \text{ kJ mol}^{-1}$$
$$2Cl_2 + Si \longrightarrow SiCl_4 \qquad \Delta H = -663 \text{ kJ mol}^{-1}$$
$$2Br_2 + Si \longrightarrow SiBr_4 \qquad \Delta H = -415 \text{ kJ mol}^{-1}$$

The reaction with F_2 is much more exothermic than with the other two halogens. Even if under the present experimental conditions the lower halides are formed, it is clear that the bond enthalpies decrease in the order Si-F>>Si-Cl>Si-Br. It has been argued that activation energies can be lowered by the formation of strong bonds[83]. In the presence of such an effect, the activation enthalpies would be expected to follow the observed order.

The electronegativity of F is the largest with a value of 4.0 compared to 3.0 for Cl and 2.8 for Br[84]. If, as discussed in section 4.6, the formation of the negative ion of the halogen atom on the silicon surface is important in the reaction, then these electronegativities would also yield an order of reactivity consistent with experimental results.

Finally, atomic size is likely to contribute to differences in reactivity. Steric constraints resulting from the reaction with a non-mobile surface bound species, would favor the smaller F atom, with a Van der Waals' radius of 1.35 Å, compared to the larger Cl (1.80 Å) and Br (1.95 Å) atoms and to a lesser extent this would favor Cl over Br.

Because of these three factors, a reaction order other than F>Cl>Br in the etching of a semiconductor surface might appear unlikely. However, deviations from such an order are observed. For example, the F atom etching of GaAs occurs slowly at low temperatures due to a low volatility of the gallium fluorides[85]. In contrast, the reaction of Cl with GaAs occurs rapidly[57] with a reported first order rate constant of 3.5×10^4 nm min^{-1} Torr^{-1} at 100 °C. Br atoms also

readily react with GaAs[58] yielding a slightly lower rate constant of 3.1×10^3 nm min^{-1} Torr^{-1} at 100 °C.

4.4.2 Cl$_2$ and Br$_2$ Etching of Silicon

4.4.2.1 Reaction Rates of Cl$_2$ and Br$_2$

A direct comparison of the reaction rates for Br$_2$ and Cl$_2$ etching of intrinsic (BN1) silicon can made by plotting the etch rates versus etchant pressure measured at the two temperatures of 540 and 570 °C. The resulting plot is presented in Figure 4.22. The Cl$_2$ etch rates measured at the two temperatures are higher than the corresponding Br$_2$ rates. The Cl$_2$ etch rate is approximately 1200 nm min^{-1} at 20 Torr and 570 °C which is roughly 2.5 to 3 times larger than that obtained for Br$_2$ under the same conditions. A similar difference in reaction rates is observed at the lower temperature of 540 °C for the two etchants. Although Cl$_2$ does etch faster than Br$_2$, the difference in reactivity is not as great as that observed for Cl and Br atoms.

In contrast to the differences in reactivity between Cl$_2$ and Br$_2$ etching of intrinsic silicon, virtually no difference is observed for n-type silicon. This is apparent in Figure 4.23 where etch rate versus etchant pressure is plotted for the etching of n-type (BN2) silicon at 385 and 410 °C. The rates for Cl$_2$ and Br$_2$ etching are almost identical under the pressures and temperatures studied. This is very different from that observed in Cl and Br atom etching of n-type silicon where large differences in reaction rates were observed.

4.4.2.2 Activation Enthalpies of Cl$_2$ and Br$_2$

It is also possible to compare the activation enthalpies for the Br$_2$ and Cl$_2$ reactions presented in Tables 4.2 and 4.4 respectively. The first order rate constant k_4 was found to have an activation enthalpy of 109 ± 23 kJ mol^{-1} for Br$_2$ etching of intrinsic silicon. Unfortunately no corresponding value was determined for Cl$_2$. For Br$_2$ etching of n-type silicon, activation enthalpies of 83 ± 27 and 75 ± 21 kJ mol^{-1} were determined for the two n-type wafers. Considering the experimental uncertainties, these are not very different from the 87 ± 18 kJ mol^{-1} observed for Cl$_2$ etching of n-type silicon. Because of the large uncertainties in activation enthalpies for k_4, and
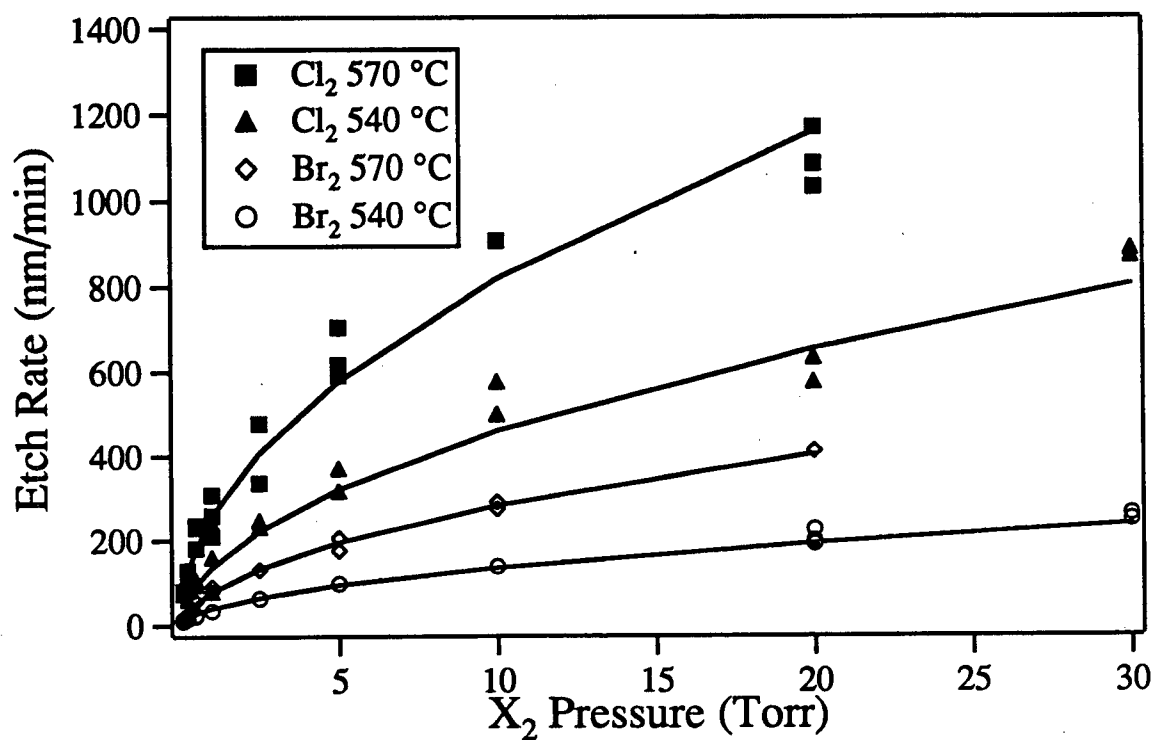
Figure 4.22 Etch Rates of intrinsic polycrystalline silicon versus Cl_2 or Br_2 pressure.
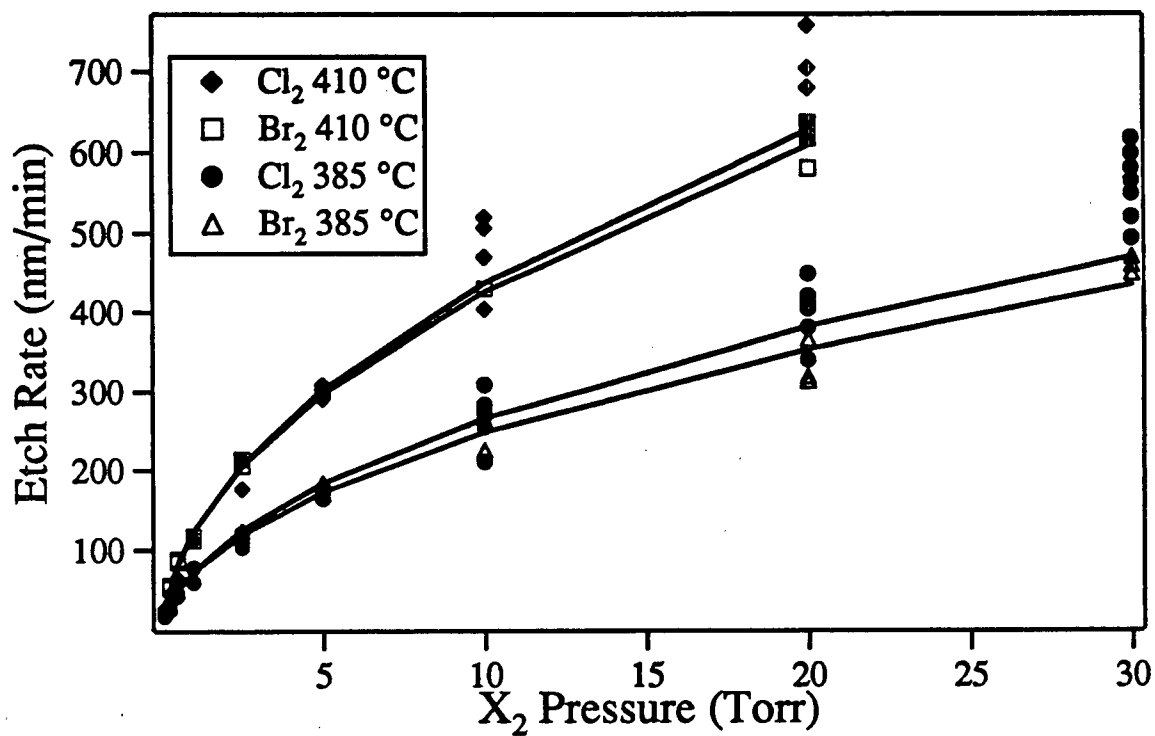
Figure 4.23 Etch rates for n-type polycrystalline silicon versus Cl_2 or Br_2 pressure.

the limited data available it would be unwise to conclude that we have detected a difference between the values of k_4 obtained for Cl_2 and Br_2.

The activation enthalpies for the half order composite rate constant $(k_4/k_{-4})^{1/2}k_5$ were determined with greater certainty than k_4 and as a result a trend in the Cl_2 and Br_2 values emerges. For intrinsic silicon, a value of 131 ± 8 kJ mol^{-1} was calculated for Br_2 etching with a lower value of 116 ± 7 kJ mol^{-1} obtained for Cl_2 etching. It was pointed out in sections 4.3.1 and 4.3.2 that the rate constant $(k_4/k_{-4})^{1/2}k_5$, which is equivalent to the constant C_1 in the empirical etch rate expressions, accounted for the majority of the observed reactivity, especially at high pressures, i.e. etch rate $\approx (k_4/k_{-4})^{1/2}k_5 (pressure)^{1/2}$. Hence the slightly higher activation enthalpy of $(k_4/k_{-4})^{1/2}k_5$ for Br_2 etching is consistent with the slightly lower reaction rates observed in Figure 4.22.

In etching n-type silicon, the activation enthalpies for $(k_4/k_{-4})^{1/2}k_5$ for the etchants Cl_2 and Br_2 are very similar. A value of 82 ± 3 kJ mol^{-1} was determined for Cl_2, while values of 86 ± 4 and 95 ± 8 kJ mol^{-1} were found for Br_2 etching of the two n-type wafers. The similarity in activation enthalpies is also reflected in the almost identical Cl_2 and Br_2 reaction rates of n-type silicon.

Activation enthalpies for the etching reaction were determined from data at only three temperatures spanning a narrow range. Ideally etch rates should have been determined for more temperatures over a wider range, but doing so as a function of pressure was difficult for two reasons. Firstly there was a limited range of etch rates which could be measured accurately. Choosing a wider temperature range would not allow the determination of etch rates over the full pressure range because of either too high or too low an etch rate. The second reason was the considerable time required to collect such pressure dependent data at several temperatures. As a compromise, etch rates were measured over a wide temperature range at a pressure of 1 Torr. The intention was to see whether or not the activation enthalpies determined from the pressure dependent data collected at three temperatures were applicable over a wider temperature range. A change in activation enthalpy in some temperature range would indicate a change in reaction mechanism.

The activation enthalpies were determined from the Arrhenius plots of ln (etch rate) versus 1/T for Cl_2 and Br_2 etching presented in Figures 3.19, 3.27 and 3.28. These values are presented in Table 4.5 along with values for $(k_4/k_{-4})^{1/2}k_5$ summarized from Table 4.2 and 4.4. Because the etch rates were not simply proportional to the square root of the etchant pressure, as shown by the empirical etch rate expression (3.2), the activation enthalpies determined at a pressure of 1 Torr will differ slightly from those determined from $(k_4/k_{-4})^{1/2}k_5$. However, the difference, arising from the contribution of C_2 in the empirical rate expression (3.2), is small and the resulting activation enthalpies should to comparable to those obtained from $(k_4/k_{-4})^{1/2}k_5$.

The activation enthalpies obtained at 1 Torr etchant compare well with those determined for $(k_4/k_{-4})^{1/2}k_5$ and provide no evidence for a change at either end of the temperature scale. Concentrating on the more accurately determined data for the three wafers from Bell Northern Research (BN1, BN2, and BN3), the following comparison can be made: 125 kJ mol^{-1} and 131 kJ mol^{-1} for Br_2-intrinsic, 83 and 86 kJ mol^{-1} for Br_2-n-type (BN2), 91 and 95 kJ mol^{-1} for Br_2-n-type (BN3), 99 and 116 kJ mol^{-1} for Cl_2-intrinsic, and 84 and 82 kJ mol^{-1} for Cl_2-n-type (BN2). The conclusion to be drawn from this rather large set of numbers is that the activation enthalpies determined for the pressure dependent data do appear to be the same as those over the wider temperature range.

The activation enthalpies for Cl_2 and Br_2 etching of silicon discussed above can be compared with previously reported values, which are summarized in Table 4.6. The 116 kJ mol^{-1} for Cl_2 etching of intrinsic silicon is comparable to the 115 kJ mol^{-1} reported by Jackman et al.[38] The 82 kJ mol^{-1} determined for Cl_2 and n-type silicon is larger than the 56 kJ mol^{-1} reported by Ogryzlo et al.[41] for variously doped n-type wafers. However, their activation enthalpy was determined from etch rates measured at various pressures near 0.3 Torr assuming a first order pressure dependence was assumed. The lack of a first order pressure dependency at this pressure, as observed in the present study, may have led to the lower value of 56 kJ mol^{-1}. The only reported activation enthalpy for the Br_2 reaction is a value of 119 kJ mol^{-1} determined by Jackman et al.[44] for the desorption of $SiBr_4$ in a thermal desorption spectroscopy study. This compares

Table 4.5 Activation enthalpies of the rate constant $(k_4/k_{-4})^{1/2}k_5$ and for etch rates measured at 1 Torr pressure for Br_2 and Cl_2 etching of silicon.

Etchant	Wafer	Activation Enthalpy (kJ mol^{-1})
Br_2	intrinsic (BN1)	131± 8
Br_2 (1 Torr)	intrinsic (BN1)	125 ± 7
Br_2	n-type (BN2)	86 ± 4
Br_2 (1 Torr)	n-type (BN2)	83 ± 4
Br_2	n-type (BN3)	95 ± 8
Br_2 (1 Torr)	n-type (BN3)	91 ± 3
Br_2	intrinsic (AT1)	118 ± 15
Br_2 (1 Torr)	intrinsic (AT1)	129 ± 8
Br_2	n-type (AT2)	100 ± 13
Br_2 (1 Torr)	n-type (AT2)	85 ± 2
Cl_2	intrinsic (BN1)	116 ± 7
Cl_2 (1 Torr)	intrinsic (BN1)	99 ± 16
Cl_2	n-type (BN2)	82 ± 3
Cl_2 (1 Torr)	n-type (BN2)	84 ± 4
Cl_2 (1 Torr)	n-type (BN3)	86 ± 5

Table 4.6 Previously reported values of activation enthalpies for the etching of silicon by F_2, Cl_2 and Br_2.

Etchant	Silicon Type	Activation Enthalpy (kJ mol^{-1})	Determined by Measurement of	Reference
F_2	silicon	50	Weight Loss	13
F_2	silicon (100), (110) and (111)	33	Etch Depth	14
F_2	silicon (100)	38	Etch Depth	15
F_2	silicon (110)	38	SiF$_2$ Production	16
Cl_2	n-type polycrystalline silicon	56	Etch Depth	40
Cl_2	silicon (100)	115	SiCl$_4$ Production	38
Br_2	silicon (100)	119	SiBr$_4$ Production	43

favorably with the 131 kJ mol^{-1} determined in the present study, although it should be noted that they are following a somewhat different reaction.

4.4.2.3 Significance of Activation Enthalpies for F_2, Cl_2 and Br_2 Etching

The activation enthalpies for F_2 etching of silicon are considerably lower than those for Br_2 and Cl_2. As seen in Table 4.6, values range from 33 to 50 kJ mol^{-1} for F_2 etching of various crystal faces of silicon. These values are considerably lower than the 116 and 131 kJ mol^{-1} activation enthalpies determined for the half order rate constant $(k_4/k_{-4})^{1/2}k_5$ for Cl_2 and Br_2 etching respectively. The lower activation enthalpies for F_2 etching is also accompanied by a faster reaction rate. Comparable etch rates are observed for F_2[14], Br_2 and Cl_2 at temperatures of 100, 480 and 520 °C respectively. The higher reactivity of F_2 over Cl_2 and Br_2 is not unreasonable based on the factors discussed for atom etching in section 4.4.1, such as high electronegativity, small size and the favorable ΔH for the reaction. However the small differences in Cl_2 and Br_2 reactivities and activation enthalpies for the rate constants k_4 and $(k_4/k_{-4})^{1/2}k_5$ are in contrast to the large differences observed in Cl and Br atom etching. The reason for this is not obvious. One factor may be the bond energies of the diatomic halogens. The 243 kJ mol^{-1} bond strength of Cl_2 is higher than the 198 kJ mol^{-1} for Br_2. This could then favor the dissociation of Br_2 on the surface, provided that the difference is reflected in the relative position of Cl_{ads} and Br_{ads} on the potential energy level diagrams in Figures 4.11, 4.12, 4.13 and 4.20. Such a difference could result in more adsorbed intermediates on the silicon surface in the case of Br_2 and could help to offset the smaller size, higher electronegativities and stronger Si-X bond strengths of Cl. If as previously suggested, the reaction of molecules proceeds through a different transition state, then these chemical properties which favor Cl over Br atoms, may not be as important in the reaction with the diatomics Cl_2 and Br_2.

4.5 Effect of Dopant on the Etch Rate

4.5.1 Earlier Models for Fluorine Etching

The effect of dopants on the etch rate of silicon is not a new phenomena and has received considerable attention in both experimental, as well as theoretical studies. Fluorine etchants have been employed in all but two of these studies, with chlorine atoms and molecules used as etchants in the other two[41,42]. This earlier work can be summarized as follows. The etch rates measured for n-type silicon are enhanced compared to those obtained for intrinsic silicon, while those for p-type silicon are suppressed. It has been shown by Baldi and Beardo[86] and Berg et al.[87] that the effect of dopants on the etch rate is related to the active carrier concentration and not the total doping level. In other words, the etch rates of samples implanted with dopants are not affected until the samples are annealed and the dopants become electrically active. Prior to annealing, most of the implanted dopant atoms are located at interstitial sites and do not contribute to the electrical conductivity of the silicon. Once annealed, however, the dopants take up lattice sites and are able to contribute electrons to the conduction band or a hole to the valence band. This strongly suggests that the effect of dopants on the etch rate of silicon is not related to differences in the chemistries between the dopant and silicon atoms, but rather to differences in the electrical behavior of the silicon brought about by their presence. This dependence on electrical behavior is not surprising considering a heavily doped n-type silicon wafer may contain dopant atoms at a concentration of only 100 to 1000 ppm, but their presence will increase the number of electrons in the conduction band by 3 or 4 orders of magnitude. Winters and Haarer[88] found the enhancement in etch rates for n-type silicon to be only a factor of 2.5 when employing fluorine etchants, while Ogryzlo et al.[41,42] reported larger enhancements of up to a factor of 100 when employing chlorine etchants.

One proposed mechanism attributes the enhanced etch rates of n-type silicon to a charge transfer reaction between the silicon surface and the halogen atom[41,42,85] resulting in an enhanced rate of chemisorption of the halogen. The more electrons available at the surface for charge transfer, the greater number of effective adsorption sites and the faster the etch rate. Hence n-type silicon with the highest surface concentration of electrons etches the fastest, followed by intrinsic and finally p-type silicon, which has the lowest surface concentration of electrons.

171

A second proposal to account for the dopant effects in fluorine etching is a space charge mechanism[87,89]. The F atom on a silicon surface is believed to have a substantial amount of negative charge associate with it because of its large electronegativity. Once negatively charged, the diffusion of F⁻ into the silicon lattice can be enhanced by the presence of positive charges on the dopant donor atoms near the surface. It is proposed that the etch rates of n-type and p-type silicon are directly related to the degree of this field assisted diffusion of F⁻ from the surface into the silicon lattice. An x-ray photoelectron spectroscopy study by Yarmoff and McFeely[90] on fluorine etching of both n- and p-type silicon found that such a simple model is not supported by experimental results. The authors found the reaction or corrosion layer for n-type silicon was slightly thinner than it is for either intrinsic or p-type silicon, indicating that F does not penetrate more deeply into the lattice of the n-type material as suggested. It was concluded that changes in the diffusion rate of F atoms through the reaction layer may only partially contribute to enhanced or depressed etch rates and that a substantial portion of the dopant effect can only be explained by a "chemical mechanism". This is to say that the rate constants for the individual elementary steps, which lead to the formation of product, are themselves affected by the presence of dopant atoms.

In a theoretical study, Garrison and Goddard[91] suggested that in fluorine etching of silicon the reacting species is a F radical, and not a negatively charged F⁻. The fluorine atom accepts an electron from the Si-Si bond, thereby weakening it and allowing the formation of a F-Si bond. In n-type silicon there is additional electron density available which can facilitate this reaction thus yielding a faster reaction rate. The deficiency of electron density in p-type silicon leads to a decrease in the reaction rate.

In a second theoretical study, Van der Walle et al.[92] have suggested etching proceeds by the reaction of a negatively charged F⁻ with a Si-Si bond to form a neutral Si-F bond. In the process a negative charge must be removed from the reacting species. If holes are present to react and annihilate the electron, then the reaction will proceed more rapidly. Heavily doped n-type silicon has a greater concentration of holes near the surface (in the so called depletion layer) than either intrinsic or lightly doped silicon, and as a result reacts at a faster rate. The formation of a depletion layer near the surface arises when electrons migrate to occupy surface states, leaving

behind the positively charged immobile donors. For a further discussion of the depletion layer see section 1.2.3.

The fact that such wide ranging mechanisms have been proposed to explain the doping effect in silicon etching is an indication of the amount of work still required before a full understanding is achieved. Whether any of these mechanisms, which are directed specifically at fluorine etching of silicon, will apply to silicon etching by other halogen etchants is yet to be seen. However, these mechanisms do provide a basis on which the present results can be discussed.

4.5.2. Effect of Dopants on Chlorine and Bromine Etching of Silicon

In the present study, all four etchants (Br_2, Br, Cl_2 and Cl) reacted more rapidly with n-type than with intrinsic polycrystalline silicon. Since different temperature ranges were employed in etching the various wafers, a direct comparison of the etch rates is not possible. However an estimate of the enhancement in etch rate due to the presence of n-type dopants can be made by calculating the etch rate for both the intrinsic and n-type wafers at some intermediate temperature. This has already been done in section (4.2.1) for Br atoms, where an enhancement factor of 340 was determined at 300 °C, and in section (4.2.2) for Cl atoms, where a factor of 89 was determined at 125 °C. Similarly, enhancements can be calculated for the molecular etchants Br_2 and Cl_2 using equations (4.23), (4.24), (4.26), (4.27), (4.28), (4.47) and (4.48). The enhancements determined from these calculations are summarized in Table 4.7. The Cl_2 etch rates for n-type silicon were enhanced by a factor of 11. For Br_2 etching the enhancement factors for the three n-type wafers increase from 70, to 77 and finally to 90 with increasing number density of dopant atoms in the three wafers (5×10^{18}, 5×10^{19} and 8×10^{19} atoms cm^{-3} respectively). With such a narrow range of doping levels in the three samples, it is difficult to determine quantitatively the dependence of etch rate enhancement on doping concentration.

There are two important conclusions to drawn from the data in presented in Table 4.7. Firstly, the enhancements observed for etching by atomic etchants are larger than those observed for etching by molecular etchants. This is true when one compares Br with Br_2 etching, as well as

173

Table 4.7 Relative etch rates for intrinsic and n-type wafers employing Br_2, Br, Cl_2 and Cl as etchants. Calculations for each etchant were done at the temperature indicated in parentheses.

Wafer	Br_2 (470 °C)	Br (300°)	Cl_2 (470 °C)	Cl (125 °C)
AT1 (intrinsic)	1.4			
AT2 (n-type)	90			
BN1 (intrinsic)	1	1	1	1
BN2 (n-type)	70	340	11	89
BN3 (n-type)	77			

Cl with Cl_2 etching. Secondly, the enhancements observed for Br are greater than those observed for Cl and the enhancements for Br_2 are greater than those observed for Cl_2.

The greater enhancements in etch rates due to doping, which are observed with atomic etchants relative to molecular etchants, is significant because it provides further evidence against a gas phase dissociation mechanism (see section 4.4.1.) for etching of silicon with Br_2 or Cl_2. If dissociation of the molecules did occur in the gas phase prior to adsorption onto the silicon surface, one would expect to see the same enhancements for n-type silicon using either molecular or atomic etchants. However the data presented in Table 4.7 shows a doping enhancement factor of 340 for Br atoms, but only a factor of 70 for Br_2. Similarly, the enhancement factor is 89 for Cl atoms, but only 11 for Cl_2.

The data presented in Table 4.7 suggests that the mechanism by which atom etch rates are enhanced could be different from the mechanism which is responsible for enhancements in molecule etch rates. For this reason, the dopant effect for atomic and molecular etchants will be discussed separately.

4.5.2.1 Possible Mechanisms for Dopant Effect in Cl and Br Atom Etching

The presence of n-type dopants in silicon significantly enhances the etching by both Cl and Br atoms. Enhancement factors of 89 and 340 were observed for Cl and Br atoms respectively, and these are due almost entirely to an increase in the preexponential factors of the rate constants. Very little of the enhancement resulted from a lowering of the activation enthalpy. Hence any mechanism proposed to account for the effect of dopants on atom etching rates must account for this increase in terms of an increased reaction probability which is not determined by a change in energy barrier for the reaction.

Ogryzlo et al.[41] observed that the enhancement in etch rates for Cl atoms was sensitive to the crystallographic orientation of the surface. The etch rates for the (111) face, in addition to being slower than for the (100) face, also displayed a greater sensitivity to dopant concentrations. As the concentration of dopant increased, the difference in etch rates for the two faces was minimized. At very high dopant concentrations of 10^{20} atoms cm^{-3}, the etch rates for the two faces were almost

identical. Flamm[93] has suggested that once a monolayer of Cl atoms chemisorb on the closely packed (111) surface, a steric barrier is established which discourages further attack by gas phase Cl atoms. This situation is illustrated in Figure 4.24a. In heavily doped n-type silicon, the large number of electrons in the conduction band facilitates charge transfer to the chemisorbed Cl atoms. The resulting bond is more ionic and allows the Cl atom to move from its position directly on top of the silicon surface atoms, thereby exposing silicon surface to further attack by gas phase Cl atoms, as shown in Figure 4.22b, and leading to enhanced etch rates. On the (100) face, the termination of the two surface states on each silicon atom by Cl atoms is such that the surface is still open to further attack by gas phase Cl atoms. Hence the etch rates for the (100) face are faster than those for the (111) face at low dopant levels, and do not increase as rapidly as the dopant concentration is increased.

This rather simple mechanical mechanism does explain how the presence of dopant atoms is capable of increasing the number of reactive sites on the surface, thereby increasing the preexponential factor in the rate constant. It may also suggest why the enhancement factor for Br atoms is larger than for Cl atoms, as observed in the present study. The larger Br atoms provide a more effective steric barrier to further atom attack, resulting in lower etch rates. The donation of electrons from dopant atoms into the conduction band facilitates charge transfer to chemisorbed Br atoms resulting in a more ionic surface bond. The change in bond geometry opens up additional chemisorption sites making it easier for the atoms to react with the silicon lattice. Although both Br and Cl atoms benefit from the formation of ionic bonds, the relative increase in chemisorption sites is greater for the larger Br atoms. Without direct experimental evidence for such an effect, such as through the measurement of "surface" vibrational frequencies, this model is somewhat speculative. However, it is the first mechanism that addresses the experimental fact that the n-type dopants increase only the preexponential factor of the rate constant.

There is an alternative to the explanation by Flamm for the effect of n-type dopants on Br and Cl atom etch rates. The large preexponential factors of the first order rate constant suggest the reaction of atoms with silicon is preceded by an adsorption equilibrium step in which atoms are physisorbed to the surface. The binding energy of the electronegative halogen atoms to the surface

(a)
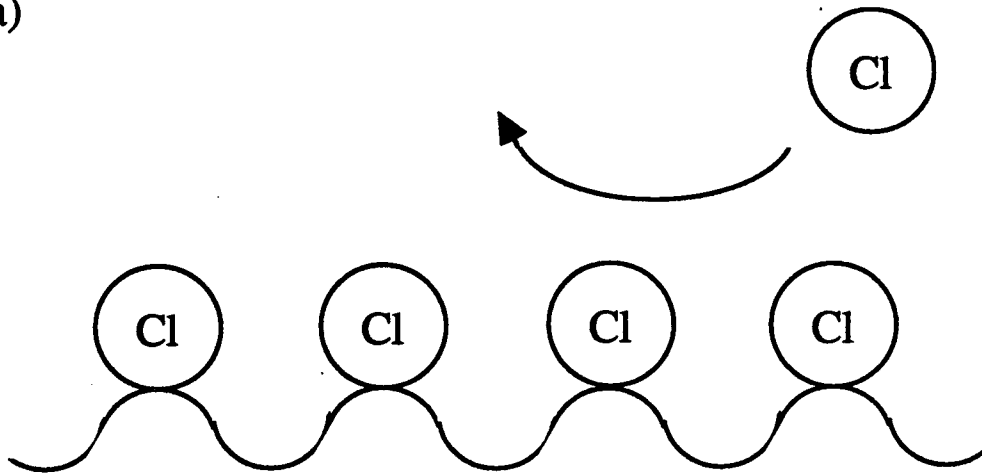
Intrinsic silicon

(b)
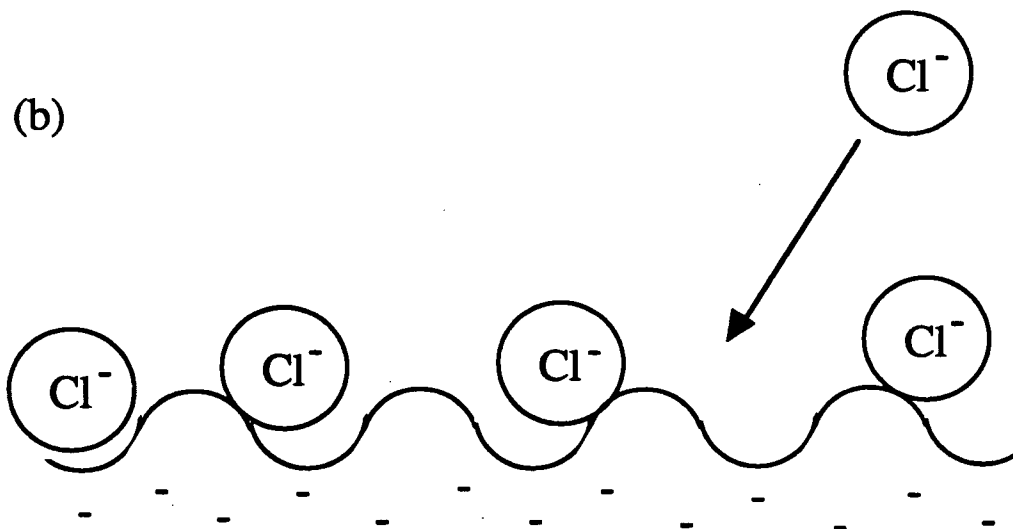
n-type silicon

Figure 4.24 Mechanism proposed by Flamm[93] to explain effect of n-type dopant on the etching of silicon by Cl atoms.

could well be increased by the presence of electron donors in silicon. A stronger binding energy for Br_{ads} or Cl_{ads} would shift the preadsorption equilibrium to favor a higher concentration of adsorbed halogen atoms, thereby increasing the preexponential factor and the overall reaction rate.

4.5.2.2 Possible Mechanisms for Dopant Effect in Cl_2 and Br_2 Etching

The enhancement in Br_2 and Cl_2 etch rates with increasing dopant concentration can be traced to a change in the activation enthalpies for the first order rate constant k_4 and the half order composite rate constant $(k_4/k_{-4})^{1/2}k_5$. From the values in Table 4.2 for Br_2 etching, the activation enthalpy for k_4 drops from 109 ± 23 kJ mol^{-1} for intrinsic silicon to 83 ± 27 and 75 ± 21 kJ mol^{-1} for the two n-type samples. Because of the relatively large uncertainties in these values for k_4, it can be argued that this difference lies within experimental error. The change in activation enthalpies for $(k_4/k_{-4})^{1/2}k_5$ is more convincing for both Br_2 and Cl_2 etching. The energy barrier drops from 131 ± 8 kJ mol^{-1} for intrinsic silicon to 86 ± 4 and 95 ± 8 kJ mol^{-1} for the two n-type wafers. For Cl_2 etching, an activation enthalpy for intrinsic and n-type silicon was determined only for the composite rate constant $(k_4/k_{-4})^{1/2}k_5$. From Table 4.4, this energy barrier drops from 116 ± 7 to 82 ± 3 kJ mol^{-1}.

The change in activation enthalpy with doping is in contrast to the changes observed in atom etching where the enhancement in etch rates was reflected only in a change in the preexponential factors of the rate constants. In Br_2 etching, it appears the additional electron density in the conduction band acts principally to lower the energy of the second maximum in the energy curve diagrams in Figure 4.12, to the values found in Figures 4.13 and 4.21. Since the position of the intermediates Br_{ads} and Cl_{ads} in these diagrams is not known, it is difficult to say whether the dopant lowers the activation enthalpy of k_5 of the position of Br_{ads}, or both. If, as Flamm suggests, the presence of dopants produces a more ionic bond, then Br_{ads} would lie at a lower energy and the drop in activation enthalpy could be due at least partly to the higher equilibrium concentration of Br_{ads} that results. If the reaction step characterized by k_5 is the disproportionation of two surface silicon halide species, as indicated in Figure 4.14a, then the extra electron density in n-type silicon may facilitate the breaking of one Si-X bond and the formation of

a second Si-X bond. Garrison and Goddard[81] have proposed a similar mechanism for fluorine etching of silicon whereby the extra electron density present in n-type silicon helps to weaken the Si-Si, thus facilitating the insertion of a F atom.

4.6 Comments on Future Work

Half order pressure dependencies for the etching of silicon by Br_2 and Cl_2 have not been reported in earlier work. A reexamination of previously reported measurements of the etch rates of silicon employing Br_2 and Cl_2 suggests that the presence of half order kinetics was simply not recognized in the earlier work. The reversible dissociative adsorption mechanism proposed to explain the half order kinetics may also be applicable in other surface reactions involving diatomics. The most likely system to study first would be F_2 etching of silicon. Although the two studies by Chen et al.[14] and Squire et al.[16] observed first order kinetics for the reaction, the pressure dependence was determined at F_2 pressures below a milliTorr. This is not unreasonable since our work also predicts first order kinetics at low pressures in the etching of silicon by Br_2 and Cl_2. For this reason, it would be interesting to determine the pressure dependence of the F_2 reaction with silicon at higher pressures. Because of the high reactivity of F_2 with silicon even at room temperature, it may be necessary to lower the reaction temperature in order to obtain reasonable etch rates at the higher pressures. However this should not be difficult to achieve.

With kinetic information available for the three halogens F_2, Cl_2 and Br_2, it would be interesting to examine the reaction of I_2 with silicon. There has been only one study of I_2 reactions with silicon in the form of a thermal desorption spectroscopy study by Jackman et al.[44]. The authors found that room temperature exposure to I_2 followed by heating of the silicon substrate produced no silicon iodide products. It may be that high temperatures with simultaneous exposure to I_2 are required to produce an etching reaction. Although the volatility of SiI_4 (b.p. 288 °C) is lower than that for $SiBr_4$ (b.p. 154 °C), $SiCl_4$ (b.p. 58 °C) and SiF_4 (b.p. -86 °C), product desorption should not be a problem if the reaction is performed at a temperature of several hundred degrees.

It would also be useful to examine the etching of silicon for a number of n-type wafers spanning a larger range of dopant concentrations in an effort to quantify the dopant effect. In addition to etching n-type polycrystalline silicon films, the etching of n-type single crystal wafers should be explored to see if the effect of dopant is sensitive to crystallographic orientation as observed in Cl atom etching[42].

Once the kinetics of the etching of silicon by bromine and chlorine are fully understood as a function of dopant concentration and crystallographic orientation, it would be interesting to examine the effect of laser irradiation on the etching process. Since high temperatures are required for the reaction between silicon and the molecular halogens Br_2 and Cl_2, it may be possible to provide the energy needed for reaction using a laser beam. This would allow selective etching of the surface without the use of a mask. Such direct writing techniques are being widely studied for Cl_2-silicon systems[94,95,96,97], but as of yet only limited work has been done on the Br_2-silicon system[76]. An excimer laser is presently located in our laboratory and would provide an excellent source of UV photons in order to carry out such a study.

Chapter 5. Summary and Conclusions

A summary of the etch rate data and rate constants determined in this study is presented at the end of this chapter. The reaction of Br atoms with silicon was shown to be first order with respect to atom partial pressure and the reaction with Cl atoms was assumed to be first order in Cl. Absolute reaction rates for Cl and Br atom etching of intrinsic and n-type polycrystalline silicon, with a dopant concentration of 5×10^{18} atoms cm^{-3}, were measured as a function of substrate temperature and the first order rate constant k_1 was determined. The reactivity of Cl atoms with n-type silicon was 89 times greater than with intrinsic silicon. This enhancement was attributed primarily to an increase in the preexponential factor in k_1, with the activation enthalpy remaining unchanged at 28 kJ mol^{-1}. The enhancement factor of 340 in Br atom etch rates of n-type silicon was also due, for the most part, to an increase in the preexponential factor in k_1. Differences in the activation enthalpies of 63 and 55 kJ mol^{-1} for intrinsic and n-type silicon respectively, accounted for only a small fraction of the change. The preexponential factors in k_1 were larger than those expected based on Cl and Br collision frequencies and this was interpreted as evidence for a preadsorption step in these reactions.

The reaction rates for Br_2 and Cl_2 etching of intrinsic and n-type polycrystalline silicon, as well as for Br_2 etching of the (100) face of single crystal silicon, were measured as a function of etchant pressure and substrate temperature. The etch rates were found to display a non-linear dependence on pressure. Plotting etch rates versus (pressure)$^{1/2}$ yielded straight line fits and for the more accurately determined data sets, the intercepts were all negative. Assuming an Arrhenius temperature dependence for the slopes and intercepts, empirical expressions for the etching of the various silicon wafers were determined. The half order pressure dependency of the reaction was found to be consistent with a reversible dissociative adsorption mechanism comprised of at least the following two steps.

$$Br_2 \underset{k_{-4}}{\overset{k_4}{\rightleftharpoons}} 2\, Br_{ads}$$

$$Br_{ads} \xrightarrow{k_5} SiBr_x$$
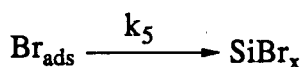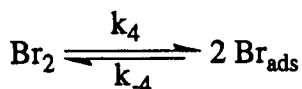
The first step is the reversible dissociation of Br_2 (or Cl_2) molecules on the silicon surface forming bound halogen atoms. These bound species then go on to react in a first order reaction, which is rate controlling at the temperatures and pressures employed in this study, forming the product $SiBr_x$ (or $SiCl_x$), where x=1,2,3 or 4 depending upon the temperature. At low pressures the half order kinetics was shown to break down, with the first order dissociative adsorption step becoming rate controlling. Evidence was presented that indicated an alternative mechanism in which gaseous atoms were formed by the reversible dissociation of Cl_2 and Br_2 prior to adsorption on the silicon surface was unacceptable.

From the slopes of the etch rate versus (pressure)$^{1/2}$ plots, a composite half order rate constant $(k_4/k_{-4})^{1/2}k_5$ was determined and from the intercepts it was possible to evaluate the first order rate constant k_4, which controls the dissociation of Br_2 or Cl_2 on the surface. The activation enthalpies for the half order rate constant for Cl_2 and Br_2 etching of intrinsic silicon were 116 and 131 kJ mol^{-1} respectively. An activation enthalpy for k_4 of 109 kJ mol^{-1} was determined for Br_2 etching. The presence of n-type dopant atoms, at a concentration of 5×10^{18} atoms cm^{-3}, was effective in increasing the reaction rate by factors of 11 and 70 for Cl_2 and Br_2 respectively. This was principally due to a lowering of the activation enthalpies of the rate constants. For Br_2 and Cl_2 etching of n-type silicon, the activation enthalpies for the composite rate constant $(k_4/k_{-4})^{1/2}k_5$ were 82 and 86 kJ mol^{-1} respectively. For Br_2 etching of n-type silicon, the activation enthalpy for the first order rate constant k_4 was 83 kJ mol^{-1}.

The high temperatures required to produce reasonable reaction rates for Cl_2 and Br_2 etching of silicon will certainly limit their practical application as etchants in device fabrication. The lower temperatures required for Cl and Br atom etching, as well as the large enhancement factors in etching n-type silicon, make these species more attractive, especially if selective removal of heavily doped n-type material if required. In practice, pure chemical etching is seldom applied in device fabrication because of its isotropic etching behavior and as a result it is unlikely these etchants will be employed directly for that purpose. However, many reactive ion etching systems are based on chlorine or bromine containing gases[98,99,100,101] and the empirical rate expressions and rate constants determined for Cl and Br atom etching of intrinsic and n-type silicon may be useful in

obtaining a better understanding of these systems. More importantly, the rate constants obtained for atomic and molecular chlorine and bromine etching of silicon will contribute to existing kinetic data, helping to further our general understanding chemical etching.

The Cl_2 and Br_2 etch rates of intrinsic polycrystalline silicon can be characterized by the expressions

$$\text{Etch Rate (Cl}_2\text{+intrinsic)} = 10^{9.6\pm0.5} \text{ nm min}^{-1} \text{ Torr}^{-1/2} \exp^{(-116\pm7 \text{ kJ/mol})/RT} (\text{Cl}_2 \text{ Pressure})^{1/2}$$

$$\text{Etch Rate (Br}_2\text{+intrinsic)} = 10^{10.1\pm0.5} \text{ nm min}^{-1} \text{ Torr}^{-1/2} \exp^{(-131\pm8 \text{ kJ/mol})/RT} (\text{Br}_2 \text{ Pressure})^{1/2}$$
$$- 10^{10.1\pm0.5} \text{ nm min}^{-1} \exp^{(-144\pm8 \text{ kJ/mol})/RT} \quad .$$

The Cl_2 etching of n-type polycrystalline silicon, with a dopant concentration of 5×10^{18} atoms cm^{-3}, can be given by the equation

$$\text{Etch Rate (Cl}_2\text{+n-type)} = 10^{8.2\pm0.2} \text{ nm min}^{-1} \text{ Torr}^{-1/2} \exp^{(-82\pm3 \text{ kJ/mol})/RT} (\text{Cl}_2 \text{ Pressure})^{1/2}$$
$$- 10^{7.1\pm0.9} \text{ nm min}^{-1} \exp^{(-77\pm12 \text{ kJ/mol})/RT} \quad .$$

The Br_2 etch rates of n-type polycrystalline silicon with dopant concentrations of 5×10^{18} and 5×10^{19} atoms cm^{-3} are given respectively by the equations

$$\text{Etch Rate (Br}_2\text{+n-type)} = 10^{8.7\pm0.3} \text{ nm min}^{-1} \text{ Torr}^{-1/2} \exp^{(-86\pm4 \text{ kJ/mol})/RT} (\text{Br}_2 \text{ Pressure})^{1/2}$$
$$- 10^{8.2\pm1.4} \text{ nm min}^{-1} \exp^{(-91\pm21 \text{ kJ/mol})/RT}$$

$$\text{Etch Rate (Br}_2\text{+n-type)} = 10^{9.4\pm0.7} \text{ nm min}^{-1} \text{ Torr}^{-1/2} \exp^{-(95\pm8 \text{ kJ/mol})/RT} (\text{Br}_2 \text{ Pressure})^{1/2}$$
$$- 10^{10.6\pm0.8} \text{ nm min}^{-1} \exp^{(-121\pm16 \text{ kJ/mol})/RT} \quad .$$

The Cl and Br atom etching of intrinsic and n-type polycrystalline silicon, with a dopant concentration of 5×10^{18} atoms cm^{-3}, is given by the following first order rate constants and the appropriate atom partial pressure.

$$k_1 \text{ (Cl+intrinsic)} = 10^{5.9\pm0.2} \text{ nm min}^{-1} \text{ Torr}^{-1} \exp^{(-28.2\pm1.2 \text{ kJ/mol})/RT}$$

k_1 (Cl+n-type) = $10^{7.9\pm0.2}$ nm min^{-1} Torr^{-1} exp $^{(-27.8\pm1.5\ kJ/mol)/RT}$

k_1(Br+intrinsic) = $10^{7.5\pm0.2}$ nm min^{-1} Torr^{-1} exp $^{(-63\pm1\ kJ/mol)/RT}$

k_1(Br+n-type) = $10^{9.3\pm0.3}$ nm min^{-1} Torr^{-1} exp $^{(-55\pm2\ kJ/mol)/RT}$

The first order rate constant k_4 and the half order composite rate constant $(k_4/k_{-4})^{1/2}k_5$ for Cl_2 etching of intrinsic and n-type silicon, with a dopant concentration of 5×10^{18} atoms cm^{-3}, are given by the expressions

k_4 (Cl_2+n-type) = $10^{8.7\pm1.4}$ nm min^{-1} Torr^{-1} exp $^{(-87\pm18\ kJ/mol)/RT}$

$(k_4/k_{-4})^{1/2}k_5$ (Cl_2+n-type) = $10^{8.2\pm0.2}$ nm min^{-1} Torr$^{-1/2}$ exp $^{(-82\pm3\ kJ/mol)/RT}$

$(k_4/k_{-4})^{1/2}k_5$ (Cl_2+intrinsic) = $10^{9.6\pm0.5}$ nm min^{-1} Torr$^{-1/2}$ exp $^{(-116\pm7\ kJ/mol)/RT}$

The two rate constants for Br_2 etching of intrinsic polycrystalline silicon are

k_4 (Br_2+intrinsic) = $10^{8.9\pm1.5}$ nm min^{-1} Torr^{-1} exp $^{(-109\pm23\ kJ/mol)/RT}$

$(k_4/k_{-4})^{1/2}k_5$ (Br_2+intrinsic) = $10^{10.1\pm0.5}$ nm min^{-1} Torr$^{-1/2}$ exp $^{(-131\pm8\ kJ/mol)/RT}$

and for two n-type polycrystalline silicon samples with dopant concentrations of 5×10^{18} and 5×10^{19} atoms cm^{-3}, the rate constants are given respectively by

k_4 (Br_2+n-type) = $10^{8.8\pm2.1}$ nm min^{-1} Torr^{-1} exp $^{(-83\pm27\ kJ/mol)/RT}$

k_4 (Br_2+n-type) = $10^{8.1\pm1.6}$ nm min^{-1} Torr^{-1} exp $^{(-75\pm21\ kJ/mol)/RT}$

$(k_4/k_{-4})^{1/2}k_5$ (Br_2+n-type) = $10^{8.7\pm0.3}$ nm min^{-1} Torr$^{-1/2}$ exp $^{(-86\pm4\ kJ/mol)/RT}$

$(k_4/k_{-4})^{1/2}k_5$ (Br_2+n-type) = $10^{9.4\pm0.7}$ nm min^{-1} Torr$^{-1/2}$ exp $^{(-95\pm8\ kJ/mol)/RT}$

1. Semiconductor International, February 1990, 13.

2. W.R. Runyan and K.E. Bean, "Semiconductor Integrated Circuit Processing Technology", Addison-Wesley, New York, 1990, p. 8.

3. S.K. Gandi, "VLSI Fabrication Principles: Silicon and Gallium Arsenide", John Wiley & Sons, New York, 1983, p. 12.

4. W.S. Ruska, "Microelectronic Processing", McGraw-Hill, New York, 1987, p. 57.

5. P. Joubert, B. Loisel, Y. Chouan, and L. Haji, J. Electrochem. Soc. 134, 2541 (1987).

6. "The electronic Structure and Chemistry of Solids", P.A. Cox, Oxford Scientific Publications, Oxford 1987, p.19.

7. J. van Zwol, J. van Laar, A.W. Kolfschoten and J. Dieleman, J. Vac. Sci. Technol. B5, 1410 (1987).

8. S.C. McNevin and G.E. Becker, J. Vac. Sci. Technol. B3, 485 (1985).

9. N. Aoto, E. Ikawa, and Y. Kurogi, J. Appl. Phys. 65, 158 (1989).

10. H. F. Winters and J.W. Coburn, J. Vac. Sci. Technol. B3, 1376 (1985).

11. D.L. Flamm, V.M. Donnelly and J.A. Mucha, J. Vac. Sci. Technol. B1, 23 (1983).

12. C.J. Mogab and H.J. Levinstein, J. Vac. Sci. Technol. 17, 721 (1980).

13. S.T. Ceyer, Nature 249, 133 (1990).

14. A.K. Kuriakose and J.L. Margrave, J. Phys. Chem. 68, 2671 (1964).

15. M. Chen, V.J. Minkiewicz and K. Lee, J. Electrochem. Soc. 126, 1946 (1979).

16. J.A. Mucha, V.M. Donnelly, D.L. Flamm and L.M. Webb, J. Phys. Chem. 85, 3529 (1981).

17. D.W. Squire, J.A. Dagata, D.S.Y. Hsu, C.S. Dulcey and M.C. Lin, J. Phys. Chem. 92, 2827 (1988).

18. J.R. Engstrom, M.M. Nelson and T. Engel, Surf. Sci. 215, 437 (1989).

19. M.J. Vasile and F.A. Stevie, J. Appl. Phys. 53, 3799 (1982).

20. D.L. Flamm, V.M. Donnelly and J.A. Mucha, J. Appl. Phys. 52, 3633 (1981).

21. C.D. Stinespring and A. Freedman, Appl. Phys. Lett. 48, 718 (1986).

22. H.F. Winters and J.W. Coburn, Appl. Phys. Lett. 34, 70 (1979).

23. D.E. Ibbotson, D.L. Flamm, J.A. Mucha, and V.M. Donnelly, Appl. Phys. Lett. 44, 1129 (1984).

24. H. F. Winters and F.A. Houle, J. Appl. Phys. 54, 1218 (1983).

25. F.A. Houle, J. Appl. Phys. $\underline{60}$, 3018 (1986).

26. J.A. Dagata, D.W. Squire, C.S. Dulcey, D.S.Y. Hsu and M.C. Lin, J. Vac. Sci. Technol. $\underline{B5}$, 1495 (1987).

27. F.R. McFeely, J.F. Morar and F.J. Himpsel, Surf. Sci. $\underline{165}$, 277 (1986).

28. J. F. Morar, F.R. McFeely, N.D. Shinn, G. Landgren and F.J. Himpsel, Appl. Phys. Lett. $\underline{45}$, 174 (1984).

29. D.E. Ibbotson, J.A. Mucha and D.L. Flamm, J. Appl. Phys. $\underline{56}$, 2939 (1084).

30. Y. Saito, O. Yamaoka and A. Yoshida, Appl. Phys. Lett. $\underline{56}$, 1119 (1990).

31. J.E. Rowe, G. Margaritondo, and S.B. Christman, Phys. Rev. B $\underline{16}$, 1581 (1977).

32. K.C. Pandey, T. Sakurai and H.D. Hagstrum, Phys. Rev. B $\underline{16}$, 3648 (1977).

33. P.H. Citrin and J.E. Rowe, Surf. Sci. $\underline{132}$, 205 (1983).

34. R.D. Schnell, D. Rieger, A. Bogen, F.J. Himpsel, K. Wandelt and W. Steinmann, Surf. Sci. $\underline{162}$, 25 (1985).

35. J. J. Boland and J.S. Villarrubia, Science $\underline{248}$, 838 (1990).

36. J.V. Florio and W.D. Robertson, Surf. Sci. $\underline{18}$, 398 (1969).

37. R.J. Madix and J.A. Schwarz, Surf. Sci. $\underline{24}$, 264 (1971).

38. F.H.M. Sanders, A.W. Kolfschoten, J. Dieleman, R.A. Haring, A. Haring and A.E. de Vries, J. Vac. Sci. Technol. $\underline{A2}$, 487 (1984).

39. R.B. Jackman, H. Ebert and J.S. Foord, Surf. Sci. $\underline{176}$, 183 (1986).

40. N. Aoto, E. Ikawa and Y. Kurogi, J. Appl. Phys. $\underline{65}$, 158 (1989).

41. E.A. Ogryzlo, D.L. Flamm, D.E. Ibbotson and J.A. Mucha, J. Appl. Phys. $\underline{64}$, 6510 (1988).

42. E.A. Ogryzlo, D.E. Ibbotson, D.L. Flamm and J.A. Mucha, J. Appl. Phys. $\underline{67}$, 3115 (1990).

43. H.S. Cheng, L.Luo, M. Okamoto, T. Thundat, S. Hashimoto and W.M. Gibson, J. Vac. Sci. Technol. $\underline{A5}$, 607 (1987).

44. R.B. Jackman, R.J. Price and J.S. Foord, Appl. Surf. Sci. $\underline{36}$, 296 (1989).

45. F.R. McFeely, J.F. Morar and F.J. Himpsel, Surf. Sci. $\underline{165}$, 277 (1986).

46. T.D. Bestwick and G.S. Oehrlein, J. Vac. Sci. Technol. $\underline{A8}$, 1696 (1990).

47. L.L. Sveshnikova, S.M. Repinskii, and A.B. Posadov, Poverkhnost. Fiz. Khimiya Mekh. 1982, $\underline{8}$, 134.

48. W.S. Ruska, "Microelectronic Processing", McGraw-Hill, New York, 1987, p. 286.

49. J.E. Lennard-Jones, Trans. Farad. Soc. 28, 333 (1932).

50. E.K. Rideal, Proc. Cambridge Phil. Soc. 35, 130 (1939); Chem. Ind. 62, 335 (1943).

51. I. Langmuir, Trans. Faraday Soc. 17, 621 (1921).

52. C.N. Hinshelwood, "Kinetics of Chemical Change", Clarendon Press, Oxford, p.145, 1926.

53. C.T. Campbell, G. Ertl, H. Kuipers and J. Segner, J. Chem. Phys. 73, 5862 (1980).

54. H. Chon and C.D. Prater, Disc. Farad. Soc. 41, 380 (1966).

55. F.C. Schouten, O.L.J. Gijzeman and G.A. Bootsma, Surf. Sci. 87, 1 (1979).

56. J.D. Beckerle, A.D. Johnson, Q.Y. Yang and S.T. Ceyer, J. Chem. Phys. 91, 5756 (1989).

57. J.H. Ha, "Reaction of Gallium Arsenide with Chlorine", Ph.D. Thesis, Department of Chemistry, University of British Columbia, 1989.

58. I.E. Salisbury, "Reactions of the (100) Face of Gallium Arsenide with Molecular and Atomic Bromine", M.Sc. Thesis, Department of Chemistry, University of British Columbia, 1990.

59. T. Takahagi, I. Nagai, A. Ishitani, H. Kuroda and Y. Nagasawa, J. Appl. Phys. 64, 3516 (1988).

60. Y. Takakuwa, M. Nogawa, M. Niwano, H. Katakura, S. Matsuyoshi, H. Ishida, H. Kato and N. Miyamoto, Jpn. J. Appl. Phys. 28, L1274 (1989).

61. M. Suemitsu, T. Kaneko and N. Miyamoto, Jpn. J. Appl. Phys. 28, 2421 (1989).

62. V.A. Burrows, Y.J. Chabal, G.S. Higashi, K. Raghavachari and S.B. Christman, Appl. Phys. Lett. 53, 998 (1988).

63. N. Hirashita, M. Kinoshita, I. Aikawa and T. Ajioka, Appl. Phys. Lett. 56, 451 (1990).

64. G.W. Trucks, K. Raghavachari, G.S. Higashi and Y.J. Chabal, Phys. Rev. Lett. 65, 504 (1990).

65. "Physical Chemistry", P.W. Atkins, W.H. Freeman and Company, San Francisco 1978, p.804.

66. E.A. Ogryzlo, Can. J. Chem. 39, 2556 (1961).

67. M.A.A. Clyne, H.W. Cruse and R.T. Watson, J.C.S. Faraday II 68, 153 (1972).

68. F.L. Nebitt, D.F. Nava, W.A. Payne and L.J. Stief, J. Phys. Chem. 91, 5337 (1987).

69. W.E. Beadle, J.C.C. Tsai and R.D. Plummer, "Quick Reference Manual for Silicon Integrated Circuit Technology", John Wiley & Sons, New York, 1985, page 2-59.

70. G.E. Jellison, Jr. and H.H. Burke, J. Appl. Phys. 60, 841 (1986).

71. A. Landauer Keaton and D.W. Hess, J. Appl. Phys. 63, 533 (1988).

72. D.E. Ibbotson, D.L. Flamm and V.M. Donnelly, J. Appl. Phys. 54, 5974 (1983).

73. T.J. Donahue and R. Reif, J. Appl. Phys. 57, 2757 (1985).

74. D.S. Fischl, G.W. Rodrigues and D.W. Hess, J. Electrochem. Soc. 135, 2016 (1988).

75. D.S. Fischl and D.W. Hess, J. Vac. Sci. Technol. B6, 1577 (1988).

76. L.L. Sveshnikova, V.I. Donin and S.M. Repinskii, Sov. Tech. Phys. Lett. 3, 223 (1977).

77. J.K.K. Ip and G. Burns, J. Chem. Phys. 51, 3414 (1969).

78. M.A.A. Clyne and A.R. Woon-Fat, Trans. Faraday Soc. 69, 412 (1973).

79. J.T. Herron, J. Chem. Phys. 67, 2864 (1963).

80. A.J. Downs and C.J. Adams, "Comprehensive Inorganic Chemistry", Chapter 26, ed. A.F. Trotman-Dickenson, Pergamon Press, Oxford 1973, p.1144.

81. R.J. Fressenden and J.S. Fressenden, "Organic Chemistry", Willard Grant Press, Boston 1979, p.226.

82. L.B. Pankratz, "Thermodynamic Properties of the Halides", United States Department of the Interior, Bureau of Mines Bulletin 674, 1984, pp. 583-595.

83. S. Glasstone, K.J. Laidler and H. Eyring, "The Theory of Rate Processes", McGraw-Hill, New York, 1941, p. 144.

84. W.L. Masterton and E.J. Slowinski, "Chemical Principles", W.B. Saunders Company, Philadelphia 1977, p. 156.

85. V.M. Donnelly, D.L. Flamm and D.E. Ibbotson, J. Vac. Sci. Technol. A1, 626 (1983).

86. L. Baldi and D. Beardo, J. Appl. Phys. 57, 2221 (1985).

87. S. Berg, C. Nender, R. Buchta and H. Norström, J. Vac. Sci. Technol. A5, 1600 (1987).

88. H.F. Winters and D. Haarer, Phys. Rev. B 36, 6613 (1987).

89. Y.H. Lee and M.M. Chen, J. Vac. Sci. Technol. B4, 468 (1986).

90. J.A. Yarmoff and F.R. McFeely, Phys. Rev. B 38, 2057 (1988).

91. B.J. Garrison and W.A. Goddard III, Phys. Rev. B 36, 9805 (1987).

92. C.G. Van der Walle, E.R. McFeely and S.T. Pantelides, Phys. Rev. Lett. 61, 1867 (1988).

93. D.L. Flamm, Pure & Appl. Chem. 62, 1709 (1990).

94. H. Okano, Y. Horiike and M. Sekine, Jpn. J. Appl. Phys. 24, 68 (1985).

95. R. Kullmer and D. Bäuerle, Appl. Phys. A 43, 227 (1987).

96. O. Mogyorosi, K. Piglmayer, R. Kullmer and D. Bäuerle, Appl. Phys. A 45, 293 (1988).

97. W. Sesselmann, E. Hudeczek and F. Bachmann, J. Vac. Sci. Technol. B7, 1284 (1989).

98. A.M. El-Masry, F.O. Fong and J.C. Wolfe, J. Vac. Sci. Technol. B6, 257 (1988).

99. J. Pelletier and M.J. Cooke, J. Vac. Sci. Technol. B7, 59 (1989).

100. T.D. Bestwick and G.S. Oehrlein, J. Vac. Sci. Technol. A8, 1696 (1990).

101. H. Crazzolara and N. Gellrich, J. Electrochem. Chem. Soc. 137, 708 (1990).